

**CONTROL AND MOTION PLANNING OF DYNAMICALLY  
WALKING BIPEDS FOR COOPERATIVE TRANSPORTATION**

by

Seyed Mohamad Shafiee Motahar

A dissertation submitted to the Faculty of the University of Delaware in partial fulfillment of the requirements for the degree of Doctor of Philosophy in Mechanical Engineering

Winter 2018

© 2018 Seyed Mohamad Shafiee Motahar  
All Rights Reserved

**CONTROL AND MOTION PLANNING OF DYNAMICALLY  
WALKING BIPEDS FOR COOPERATIVE TRANSPORTATION**

by

Seyed Mohamad Shafiee Motahar

Approved: \_\_\_\_\_  
Ajay K. Prasad, Ph.D.  
Chair of the Department of Mechanical Engineering

Approved: \_\_\_\_\_  
Babatunde A. Ogunnaike, Ph.D.  
Dean of the College of Engineering

Approved: \_\_\_\_\_  
Ann L. Ardis, Ph.D.  
Senior Vice Provost for Graduate and Professional Education

I certify that I have read this dissertation and that in my opinion it meets the academic and professional standard required by the University as a dissertation for the degree of Doctor of Philosophy.

Signed: \_\_\_\_\_

Ioannis Poulakakis, Ph.D.  
Professor in charge of dissertation

I certify that I have read this dissertation and that in my opinion it meets the academic and professional standard required by the University as a dissertation for the degree of Doctor of Philosophy.

Signed: \_\_\_\_\_

Herbert G. Tanner, Ph.D.  
Member of dissertation committee

I certify that I have read this dissertation and that in my opinion it meets the academic and professional standard required by the University as a dissertation for the degree of Doctor of Philosophy.

Signed: \_\_\_\_\_

Thomas S. Buchanan, Ph.D.  
Member of dissertation committee

I certify that I have read this dissertation and that in my opinion it meets the academic and professional standard required by the University as a dissertation for the degree of Doctor of Philosophy.

Signed: \_\_\_\_\_

Jill Higginson, Ph.D.  
Member of dissertation committee

I certify that I have read this dissertation and that in my opinion it meets the academic and professional standard required by the University as a dissertation for the degree of Doctor of Philosophy.

Signed: \_\_\_\_\_

Samuel Lee, Ph.D.  
Member of dissertation committee

## ACKNOWLEDGEMENTS

First and foremost I would like to thank my advisor Dr. Ioannis Poulakakis for his support and encouragement during my doctoral study. Without his thoughtful guidance and careful comments this PhD would have not been achievable. I would also like to thank my committee members Dr. Herbert Tanner, Dr. Thomas Buchanan, Dr. Jill Higginson and Dr. Samuel Lee for their instrumental advice. In terms of funding, the research for this dissertation is supported by National Science Foundation (NSF) through the grant NRI-1327614 and the NSF Career Award IIS-1350721.

I owe a debt of gratitude to my lab mate Sushant Veer for his constant help and for all the productive discussions we shared during the collaborative research we have carried out toward this dissertation. I would like to thank my other lab mates Dr Qu Cao, Dr Xin Liu and Jian Huang. The time that we spent together in Robotic Locomotion Lab will be a memorable part of my life. I also want to thank my friends Reza, Mohammad I and II, Ahad, Sina and Hossein for the support and friendship that I needed and for making the best out of a village life.

Lastly, I want to dedicate this thesis to my parents and siblings for their unconditional love and support in my life. I haven't been able to visit them for years, but their thoughts and kind words have always carried me forward.

## TABLE OF CONTENTS

<b>LIST OF TABLES</b> . . . . .	<b>x</b>
<b>LIST OF FIGURES</b> . . . . .	<b>xi</b>
<b>ABSTRACT</b> . . . . .	<b>xv</b>
 <b>Chapter</b>	
<b>1 INTRODUCTION</b> . . . . .	<b>1</b>
1.1 Contributions . . . . .	4
1.1.1 Controller Design for Biped’s Adaptive Behavior in Response to Leader’s Intention: 2D and 3D models . . . . .	4
1.1.2 Stable Navigation of 3D Dynamically Walking Bipedal Walkers	5
1.2 Structure of the Thesis . . . . .	6
<b>2 LITERATURE SURVEY</b> . . . . .	<b>8</b>
2.1 Bipedal Robots . . . . .	9
2.2 Locomotion Controllers . . . . .	12
2.3 Integrating Locomotion and Manipulation for Cooperation . . . . .	15
2.4 Motion Planning . . . . .	19
<b>3 BIPED-LEADER COOPERATIVE TASK: PLANAR MODEL</b> . . . . .	<b>23</b>
3.1 Walking under Interaction Forces . . . . .	23
3.1.1 Planar Biped Model . . . . .	23
3.1.2 Cooperation Model . . . . .	24
3.1.3 Swing Phase Dynamics . . . . .	27

3.1.4	Double Support Phase . . . . .	28
3.2	Coupled Locomotion and Arm Control . . . . .	30
3.2.1	Virtual Constraint for the Locomotion Task . . . . .	31
3.2.2	Impedance Regulation for the Manipulation Task . . . . .	31
3.2.3	Controller Design . . . . .	32
3.2.4	Effect of Interaction Force on Locomotion . . . . .	34
3.2.5	Closed Loop Hybrid System . . . . .	35
3.3	Reduced-order Stiff Manipulator System . . . . .	38
3.3.1	Effect of External Force on a Step . . . . .	39
3.3.2	Effect of External force on Gait Constraints . . . . .	45
3.3.3	No Fall Conditions under External Force . . . . .	46
3.4	Examples . . . . .	47
3.4.1	Adaptation to the Leader's Change of Speed . . . . .	49
3.4.2	Effectiveness of the Arm's Impedance Controller . . . . .	51
3.4.3	Switching from Flat Ground to Upstairs and Downstairs . . . . .	53
3.5	Discussion . . . . .	56
<b>4</b>	<b>BIPED-LEADER COOPERATIVE TASK: 3D MODEL . . . . .</b>	<b>57</b>
4.1	Walking under Interaction Forces . . . . .	57
4.1.1	Three-Dimensional Model . . . . .	57
4.1.2	Swing Phase . . . . .	59
4.1.3	Double Support Phase . . . . .	60
4.2	Coupled Locomotion and Arm Control . . . . .	62
4.2.1	Virtual Constraints for the Locomotion Task . . . . .	62
4.2.2	Impedance Regulation for the Manipulation Task . . . . .	63
4.2.3	Controller Design . . . . .	64
4.3	Effect of External Force on Locomotion . . . . .	65
4.3.1	Effect of External Force on Stepping Pattern . . . . .	65
4.3.2	Effect of External Force on Symmetry under Yaw Rotation . . . . .	65

4.3.3	Effect of External Force on Zero Dynamics . . . . .	68
4.4	Examples . . . . .	72
4.4.1	An Example of Periodic Gait under External Force . . . . .	73
4.4.2	Optimized Periodic Gait with Respect to External Force . . . . .	74
4.4.3	Straight Walking with Leader . . . . .	75
4.4.4	Steering the Biped to a Goal Region . . . . .	78
4.5	Discussion . . . . .	80
<b>5</b>	<b>A SWITCHED SYSTEM APPROACH TO MOTION PLANNING OF LIMIT CYCLE ROBOTIC SYSTEMS WITH APPLICATION TO 3D BIPEDAL WALKERS . . . . .</b>	<b>81</b>
5.1	Problem Formulation . . . . .	82
5.2	Stable switching among multiple equilibria . . . . .	83
5.2.1	Set Constructions . . . . .	83
5.2.2	Stability of the switched system with dwell-time . . . . .	85
5.3	Application to 3D Bipedal Walking . . . . .	88
5.3.1	A Model of 3D Bipedal Walking . . . . .	88
5.3.2	Equivariance-Preserving Control Law . . . . .	90
5.3.3	HZD Based Controller Design . . . . .	92
5.3.4	Generating Motion Primitives . . . . .	95
5.3.5	Stable Composition of Gait Primitives . . . . .	97
5.3.5.1	Estimation of Basin of Attraction . . . . .	97
5.3.5.2	Computation of Minimum Dwell Time for Stability . . . . .	99
5.3.6	Planning with Motion Primitives . . . . .	100
5.3.6.1	Nominal Motion Primitives . . . . .	102
5.4	Discussion . . . . .	109
<b>6</b>	<b>CONCLUSION AND FUTURE WORK . . . . .</b>	<b>111</b>
6.1	Conclusion . . . . .	111

6.2	Future Work . . . . .	113
6.2.1	Prioritizing between Adaptive Response and Obstacle Avoidance	113
6.2.2	Improving Adaptive Response . . . . .	114
6.2.3	Experimental Validation . . . . .	115
	<b>BIBLIOGRAPHY . . . . .</b>	<b>116</b>

## LIST OF TABLES

3.1	Mechanical Parameters of the planar Bipedal Model . . . . .	25
4.1	Mechanical Parameters of the 3D Bipedal Model . . . . .	58
5.1	Selected Nominal Motion Primitives . . . . .	104
5.2	Dwell Time Values Based on Allowable Drift . . . . .	107

## LIST OF FIGURES

1.1	The hierarchical components for achieving complex tasks with bipedal robots. The high-level planner and the low-level controller need to communicate properly for the successful completion of the task. . .	3
1.2	(a) Biped-leader cooperation model. (b) Steering the biped to a goal region via interaction force while avoiding obstacles. . . . .	4
1.3	(a) The walking arcs for a family of gait primitives. The number on each arc shows the change in heading angle. (b) Motion planner constructs an obstacle-free path while the biped stably executes it.	5
2.1	Photos of (a) RABBIT [13], (b) MABEL [34], (c) MARLO [10], (d) ASIMO [1] and (e) DRC-HUBO [120]. . . . .	10
2.2	Guiding the motion of NAO via physical interaction. Photo adopted from [7]. . . . .	18
2.3	(a) Sequential composition of funnels. The dwell time condition is computed so that that any two funnels are composable. Each funnel corresponds to a motion primitive. (b) High-level and low-level interconnections. Planner respects the dwell time constraint and produces a switching signal accordingly. (c) execution of the suggested path. Stability of the biped is ensured by the dwell time constraint. . . . .	20
3.1	Planar model of the biped with a choice of generalized coordinates. The values of each link’s length, mass and inertia is given in Table 3.1.	24
3.2	(a) Planar model of biped-human team in a cooperative transportation of an object. (b) Impedance model of interaction. . .	26
3.3	An example of a force profile. The force over the duration of each step can be expressed as a function of the monotonic angle $\theta$ . . . .	40

3.4	<b>Left:</b> Biped response when the average speed of the leader is higher than that of the biped. <b>Right:</b> Biped response when the average speed of the leader is lower than that of the biped. (a) and (b) Average speed of leader (solid red line) and average speed of biped (blue marker). (c) and (d) Horizontal component of interaction force. (e) and (f) Zero dynamics state at the end of each step $\zeta^-$ (blue markers) and fixed point of each step $\zeta_k^*$ as in (3.47) (red markers). (g) and (h) Convergence of limit cycles. Black is the base (unforced) limit cycle, gray is the transitioning and red is the final limit cycle.	50
3.5	(a) Speed convergence of the biped (dashed blue line) to intended speed of leader (solid red line) for different impedance values of manipulator. (b) RMS of the interaction force as a function of manipulator impedance. . . . .	52
3.6	<b>Left:</b> Simulation results when transitioning from flat ground to upstairs. <b>Right:</b> Transitioning from flat ground to downstairs. (a) and (b) Snapshots of walking. Black and red links correspond to the stance and swing foot respectively. (c) and (d) Average walking speed of the biped (blue markers) and desired speed of leader (red line). (e) and (f) Interaction force. Solid blue is the horizontal component and dashed red is the vertical component. . . . .	55
3.7	The hierarchical components for a cooperation task. The leading co-worker plans a trajectory $p_L$ (high-level) and guides the robot to follow it by applying a suitable force $F_e$ at the biped's end effector.	56
4.1	(a) 3D biped model with a choice of generalized coordinates when supported on leg 1. (b) 3D biped model with a choice of generalized coordinates when supported on leg 2. Each link has a length and a mass that is modeled by point mass located at the center of the link. The values of these parameters are given in Table 4.1. . . . .	59
4.2	Comparison of the behavior of two periodic gaits in response to the external force $F_e = (5, 0, 0)^T N$ . (a) Average speed (b) Trajectory of biped's COM. The green color refers to the periodic gate that minimizes (4.33); i.e. the change in the heading angle of biped is less sensitive to the external force in the X direction. . . . .	74

4.3	<p><b>Left:</b> Response of a 3D biped when the leader walks along the X direction with higher average speed than that of the biped. <b>Right:</b> Response of a 3D biped when the leader walks along the X direction with lower average speed than that of the biped. (a) and (b) Intended average speed of leader (dashed red line) and average speed of biped (blue marker). (c) and (d) Component of interaction force in the X direction. (e) and (f) Intended trajectory of leader (dashed red line) and trajectory of biped’s end effector (solid blue line) in the X-Y plane. . . . .</p>	76
4.4	<p><b>Left:</b> Response of a 3D biped when the leader walks along the X direction with higher average speed than that of the biped. <b>Right:</b> Response of a 3D biped when the leader walks along the X direction with lower average speed than that of the biped. (a) and (b) Convergence of limit cycles in terms of <math>\theta</math> and <math>\dot{\theta}</math>. (c) and (d) Convergence of limit cycles in terms of <math>q_1</math> and <math>\dot{q}_1</math>. Black is the base (unforced) limit cycle, gray is the transitioning and red is the final forced limit cycle. . . . .</p>	77
4.5	<p>(a) Biped-leader cooperation in an environment with obstacles. The intended trajectory of the leader is denoted as red line. (b) X component (blue) and Y component (dashed red) of the interaction force. (c) Intended average speed of the leader (red) and average speed of the biped (blue). (d) Convergence of limit cycles in terms of <math>\theta</math> and <math>\dot{\theta}</math>. (e) Convergence of limit cycles in terms of <math>q_1</math> and <math>\dot{q}_1</math>. Black is the base (unforced) limit cycle, red is the final forced limit cycle and gray correspond to transition. . . . .</p>	79
4.6	<p>The hierarchical components for a cooperation task in 3D space. The leading co-worker plans a trajectory <math>p_L</math> and guides the robot to follow it by applying a suitable force at the biped’s end effector. . . . .</p>	80
5.1	<p>Schematic of the set construction for two discrete systems with different equilibria. The open domain <math>\mathcal{D}</math> of the discrete maps is represented by the black dotted outer boundary. The largest positive invariant sub-level sets <math>\mathcal{D}_1</math> and <math>\mathcal{D}_2</math> in the domain <math>\mathcal{D}</math> are represented by red. <math>\overline{\mathcal{M}}(\kappa)</math> is represented by green, and <math>\mathcal{N}(\kappa)</math> is represented by blue. The <math>\overline{\mathcal{M}}(\kappa)</math> construction lies entirely within <math>\mathcal{D}_1 \cap \mathcal{D}_2</math>. . . . .</p>	86
5.2	<p>Robot model with a choice of generalized coordinates when supported on left leg. . . . .</p>	90

5.3	Estimates of the basin of attraction for each of the motion primitives in $\mathbb{G}$ (dashed ellipses), and computation of $\overline{\mathcal{M}}(\kappa)$ (union of solid ellipses), which is entirely inside the intersection of basin of attractions. The colors blue, red and green correspond to the primitives $\mathcal{R}_0$ , $\mathcal{R}_1$ and $\mathcal{R}_2$ respectively. Note that the fixed points of $\mathcal{R}_1$ and $\mathcal{R}_2$ and their corresponding $\mathcal{M}(\kappa)$ sets are almost coinciding. The set $\overline{\mathcal{M}}(\kappa)$ of (5.8) corresponds to $\kappa = 0.0002$ resulting in the dwell time $N_d = 1$ . . . . .	99
5.4	An example of stable composition of motion primitives. The sequence is $(\mathcal{R}_0, \mathcal{R}_1, \mathcal{R}_1, \mathcal{R}_1, \mathcal{R}_1, \mathcal{R}_2, \mathcal{R}_2, \mathcal{R}_2, \mathcal{R}_2, \mathcal{R}_0)$ . (a) animation of the walking sequence. (b) Evolution of stance hip torque corresponding to joint $q_5$ . (c) Evolution of swing hip torque corresponding to joint $q_8$ . . . . .	101
5.5	Nominal motion primitives for a family of primitives. The number on each arc shows the change in the heading angle. Blue corresponds to turning when support is on the left leg and red when support is on the right leg. . . . .	103
5.6	Two walking environments. The nominal plans using NMP are shown as red circles and the simulated trajectories of biped's CoM are indicated by blue lines. In the environment (a), the biped takes 24 strides to reach the goal (marked by black rectangle) and the final drifting error is 6.3 cm. In the environment (b), the biped takes 90 strides to reach the goal and the final error is 1.20 m. . . . .	108
5.7	The hierarchical components for motion planning. Based on the gait primitives and the dwell time constraint, the high-level planner constructs an obstacle-free path, which is then sent to the low-level locomotion controller for execution. . . . .	110
6.1	A human carrying an object with the humanoid robot HUBO (photo courtesy of Prof. P. Oh, Drexel University). . . . .	115

## ABSTRACT

There is an increasing demand for assistive bipedal robots that are capable of physical interaction with other agents possibly humans to accomplish collaborative tasks, such as coordinated object transportation. In such collaborative scenarios, we can rely on the environment mapping and path planning skills of the leading collaborator to choose an obstacle-free trajectory for the team. This intended trajectory may not be directly accessible by the robot; however, the interaction forces developed between the robot and the collaborator offer cues on how the robot should adapt its behavior to accomplish the task. As its first objective this thesis proposes a method that empowers a biped to actively modify its speed and heading angle in response to the resulting interaction forces, allowing a collaborator to effectively walk the biped along a desired path. The proposed method is based on integration of impedance control to provide compliance at biped's manipulator, with position control to synchronize the actuated degrees of freedom in a way that the generated walking gaits are adaptable to external activity. The feasibility of the method is illustrated on both planar and three dimensional bipedal robots that track the intended trajectory of leader with the sole knowledge of interaction force.

Bipedal robots should also be capable of navigating an environment autonomously, that is without the help of a leading collaborator. Planning the motion of biped through a workspace populated by obstacles can be decomposed into two hierarchical components. At the high level, a planner is responsible for the generation of an obstacle free path that respects the geometry of the workspace. At the low level, a controller should take into account the stability of the platform as it executes the descending plan. Certain stability issues and unfaithful execution of the plan may arise if the

high-level planning and low-level stability goals are considered in isolation. The second objective of this thesis is to bridge this gap by proposing a framework that unifies low-level stability and high-level planning objectives for systems that move in the environment via cyclic interactions, such as dynamically walking bipeds, in order to stably navigate them through a cluttered environment. The framework is based on extracting motion primitives in the form of limit cycle locomotion behaviors. The planner outputs a sequence of motion primitives that has to be followed by the robot in order to reach a goal location while avoiding obstacles. In this setting, a discrete-time switched system with multiple equilibria – each corresponding to a motion primitive – emerges as a natural formulation of the problem which projects the stability of the motion sequence to that of the switched system. We then show that the solution of the switched system can be confined in a safe region – characterized as the union of sub-level sets of Lyapunov functions – by imposing a bound on the dwell time of the switching signal. The approach is implemented on an underactuated 3D biped, and locally exponentially stable gait primitives are extracted using Hybrid Zero Dynamics (HZD) controllers. The dimensional reduction afforded by HZD allows the estimation of the basin of attraction of the gait primitives using sums-of-squares techniques, which facilitates the computation of the bound on the dwell time.

Overall, this thesis contributes to the cooperation and autonomous navigation of dynamically (limit-cycle) walking bipedal robots in two ways. First, it takes a step toward the development of controllers for cooperative object transportation tasks, in which a bipedal robot assists a human to carry an object along a path that is enforced by the human. Secondly, it bridges the gap between high-level motion planning algorithms and low-level *limit-cycle* locomotion controllers so that the descending commands of the planner can be faithfully executed by the biped.

## Chapter 1

### INTRODUCTION

The need for intelligent robots capable of cooperative interaction with humans is growing in the modern society. This type of cooperation can take advantage of both human decision making ability and robot precise command following capability. Owing to their anthropomorphic characteristics, humanoid robots are ideal for accomplishing tasks that require physical collaboration with humans in typical human-centric environments.

Assistive bipedal robots must be capable of complying with the geometry of the environment while simultaneously engaging in tasks that involve physical interaction with humans (or other robots) by means of their manipulators. In a number of such tasks – cooperative object transportation between a robot and a leading co-worker is one example – the robot’s walking pattern should be adapted according to interaction forces that can be interpreted as signals of collaborator’s intention.

Consider a scenario in which a bipedal robot must autonomously navigate in an environment cluttered by obstacles in order to reach the region where the human needs assistance. For the successful completion of this task, there is a need for a high-level planner that generates an obstacle-free path that conforms to the geometry of the environment, and a low-level controller that executes the descending plan, while ensuring stable operation of the platform. When the high-level planning and low-level stability objectives are treated in isolation, the platform may not be able to faithfully execute the plan, or may fail due to instability. Therefore, it is necessary to develop a framework that seamlessly integrates *limit-cycle* locomotion controllers with motion planning algorithms to enable the bipedal robot navigate in an environment cluttered by obstacles.

Once the biped arrives at the goal region, it needs to engage in a cooperative task that requires it to follow the commands of the leading co-worker. These commands may not be explicitly available to the biped; rather, they may be implicitly available as interaction forces that the robot perceives at the end effector of its manipulators. In this setting, the biped must adapt its locomotion in response to these interaction forces, while ensuring that it does not fall down. In addition, to reduce the effort on behalf of the collaborator and to increase the safety of the cooperative task, the biped needs to exhibit compliance at the port of interaction. This necessitates the design of a unified manipulation and locomotion controller that enables the robot to respond to a collaborator’s intentions on both the locomotion and manipulation levels, adapting its movement to the interaction forces without compromising stable and safe operation.

There has been a vast amount of research on providing humanoid robots with navigation and cooperation capabilities. However, the proposed controllers work within the Zero Moment Point (ZMP) framework, which yields quasi-static motions that are not natural and energy efficient. On the other hand, in dynamic locomotion<sup>1</sup>, which is abundant in nature, the robot can be statically unbalanced and continually fall at some points of the gait cycle while the overall motion remains stable. In stark contrast to humanoids walking under the ZMP stability criterion, locomotion control methods for dynamically walking bipeds have been developed largely in isolation from high-level motion planning objectives. Indeed, most of the existing literature on dynamic walkers focuses on designing low-level controllers for generating and stabilizing periodic motions without examining how the resulting locomotion behaviors can be “shaped” to adapt to high-level motion planning considerations. The objective of this thesis is to integrate high-level tasks with low-level locomotion controllers to enable such robots to cooperate with a leading co-worker and to autonomously navigate in a cluttered environment; see Fig. 1.1. To this end, this thesis proposes two approaches that are suitable for cooperation and navigation scenarios. In the cooperation scenario, the

---

<sup>1</sup> Throughout this dissertation the term dynamic locomotion indicates limit-cycle locomotion.

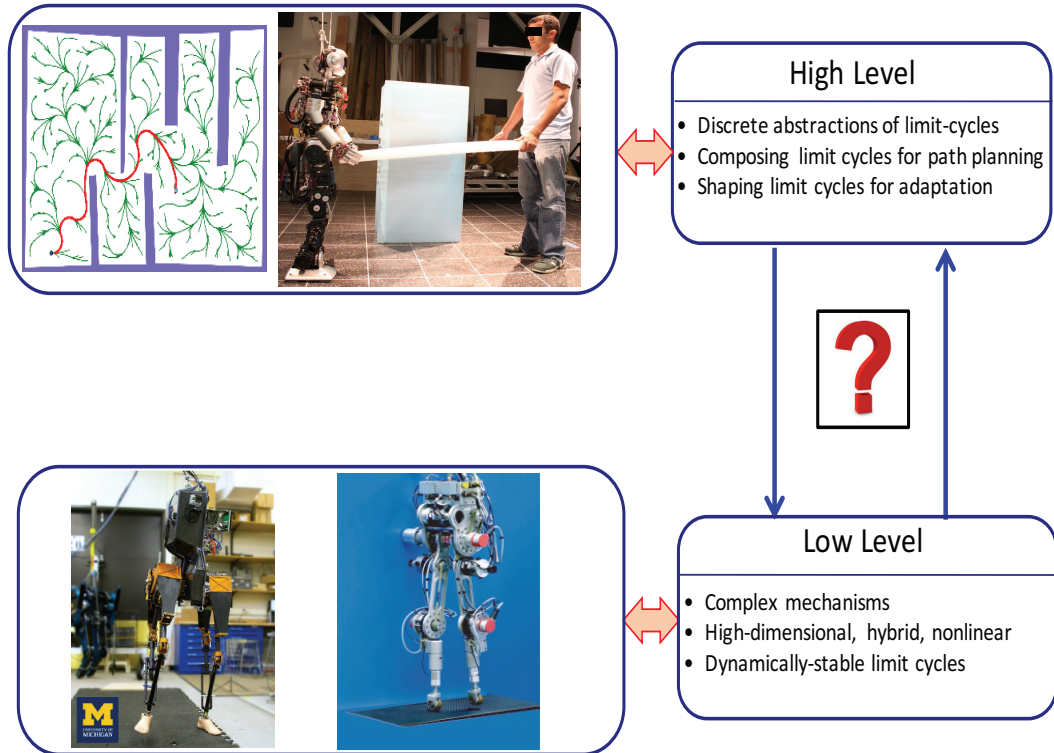


**Figure 1.1:** The hierarchical components for achieving complex tasks with bipedal robots. The high-level planner and the low-level controller need to communicate properly for the successful completion of the task.

leading co-worker acts as a high-level path planner that communicates its intention by applying a suitable force on the robot. The low-level locomotion controller is then designed so that the resulting limit cycle can be shaped by the interaction force in a way that the robot follows leader's intended path. In the autonomous navigation scenario, the high-level path planning algorithm composes different limit-cycle behaviors to generate an obstacle-free path in the environment while the low-level locomotion controller is responsible for executing the suggested path. The question that arises in these situations is how the high-level planner and low-level controller communicate. This thesis answers this question by providing information that need to be exchanged between these two components so that the task can be successfully accomplished.

## 1.1 Contributions

This thesis contributes to the cooperation and navigation of dynamically walking bipeds in a number of ways that can be summarized as follows.

### 1.1.1 Controller Design for Biped's Adaptive Behavior in Response to Leader's Intention: 2D and 3D models

This thesis proposes a method that enables a biped to adjust its walking pattern in response to the interaction forces developed as the biped physically cooperates with a leading co-worker; see Fig. 1.2(a). The proposed approach combines impedance control to regulate the manipulator's motion in response to the interaction force, with position control to coordinate the actuated degrees of freedom of the biped's legs in order to generate dynamic walking motions that can be adapted to external activity. In the planar model, analytical expressions on a step-to-step basis are derived that describe how the interaction force influences the biped's motion. With the help of these expressions, explicit conditions are obtained that predict the success of the biped in completing a step based on the state of the robot at the beginning of a step and the force applied over that step. Having these conditions met, with mere knowledge of

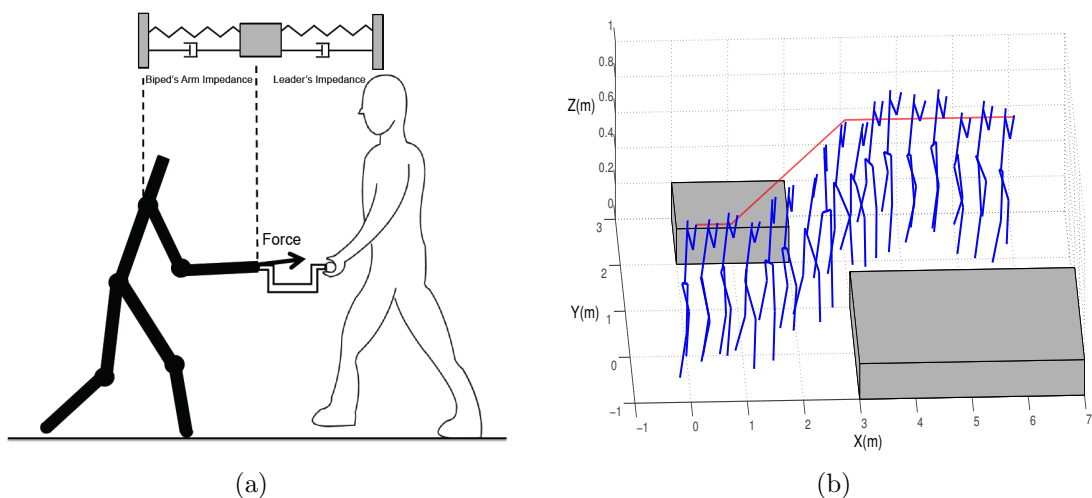


**Figure 1.2:** (a) Biped-leader cooperation model. (b) Steering the biped to a goal region via interaction force while avoiding obstacles.

the interaction force – that is, *without* knowing the intended trajectory of the leading collaborator – the biped is capable of altering its speed as it walks on flat ground or up and down stairs of known geometry by changing its stride frequency while keeping its stride length constant. In the 3D model, in addition to the aforementioned adaptations, it is shown in simulation that the biped also adjusts its heading angle in response to the interaction force. This property allows the leader to guide the motion of the biped so as to avoid collision with obstacles; see Fig. 1.2(b). These results have appeared in [70, 72, 105].

### 1.1.2 Stable Navigation of 3D Dynamically Walking Bipedal Walkers

The second contribution of this thesis is to present a framework for navigation of 3D dynamically walking bipeds in spaces cluttered by obstacles. The framework is based on extracting gait primitives in the form of limit-cycle locomotion behaviors, which are then composed by a higher-level planning algorithm with the purpose of navigating the biped to a goal location while avoiding obstacles; see Fig. 1.3. By formulating motion planning as a discrete-time switched system with multiple equilibria

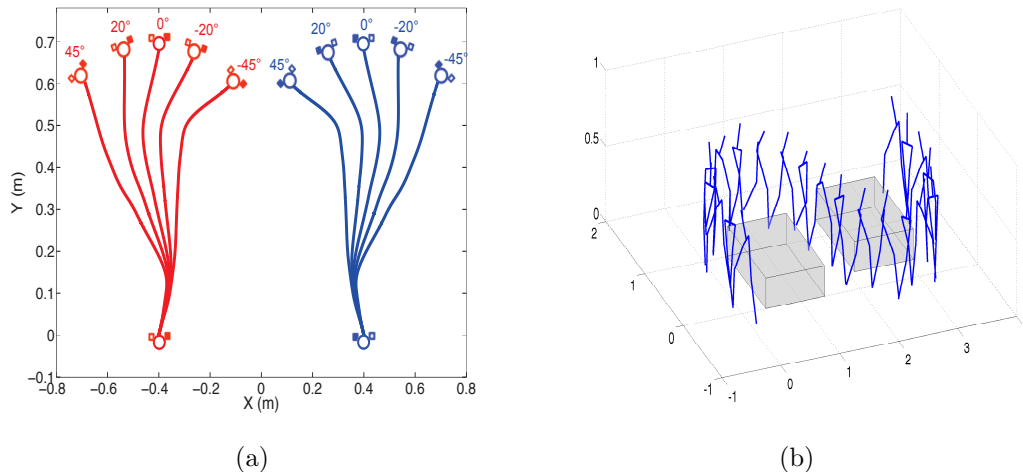


**Figure 1.3:** (a) The walking arcs for a family of gait primitives. The number on each arc shows the change in heading angle. (b) Motion planner constructs an obstacle-free path while the biped stably executes it.

– each corresponding to a gait primitive – analytical conditions are provided that constrain the frequency of the switching signal provided by the planner so that the biped is guaranteed to stably execute a suggested plan. Effectively, these conditions distill the limitations of the system dynamics in a form that can be readily incorporated to the planning algorithm. We demonstrate the feasibility of the method in the context of a three-dimensional bipedal model, walking dynamically under the influence of a Hybrid Zero Dynamics (HZD) controller. It is shown that the dimensional reduction afforded by HZD greatly facilitates the application of the method by allowing certificates of stability for gait primitives using sums-of-squares programming. These results have appeared in [71, 107].

## 1.2 Structure of the Thesis

The organization of the rest of this thesis is as follows. Chapter 2 provides a brief overview of the related work on locomotion controllers, integrating locomotion and manipulation for cooperation and motion planning with bipedal robots.

Chapter 3 investigates the cooperation task of the biped-leader team in a planar setting. The walking cycle is mathematically modeled as a periodic solution of a hybrid system that is composed of a continuous swing phase and a discrete impact map. A coupled locomotion and manipulation controller is then proposed that generates dynamic walking gaits and simultaneously provides compliance in the biped’s arm. The proposed controller takes advantage of the underactuated nature of the robot to respond to the interaction forces. The availability of closed form solutions for the reduced system allows us to quantify speed change based on interaction force. Finally, the method is applied in the case of a bipedal robot model walking over flat ground and up and down stairs of known geometry under the influence of a desired trajectory that is unknown to the biped and represents the intention of a collaborator.

Chapter 4 demonstrates that the control method presented in Chapter 3 can be extended to underactuated 3D bipedal robots. Particularly, the controller is designed so that in addition to speed, the heading angle of the biped also responds to the interaction

force. Although analytical solutions cannot be derived for the 3D case due to the high dimensionality of the reduced system, several simulation examples demonstrate that the biped is able to follow the intended direction of the leader. The biped can then rely on the leader’s knowledge of the environment in order to avoid the obstacles on the way, and to be steered to the goal region.

Chapter 5 deals with the case when the biped has to autonomously navigate within an obstacle-cluttered environment without the help of a leading co-worker. Instead, a high-level planner with knowledge of the environment can be used to provide an obstacle-free path by composing limit-cycle primitives. In this setting, a discrete-time switched system with multiple equilibria – each corresponding to a motion primitive – emerges as a natural formulation of the problem which relates the stability of the motion sequence to that of the switched system. It is shown that the solution of the switched system can be confined in a safe region – characterized as the union of sub-level sets of Lyapunov functions – by imposing a bound on the dwell time of the switching signal. More importantly, the availability of the closed-form relations allows adjusting the size of the desired region as a function of the bound on the dwell time. Increasing the bound on the dwell time reduces the size of the safe region, resulting in smaller deviation from the nominal path, while adversely affecting the flexibility of the planner in generating a feasible path. The framework is demonstrated on a 3D bipedal robot model that implements an HZD control law to generate locally exponentially stable motion primitives. The inherent reduction in dimension offered by HZD enables the use of sums-of-squares (SOS) techniques to estimate the basin of attraction of the motion primitives, resulting in analytical expressions for the dwell-time bound for stability.

Finally, Chapter 6 provides concluding remarks and suggests future directions.

## Chapter 2

### LITERATURE SURVEY

This chapter presents the literature review about bipedal robots and motivates the development of the methods presented in this thesis. The discussion begins with the history of prototype development of various passive and powered bipedal robots in chronological order in Section 2.1.

Section 2.2 presents relevant work on two of the main approaches for bipedal locomotion control design, namely, Zero Moment Point (ZMP) and limit-cycle based controllers. The latter is the focus of this thesis. Section 2.3 provides an overview of the relevant work on manipulation controllers and its integration with locomotion controllers. It should be mentioned here that the majority of these studies implement the ZMP criterion for stability to enable humanoids perform various complicated tasks such as cooperating with humans and transporting objects over distances. The objective of this thesis is to enable limit-cycle walkers to perform similar tasks in a provably stable fashion.

Section 2.4 presents recent advances in motion planning of bipedal robots. As will be seen in this section, there are only very few works that explicitly take into account high-level motion planning objectives in the context of limit-cycle walkers. Furthermore, none of these studies establish analytical guarantees for stable composition of motion primitives. This shortcoming motivates the work in this thesis that attempts to provide a framework within which stable operation as the biped executes the path suggested by the planner is ensured.

## 2.1 Bipedal Robots

The development of bipedal robot prototypes has received considerable attention in recent years. There are generally two classes of bipedal robots: humanoids and dynamically walking robots. Humanoid robots are capable of performing a large array of tasks at the expense of a complex mechanical design. On the other hand, dynamically walking bipeds are generally less complex mechanical systems than humanoids and are capable of more natural and energy efficient walking motions.

An extreme example of dynamically walking bipeds are passive dynamic walkers. These systems walk downhill powered only by gravity – that is, without any motor actuating their joints. In more detail, in passive walking gaits, the portion of energy that is being dissipated at impacts is compensated by the potential energy as the robot walks down the slope. The first passive biped was built by McGeer in the late 1980s [65]. It consisted of two straight legs each having two parallel links to keep the motion in the sagittal plane. The biped could successfully walk down a slope of 1.4 degrees with the speed of 0.4 m/s. To provide a simple solution for foot clearance from the ground, a knee joint was added to the leg which in some cases enhanced the overall stability of the walking gait [65]. In late 1990s, Collins et al. built a three dimensional passive biped that had common features with McGeer’s planar biped. However the biped was prone to lateral instability due to the addition of roll and yaw degrees of freedom in the three dimensional model. To reduce the fluctuation of angular momentum induced by swinging legs, counter-swinging arms were attached to the opposing legs so that right leg and left arm swing forward at the same time. Using this strategy the biped could stably walk down a 3.1 degree slope with the speed of 0.5 m/s [18].

Although the study of passive robots is important in understanding the basic cyclic walking behavior, the use of actuation can enhance the stability and versatility of the generated motions. One of the first powered bipeds capable of stable walking was called WL-5; a three dimensional biped with 11 DOF that was built in Japan in 1972 [46]. In the mid 1980s, Miura et al. constructed a series of small-sized bipeds, called Biper, some of which were able to walk forward, backward and sideways [67].

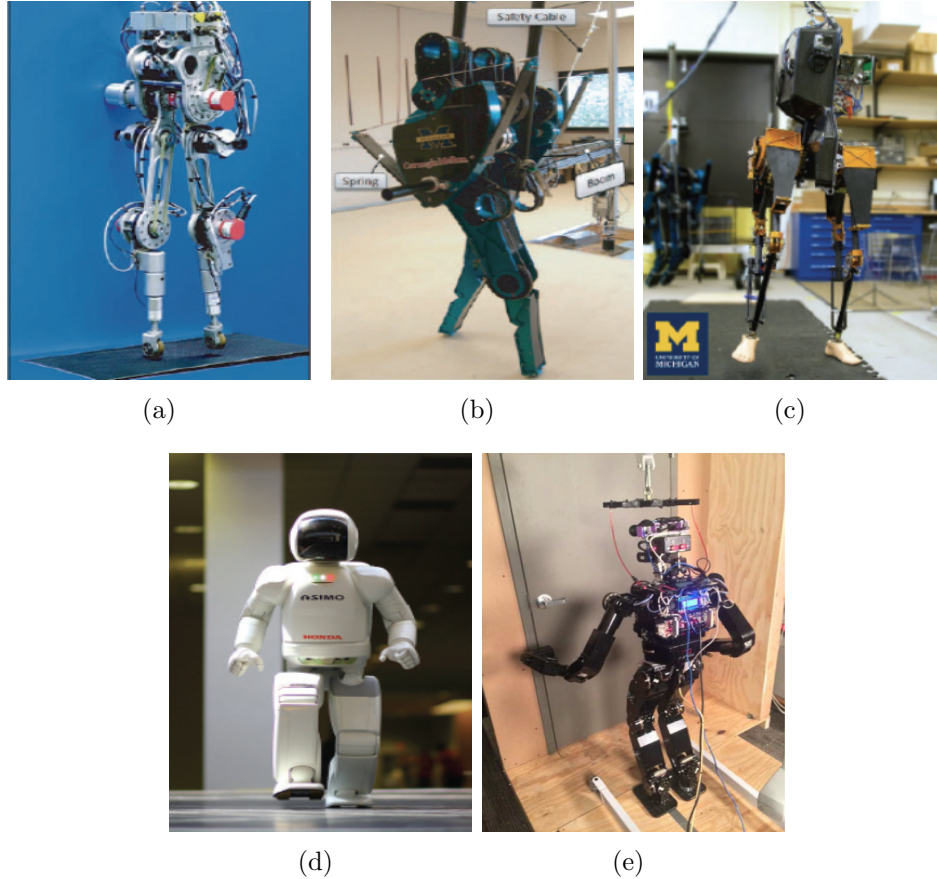


**Figure 2.1:** Photos of (a) RABBIT [13], (b) MABEL [34], (c) MARLO [10], (d) ASIMO [1] and (e) DRC-HUBO [120].

The controller was designed to enforce a trajectory on the joints that was generated based on the motion of an inverted pendulum. In the late 1980s, Furusho et al. built a medium-sized, 0.98 m tall biped, called BLR-G2 that could walk at the speed of 0.18 m/s [25]. In the late 1990s, a planar biped named Spring Flamingo was built at the MIT Leg Lab [86]. It had six degrees of freedom each controlled by a series elastic actuator. The use of series elastic actuators improved the force control performance and increased the shock tolerance of the walking gait. The biped was capable of walking over sloped terrains with the speed of 1.2 m/s. In the late 1990s, the French National Research Council constructed a 5 DOF planar biped RABBIT; see Fig. 2.1(a), with the purpose of providing a platform to study the control aspects of limit-cycle walkers [13]. The

model of RABBIT is used in this thesis and its morphological characteristics can be found in Table 3.1. In 2007, MABEL a five link planar biped was collaboratively built by University of Michigan and Carnegie Mellon University; see Fig. 2.1(b). Compliant elements were introduced in the robot's power train to enhance the energy efficiency and agility of the walking gait [34]. MABEL is able to reach speeds of up to 3.6 m/s. Both RABBIT and MABEL are attached to a safety boom for lateral stability. In 2012, a 3D bipedal robot MARLO was built by the same group that could walk without the need of a supporting boom; see Fig. 2.1(c). The use of virtual constraints in the lateral plane allowed the robot to extend planar walking to 3D walking. MARLO has 13 DOF and is highly underactuated with only 6 actuators [10].

One of the most advanced bipedal robots that is capable of operating in human environments is the humanoid ASIMO, developed by HONDA. The robot has a total of 34 DOFs which offer a wide range of possible motions; see Fig. 2.1(d). ASIMO can adjust its body posture, step length, speed and the direction it is stepping in. It is equipped with visual sensors that detect the ground surface and obstacles, enabling it to autonomously navigate the environment. It also has face and voice recognition features that allow it to interpret and respond to the commands of its companion. ASIMO can walk with the speed of 0.75 m/s and run upto speed of 2.5 m/s [1]. Another humanoid robot, the DRC-HUBO, was the winner of the DARPA<sup>1</sup> robotic challenge in 2015; see Fig. 2.1(e). One of the prominent features of DRC-HUBO during the competition has been its ability to transform from walking robot to rolling on four wheels by bending and using wheels incorporated in its knees, which indicates that humanoid robots have not yet reached at the point of accomplishing realistic tasks such as those required in the 2015 DARPA robotic challenge. This robot is 1.47 m tall with a wingspan of 2.04 m, it weighs 52 kg (including battery), and it has 32 DOFs [120]. DRC-HUBO could successfully complete a variety of complex tasks such as debris removal, door opening, wall breaking and stair climbing.

---

<sup>1</sup> Defense Advanced Research Projects Agency

## 2.2 Locomotion Controllers

The majority of existing work on designing controllers for bipedal walking utilized the notion of ground reference points such as ZMP, as a stability measure of the biped [116], [56], [115], [109]. The ZMP refers to the point on the ground about which the horizontal component of the moment resulting from the ground reaction force is zero [83]. The intuition for defining the ZMP is to find a point that describes the overall behavior of the mechanism and replaces all forces acting on the mechanism by one single force [108]. If the computed location of ZMP resides within the support polygon the robot has postural balance.

This method was first implemented in 1984 on a real robot, namely the WL-12RV biped, which could walk at the highest speed of 0.375 m/sec. The control method compensated the three axes (pitch-roll and yaw) moments by following a planned trajectory of the ZMP [116]. The most popular robot that works with ZMP criterion is the humanoid ASIMO [89] which is capable of doing different tasks. Although the ZMP method evolved in different aspects such as improving mobility and agility [102], traversing different terrains [40] and more natural looking gaits [23], there exists some shortcomings which are inherent to this method. Utilizing this quasi-static method in the gait synthesis requires that the ZMP remains strictly in the interior of footprint. On the other hand, in truly dynamic methods, the hypothetical ZMP can be outside the support polygon and yet the biped does not experience instability. This strict condition in the ZMP approach limits the speed of achieved motion and results in inefficient gait cycle. Furthermore, the foot remains flat on the ground which is in contrast with human walking where the foot rotates on the ground to minimize the energy losses and contribute to powering the motion. In addition, the dependency of the method on the foot being flat on the ground precludes the use of ZMP-based methods to point-foot walking, and also to realizing gaits such as running in which the foot is not always in contact with the ground.

Contrary to ZMP-based controllers, a number of control approaches has been introduced to generate and sustain dynamic walking motions on bipedal robots by

stabilizing desired limit-cycle solutions of their dynamics. Inspired by McGeer’s passive bipedal walker [65], Spong [96] designed feedback control laws for a fully actuated compass walker, that canceled the change in gravity torque due to the change in ground slope and rendered the limit cycle slope invariant, i.e. it could walk on any slope. Later, Spong and Bullo [97] generalized the results for three-dimensional bipeds, where they gave a rigorous proof of the stability of the periodic motion. In order to simplify the analysis of the coupled and complex dynamics of 3D bipeds and to use the known planar limit cycles, geometric reduction is implemented to decouple the sagittal plane motion from the roll and yaw motions [28].

Along a different philosophy, the hybrid zero dynamics (HZD) method [111] has been proposed to generate periodic dynamic walking for a class of underactuated bipeds; the purpose of this method is to reduce the dimension of the system and facilitate the stability analysis. In this approach, input-output linearization is implemented to design a controller that produces the walking gait by zeroing a set of suitably designed outputs in the form of virtual holonomic constraints. The zero dynamics is then defined as the maximal internal dynamics of the system that are compatible with the outputs being identically equal to zero. The method was first applied on a three-link biped to generate asymptotically-stable limit cycles [33]. Since the constraints are imposed during the stance phase without regarding impacts, the zero dynamics of the system is not in general invariant under the impact. To alleviate this problem, [112] introduced the notion of hybrid invariance of the zero dynamics which was implemented through output functions in the form of Beziér polynomials. Adjusting the parameters of Beziér polynomials created an invariant surface in the continuous phase of the system as well as under the action of the impact map. This lower dimensional model of the closed-loop hybrid model is termed the Hybrid Zero Dynamics (HZD), which further facilitated the stability analysis of the full-order system. In addition, optimization could be performed on the design of holonomic constraints in order to meet actuation limitations and other gait constraints such as friction cone limitation and unilateral ground reaction forces. A new definition of stability for aperiodic walking in the sense

of “not falling” was introduced in [117] and specifically used to give a framework for switching controllers. Transitioning between discrete speeds was carried out through designing an intermediate HZD surface that connected the corresponding HZD surfaces of two different gaits. The HZD method has also been used to stabilize periodic gaits for 3D bipeds [14] and to steer the biped along a desired path with mild curvature [93].

The studies just cited have assumed point feet during the walking cycle. The role of non trivial foot for the planar and 3D bipeds have been addressed in [16] and [110]. The gait cycle is composed of a fully actuated flat footed phase and an underactuated phase to allow foot rotation in the walking gait. The ankle torques have been used to follow a desired ZMP trajectory and to enhance the stability and energy efficiency of the gait. The HZD method was successfully demonstrated in experiments for the bipeds with point [99], as well as curved [63], feet.

Recently, the class of stabilizing controllers have been extended through the use of Control Lyapunov Functions (CLF) that enforce rapid convergence to the zero dynamics [5]. The reference [26] formulated a CLF-based quadratic program to unify stability requirements and gait constraints such as torque saturation, in one single framework. Using this framework, [76] developed a robust control method that could handle significant model perturbations. Control barrier functions were further integrated into the framework, in order to adjust step length in planar bipeds [77] and in 3D bipeds [74].

Plant uncertainty and external disturbances can be detrimental to stability of dynamic walking bipeds. To enhance robustness against external disturbances, the problem of stabilizing periodic orbits has been formulated as a set of bilinear matrix inequalities to systematically design event-based controllers [37] and continuous-time controllers [36]. This approach was illustrated on a simulation model of ATRIAS, a highly underactuated 3D biped with series-compliant actuators, walking on flat ground with different contact models. Reference [75] applies  $L_1$  adaptive control in a CLF-based controller scheme, to handle nonlinear uncertainty in bipedal walking. Ultimate boundedness of the output dynamics in the presence of modeling uncertainties was

established in [52]. In case of stochasticity in the dynamics, the high-gain feedback controllers may not be able to stabilize the limit cycle due to limited control authority. The study in [11] adopts a stochastic approach to present a controller design that maximizes the expected time to failure of walking machines. The method was examined on the compass gait biped walking on uneven ground profiles. By exploiting the terrain knowledge, the controller improved the stochastic stability of the walking cycle. Recently, the robustness of the approach has been improved through the use of meshing techniques that capture the step-to-step behavior of the biped [88].

To produce more “human-like” bipedal robotic walking, the notion of canonical walking functions has been proposed in [3] and [95]; these functions are simply solutions to a linear mass-spring-damper system with suitable parameters. These parameters are then optimized to derive the outputs of the robot as close as possible to the output of human. A novel aspect of this work is the use of the hip velocity as an output function which is allowed to jump through the impact. This provides some freedom to the velocity of the hip to compensate for the shock when the system experiences an impact [3]. In addition, having the velocity of the hip as an output facilitates the optimization problem for finding gait cycles with nearby speeds. The method was applied to achieve stable walking on uneven terrain [51], going upstairs and downstairs [85] and changing speeds in 3D [84]. Particularly, for stable speed-controlled robotic walking, a finite automaton containing different speeds and their transitions was built and a supervisor was designed to govern transition among different speeds through the minimum number of steps [21].

### **2.3 Integrating Locomotion and Manipulation for Cooperation**

Aside from the locomotion control of the biped, realizing cooperative object transportation tasks requires the interaction of the bipeds arm with the leading collaborator. This can be achieved through impedance control of the biped’s manipulator. The goal of this approach is to organize the manipulator so that its response to an externally applied force corresponds to that of a mass-spring-damper system [41]. As

a consequence, the manipulator is capable of mitigating the effect of modeling error, finite positioning accuracy and imprecise modeled environment, which would lead to increased contact forces and actuator saturation if conventional position control algorithms were used [90]. The pioneering work of Hogan [41] demonstrated that, for a simplified case, the manipulator impedance should be proportional to the environmental admittance when the task is to simultaneously minimize motion error and interface force. The subsequent works has been focused on addressing issues related to robot dynamics uncertainty and unknown environmental parameters. Kelly et al. [47] proposed an adaptive impedance control with parameter estimation to reduce the effect of manipulator uncertainty. In order to enhance the force tracking capability of impedance control under unknown environmental parameters (i.e. stiffness and location), Seraji et al. [92] presented an adaptive control scheme in which the reference position was generated online as a function of force tracking error.

In the context of robot-human cooperation, a significant body of research focuses on adaptive impedance control to produce biomimetic behavior [27], and to adapt to human characteristics and intention [22,31]. From an experiment involving two humans that cooperate to carry an object, an impedance controller with varying damping parameter was designed to improve the cooperation performance of a robotic manipulator and a human agent [42]. Gribovskaya et al. proposed a haptic control method in which the robot learns the task model through demonstration and generates reference trajectories in response to the perceived force [31]. In addition, to account for the non-modeled effects of the human, an adaptive impedance control is proposed that updates the impedance parameters based on the deviation of the robot from the learned task. Since it is generally difficult to model human behavior in cooperative tasks, as was shown experimentally in [80], the work of [59] uses a neural network to estimate the intention of a human partner, and integrates it in the impedance controller such that the robot actively follows the intended motion of the human with the mere knowledge of the human force. A real-time variable impedance parameters proportional to the estimated stiffness of human arm was proposed in [104]. In this work, the end effector

position and force sensor data was used to estimate the stiffness of the human hand.

There has been a vast amount of research on integrating manipulation tasks with legged locomotion using the ZMP stability criterion. In this approach, the interaction of a bipedal robot with its environment is accounted when generating trajectories for the whole system in a way that the ZMP remains in the support polygon. The study in [119] presents a control method that adjusts step length and timing to improve the manipulability of a biped's arm in a reference trajectory tracking task. Online modification of the ZMP and fast gait generation in response to commanded hand position in human-humanoid interaction was realized in [100] and [78]; the method was experimentally implemented on the robot HRP-2. To address the problem of push recovery of humanoids, [101] uses model predictive control to compute the desired forces and footstep locations that account for future actions.

The difficulties in a cooperative transportation of an object by two humanoids have been addressed in a few studies. The work in [43] showed that mutual position shifts will occur as a result of body swinging when two humanoids carry an object. Therefore, learning algorithms were used to find the optimal motion plans that result in minimum position shift [44]. The issue of speed mismatch between the two humanoids was resolved using a control law that combines PID and fuzzy-logic controllers. [49]. Realizing the configuration similarity between two cooperating humanoids and a quadruped, the use of quadrupedal trajectory planning with the purpose of synchronizing the motion of the cooperating humanoids has been proposed in [66]. Finally, the book [38] contains several examples of humanoids that are engaged in activities that involve their manipulators, such as pushing objects, moving obstacles out of their way, or carrying objects over a distance. It should be emphasized that, in all the research efforts discussed so far, humanoid walking has been achieved through the ZMP stability criterion, resulting in quasi-static motions. Dynamically walking bipeds, have not enjoyed the popularity of their quasi-static counterparts in such activities.

In almost all cases of dynamic walking bipeds in the literature, the controllers



**Figure 2.2:** Guiding the motion of NAO via physical interaction. Photo adopted from [7].

are derived with the purpose of stabilizing locomotion alone, typically treating external forces – such as those developed during collaborative tasks for example – as disturbances that need to be rejected. To the best of the author’s knowledge, only [6] investigates how manipulation tasks can be integrated with dynamic walking gaits which are generated through the notion of partial hybrid zero dynamics [4]. In this case, however, the control law is specifically designed so that the manipulation controller does *not* interfere with locomotion. Contrary to this approach, In this thesis, we turn our attention to external forces that are applied on a dynamically walking biped *intentionally*, with the purpose of modifying its motion. An instance of this general case has been investigated with the biped Acroban [79] and NAO [7], in which a human literally “walks” the robot by applying a force on its hand. As the human moves, it holds the robot, which adapts to the external force supplied by the human by modifying its walking gait accordingly; see Fig. 2.2. Similar situations arise in applications where humans and robots cooperate to transport objects over a distance that is large enough to require the use of the locomotion system of the robot. In such cooperative tasks, the robot experiences a persistent external force that differs from disturbances

acting momentarily in a fundamental way: the robot should adapt its motion to this force rather than trying to return to its original gait. In the context of dynamically walking bipeds, realizing such human-robot teams requires a deeper understanding of how the underlying locomotion controller reacts to *persistent* external forcing.

## 2.4 Motion Planning

Planning the motion of robotic systems through a workspace populated by obstacles can be decomposed in two hierarchical components. At the high level, a planner is responsible for the generation of an obstacle-free path that respects the geometry of the workspace. At the low level, the locomotion controller should execute the descending plan ensuring stability of the platform. Clearly, if the high-level planning and low-level stability goals are considered in isolation, loss of stability and unfaithful execution of the plan may arise.

In the context of robot motion planning, the method of sequential composition seeks to integrate the planning and control components to generate global feedback control policies [9, 103]. In this approach, the state space of the robot is covered by a large set of Lyapunov funnels – each generated through a local feedback control policy – so that the system can be driven from an initial state to a desired goal region in the state space by transitioning among these local controllers. Sequential composition of fundamental behaviors encoded in motion primitives has been introduced in [19], where a symbolic planner is used to navigate a wheeled robot in a cluttered workspace. The reference [73] extended this method to achieve navigation tasks with highly dynamic mobile robots whose shape dynamics strongly influence their position dynamics in the workspace. In this work, control policies had to be devised to incorporate the natural dynamics of the robot to generate fast and graceful motion primitives. In [61], the same approach was used to achieve motion planning of a flying robot based on a precomputed library of motion primitives that account for uncertainty. Motion planning of switched dynamical systems has also been formulated as finite state automata [24] and timed automata [8], that prescribe the rules for transitioning between systems or motion

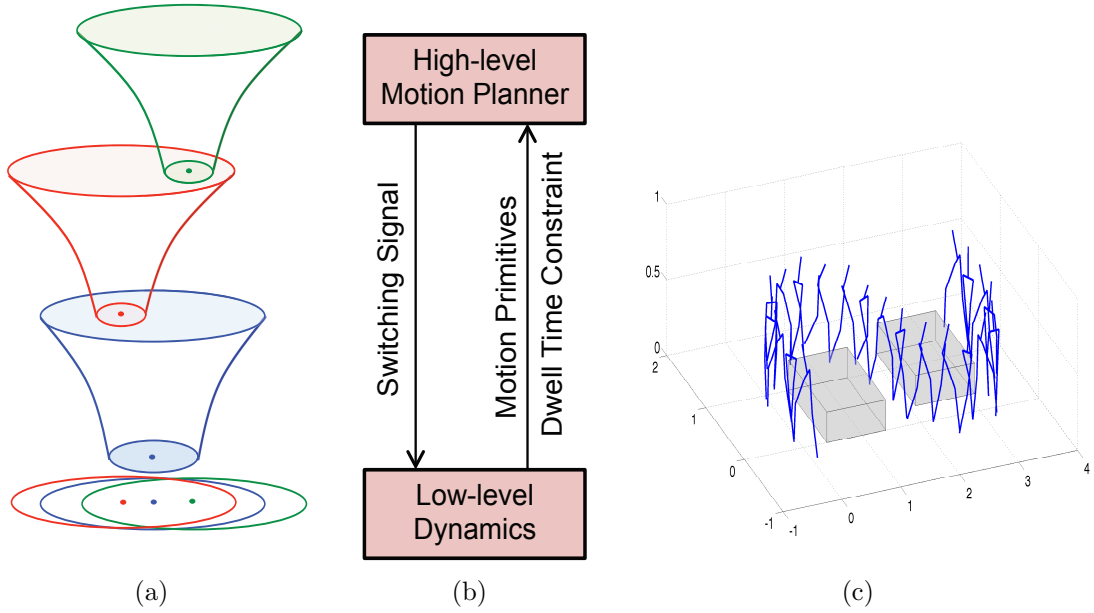


**Figure 2.3:** (a) Sequential composition of funnels. The dwell time condition is computed so that that any two funnels are composable. Each funnel corresponds to a motion primitive. (b) High-level and low-level interconnections. Planner respects the dwell time constraint and produces a switching signal accordingly. (c) execution of the suggested path. Stability of the biped is ensured by the dwell time constraint.

primitives. Our work contributes to the sequential composition approach, by providing analytical conditions of funnel compositions in any arbitrary sequence. To this end, we require each equilibrium point of a funnel to be in the intersection of domains of all funnels; see Fig 2.3(a). We then analytically compute a bound on the frequency of switching among the various precomputed primitive behaviors in order to ensure that the goal set of the funnel lies within the intersection of domains of all funnels. This condition is given *a priori* and can be readily integrated in the motion planning algorithm in a computationally efficient way; see Fig. 2.3(b). Essentially, this condition captures the low-level restrictions in achieving high-level objectives, enabling the robot to stably follow the plan generated by the motion planner; see Fig. 2.3(c).

There has been a great deal of research on motion planning of legged systems,

which, almost exclusively, deals with humanoid robots walking based on the ZMP stability criterion; see [38] and references therein for an overview of the state of the art. The availability of closed form expressions for low-level stability in the context of the ZMP formalism, resulted in efficient motion planning algorithms that achieve high-level objectives in high-dimensional spaces. In this approach, an extra layer is integrated to the high-level planner, the purpose of which is to check the balance of the biped based on the ZMP constraints and to output a statically-stable and collision-free path [53]. The reference [54] constructs a rapidly exploring random tree (RRT) from a discrete set of footstep locations to drive a humanoid to the goal region through a collision-free path. A similar method was proposed in [39] that uses a library of pre-computed motion primitives to safely navigate high-dimensional robotic systems across varied terrains. A two stage global planner is proposed in [20,118] that first generates an obstacle-free path using sampling based algorithms. In [20], the second stage consists of approximating the given path by walking trajectories that are guaranteed to be stable, while in [118], temporal and spatial reshaping has been used in the second stage to change the speed of the biped and to deform the colliding portion of the path. To reduce the search space of the planner, [12] presents a hierarchical motion planner that navigates a humanoid robot in the environment based on a motion primitive framework. Based on formulating motion planning tasks as optimization problems, [55] provides an integrated approach to locomotion planning, estimation and control for humanoid robots, which has been experimentally verified on the humanoid Atlas.

Contrary to ZMP-based walkers, only very few studies exist that account for high-level motion planning objectives for limit-cycle walkers. In the context of footstep planning, [62] uses an energy-based planner to output suitable sequences of limit cycles that enable an underactuated planar biped to traverse over uneven but known terrain. Emphasizing guaranteed performance, [77] proposed a method that combines control barrier functions for the purpose of precise foot placement, with control Lyapunov functions [5] to achieve stability. Closest to our approach is [30], which formulates motion planning of a 3D bipedal robot as a switched system and proves the *existence* of

a bound on the switching frequency in order to ensure that the entire walking sequence is stable. However, this bound is estimated on the basis of computationally intensive simulations. We contribute to this approach, an analytically tractable bound on the switching frequency, which, when respected by the planner, guarantees the stability of the biped as it executes the path. It is important to emphasize that our approach explicitly characterizes a compact set where the solution of the switched system evolves. The size of this set can be used to estimate the drift from the nominal path when the planner composes nominal motion primitives.

The stability of switched systems with a common equilibrium point is well established in the literature; see the book [60] for a thorough overview. However the results of this class of switched systems are not directly applicable in motion planning problems, like the ones this thesis studies, since each motion primitive corresponds to an equilibrium point; i.e., a fixed point of the corresponding Poincaré map. In other words, motion planning with limit-cycle motion primitives corresponds to switching among distinct fixed points of different Poincaré maps. This fact significantly complicates the analysis of the switched system that emerges. The references [113, 114] account for multiple equilibria and present their results in the framework of practical stability using direct methods. Closest to our approach is the study in [2], which uses Lyapunov functions to show that under a condition on dwell time, the solution of a continuous-time switched system with multiple globally exponentially stable equilibria stays within a compact set containing these equilibria. We extend this result to a family of discrete switched systems that are only locally exponentially stable.

## Chapter 3

### BIPED-LEADER COOPERATIVE TASK: PLANAR MODEL

This chapter describes the cooperative task of the biped-leader team in a planar setting, and presents the controller design and stability requirements that enables the biped to adapt its motion in response to leader’s intention in a stable fashion. Section 3.1 describes the walking dynamics of biped as a hybrid system and explains how the force is created through the interaction of the biped and the leader. In section 3.2, a method for integrating locomotion and manipulation controller is presented that results in adaptive locomotion response to the interaction force, and provides compliance in the arm as the biped interacts with environment. The conditions that are required for this adaptive behavior are explained in section 3.3 by analytically deriving a reduced-order system that represents the behavior of the biped. Section 3.4 provides different examples of biped-leader cooperation tasks, in which the biped is required to walk on the flat ground and up and down stairs of known geometry. Finally, Section 3.5 summarizes the contributions of this chapter and relates it to the chapters that follow. The results of this chapter have appeared in [70,105].

### 3.1 Walking under Interaction Forces

#### 3.1.1 Planar Biped Model

The model presented here is an underactuated planar biped that morphologically resembles the bipedal robot RABBIT [13], with the addition of a two-link manipulator that allows it to interact with its environment and external forces that are applied at its end effector, as shown in the schematic of Fig. 3.1. A torso and two identical legs connected to the torso via hip joints constitute the locomotion part of the model. Each leg comprises of two links, the shin and the thigh, connected through the knee joint. In

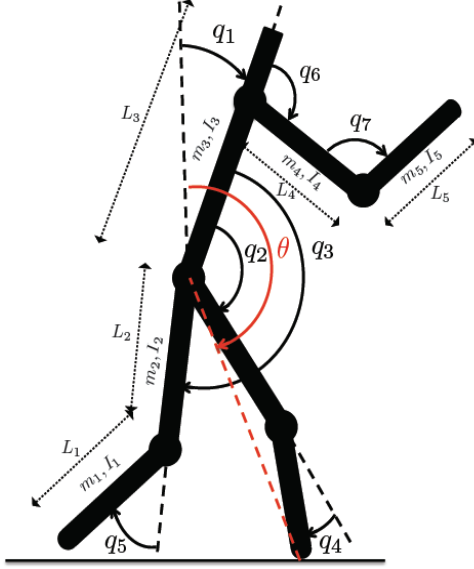


**Figure 3.1:** Planar model of the biped with a choice of generalized coordinates. The values of each link’s length, mass and inertia is given in Table 3.1.

total, the biped has seven degrees of freedom (DOF) characterized by the generalized coordinates  $q := (q_1, \dots, q_7)^T \in \mathcal{Q}$ , where  $\mathcal{Q}$  is a subset of  $[0, 2\pi)^7$  containing physically reasonable configurations of the model. The biped is controlled by four actuators located at the hip and knee joints and two actuators located at the shoulder and elbow joints. The DOF representing the contact between the stance leg end and the ground is not actuated, thus resulting in one degree of underactuation. The physical parameters of the planar model are provided in Table 3.1.

### 3.1.2 Cooperation Model

Suppose that a leading co-worker interacts with the biped by holding the end effector of the biped’s arm with the purpose of intentionally modifying its motion. An instance of this general case arises when a human and a bipedal robot cooperate to transport an object over a distance that requires the locomotion system of the robot to be engaged.

We assume that the intention of the leader can be captured by a trajectory  $p_L(t)$ ,

**Table 3.1:** Mechanical Parameters of the planar Bipedal Model

Model Parameter	Units	Label	Value
Mass	kg	$m_1$	3.2
		$m_2$	6.8
		$m_3$	12
		$m_4$	1.3
		$m_5$	1
Length	kg.m <sup>2</sup>	$I_1$	0.2
		$I_2$	0.47
		$I_3$	1.33
		$I_4$	0.04
		$I_5$	0.03
Length	m	$L_1$	0.4
		$L_2$	0.4
		$L_3$	0.63
		$L_4$	0.25
		$L_5$	0.25

which is selected to be a sufficiently smooth (continuously differentiable) function of time. In our approach, the biped does *not* have any information regarding the intention  $p_L(t)$  of the leader; the leader’s intended trajectory is perceived by the biped as an external force  $F_e(t)$  applied at its end effector. In what follows, the interaction force  $F_e(t)$  represents the only information available to the robot regarding the leader’s intention.

To simulate a cooperative task such as the one described above, the intention of the leader can be translated to the interaction force through an impedance model, as is common in the relevant literature [82, 87]; the purpose of this impedance model is to capture the leader’s response to the robot’s activity<sup>1</sup>. In more detail, we define the error between the location  $p_E(q)$  at which the end effector currently is and the location

---

<sup>1</sup> In experimental implementation, modeling the leader’s impedance is not necessary; the controller only needs to know the force  $F_e(t)$ , which can be provided to the biped via a force sensor.

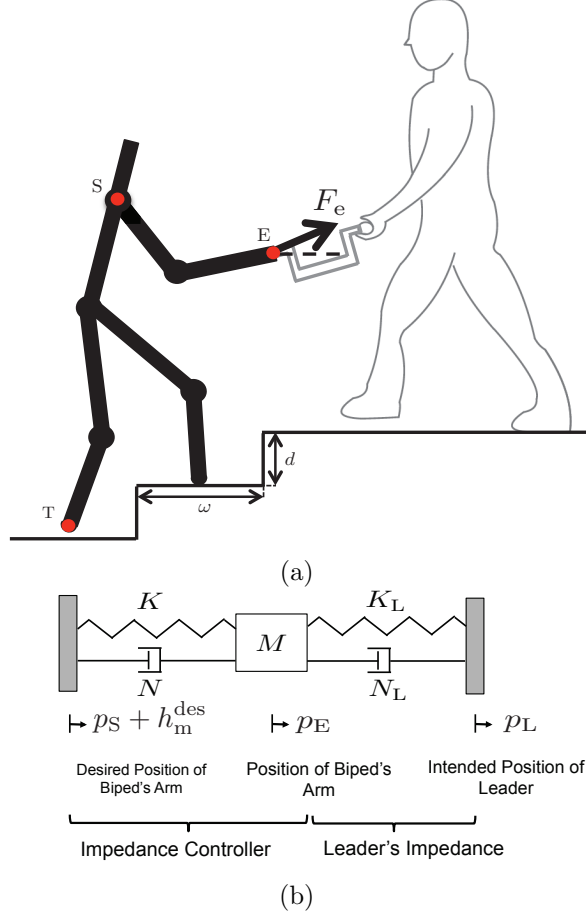


**Figure 3.2:** (a) Planar model of biped-human team in a cooperative transportation of an object. (b) Impedance model of interaction.

$p_L(t)$  at which the leader intends to drive it; i.e.,

$$y_L = h_L(t) := p_L(t) - p_E(q(t)) . \quad (3.1)$$

Then, the interaction force is computed by

$$F_e = K_L y_L + N_L \dot{y}_L , \quad (3.2)$$

where  $K_L$  and  $N_L$  are the corresponding stiffness and damping matrices; see Fig. 3.2(b).

Note that the force  $F_e(t)$  computed by (3.2) is a piecewise continuous function of time.

### 3.1.3 Swing Phase Dynamics

The walking cycle consists of a single support (swing) phase and a double support (impact) phase. The single support dynamic model can be represented by

$$D(q)\ddot{q} + C(q, \dot{q})\dot{q} + G(q) = B_\ell u_\ell + B_m u_m + J_E^T(q)F_e, \quad (3.3)$$

where  $D(q)$  is the mass matrix,  $C(q, \dot{q})\dot{q}$  is the vector of the velocity-dependent forces (centrifugal and Coriolis forces), and  $G(q)$  is gravity vector. The constant matrices  $B_\ell$  and  $B_m$  distribute the inputs  $u_\ell$  and  $u_m$  containing the torques applied at the leg and manipulator joints, respectively, to the configuration variables. Finally,  $J_E(q) := \partial p_E(q)/\partial q$ , where  $p_E$  is the position of the biped's end-effector on which the interaction force  $F_e$  acts; see Fig. 3.2(a).

Defining the state vector  $x := (q^T, \dot{q}^T)^T$  evolving in  $T\mathcal{Q} := \{x := (q^T, \dot{q}^T)^T \mid q \in \mathcal{Q}, \dot{q} \in \mathbb{R}^7\}$ , the swing phase dynamics (3.3) can be transformed to state-space form as

$$\dot{x} := f(x) + g_\ell(x)u_\ell + g_m(x)u_m + g_e(x)F_e, \quad (3.4)$$

where

$$f(x) := \begin{bmatrix} \dot{q} \\ D^{-1}(q)[-C(q, \dot{q})\dot{q} - G(q)] \end{bmatrix}, \quad (3.5)$$

$$g_\ell(x) = \begin{bmatrix} 0 \\ D^{-1}(q)B_\ell \end{bmatrix}, \quad g_m(x) = \begin{bmatrix} 0 \\ D^{-1}(q)B_m \end{bmatrix}, \quad g_e(x) = \begin{bmatrix} 0 \\ D^{-1}(q)J_E^T(q) \end{bmatrix}.$$

The evolution of the single support phase proceeds until the swing toe impacts the ground in front of the stance leg. This incident requires the definition of a switching surface  $\mathcal{S}$  as

$$\mathcal{S} := \{(q^T, \dot{q}^T)^T \in T\mathcal{Q} \mid p_v(q) = d, \dot{p}_v(q, \dot{q}) < 0\}, \quad (3.6)$$

where  $p_v$  is the height of swing leg and  $d$  is the height of the stair; see Fig. 3.2(a).

### 3.1.4 Double Support Phase

When the swing toe impacts the ground, the system enters the double support phase. The model of the double support includes an impact model that captures the physics of the interaction between the toe and the ground, and a state relabeling that switches the role of the swing and stance legs. The derivation of the model for double support phase is taken from [111, Section 3.4.2] and is explained next. The assumptions that we consider for this phase are listed as below:

- the impact is instantaneous;
- the impact is modeled as a complete plastic contact between two rigid bodies with no rebounding and slipping of the swing leg;
- the stance toe lifts off from the ground without any interactions;
- the ground reaction forces during the impact can be represented by impulses;
- the interaction force applied at biped's end effector is not impulsive, and the actuators are not able to produce impulses, hence they can be both ignored during impact;
- the impulsive force does not change the configuration of the biped, however it may result in an instantaneous change in the biped's velocities;

The contact model requires the addition of the Cartesian coordinate of stance toe  $p_C$ , resulting in the extended generalized coordinates  $q_e := (q^T, p_C^T)^T$ . The dynamics of impact can be derived using the method of Lagrange

$$D_e(q_e)\ddot{q}_e + C_e(q_e, \dot{q}_e)\dot{q}_e + G_e(q_e) = B_{\ell,e}u_\ell + B_{m,e}u_m + J_{E,e}^T(q_e)F_e + J_W^T(q_e)\delta F_g \ , \quad (3.7)$$

where  $\delta F_g$  denotes the impulsive ground reaction force at the contact point, and  $J_W(q_e) := \partial p_W(q_e)/\partial q_e$ , where  $p_W$  is the position of swing leg end. Considering the aforementioned assumptions, (3.7) can be integrated over the infinitesimal duration of the impact to obtain

$$D_e(q_e^+)\dot{q}_e^+ - D_e(q_e^-)\dot{q}_e^- = J_W^T(q_e)F_g \ , \quad (3.8)$$

where  $F_g := \int_{t^-}^{t^+} \delta F_g(\tau) d\tau$  results from integration of the impulsive force  $\delta F_g$ , and the symbols  $-$  and  $+$  refer to the moments before and after the impact, respectively. Note that since the stance leg acts as a pivot before impact, we have  $\dot{p}_C^- = 0$  and hence  $\dot{q}_e^- = (q^T, 0)^T$  is known. In addition, the fact that rebounding and slipping do not occur after the impact of swing toe with the ground results in

$$J_W(q_e^-) \dot{q}_e^+ = 0 . \quad (3.9)$$

Putting (3.8) and (3.9) together yields the following algebraic system, the solution of which provides the rates of the extended configuration variables  $\dot{q}_e^+$  and the ground reaction forces  $F_g$  immediately after impact,

$$\begin{bmatrix} D_e(q_e^-) & -J_W^T(q_e^-) \\ J_W(q_e^-) & 0 \end{bmatrix} \begin{bmatrix} \dot{q}_e^+ \\ F_g \end{bmatrix} = \begin{bmatrix} D_e(q_e^-) \dot{q}_e^- \\ 0 \end{bmatrix} . \quad (3.10)$$

Since the inertia matrix  $D_e$  is positive definite and  $J_W$  is full rank, the matrix on the left hand side of (3.10) is invertible, and the unique solution can be given as

$$\begin{bmatrix} \dot{q}_e^+ \\ F_g \end{bmatrix} = \begin{bmatrix} \bar{\Delta}_{\dot{q}_e}(q^-) \\ \Delta_{F_g}(q^-) \end{bmatrix} \dot{q}^- , \quad (3.11)$$

where

$$\Delta_{F_g} = -(J_W D_e^{-1} J_W^T)^{-1} J_W \begin{bmatrix} I \\ 0 \end{bmatrix} \quad (3.12)$$

and

$$\bar{\Delta}_{\dot{q}_e} = D_e^{-1} J_W^T \Delta_{F_g} + \begin{bmatrix} I \\ 0 \end{bmatrix} \quad (3.13)$$

After the impact, the legs swap their roles; the former swing leg becomes the new stance leg and the former stance leg becomes the new swing leg. This can be expressed

as a relabeling matrix  $R_M$  acting on  $q$  as

$$R_M = \begin{bmatrix} 1 & 0 & 0 & 0 & 0 & 0 & 0 \\ 0 & 0 & 1 & 0 & 0 & 0 & 0 \\ 0 & 1 & 0 & 0 & 0 & 0 & 0 \\ 0 & 0 & 0 & 0 & 1 & 0 & 0 \\ 0 & 0 & 0 & 1 & 0 & 0 & 0 \\ 0 & 0 & 0 & 0 & 0 & 1 & 0 \\ 0 & 0 & 0 & 0 & 0 & 0 & 1 \end{bmatrix} . \quad (3.14)$$

The result of the impact and the relabeling matrix can be described by a map  $\Delta : \mathcal{S} \rightarrow TQ$  taking the final state  $x^- \in \mathcal{S}$  of one swing phase to the initial state  $x^+ \in TQ$  of the next, i.e.

$$x^+ = \Delta(x^-) ,$$

and  $\Delta$  takes the form

$$\Delta(x^-) = \begin{bmatrix} R_M q^- \\ \Delta_{\dot{q}}(q^-) \dot{q}^- \end{bmatrix} , \quad (3.15)$$

where  $\Delta_{\dot{q}}(q^-) := \begin{bmatrix} R_M & 0 \end{bmatrix} \bar{\Delta}_{\dot{q}_e}(q^-)$ .

Combining the swing and impact phases, the model can be expressed in the form of a system with impulse effects as

$$\Sigma: \begin{cases} \dot{x} = f(x) + g_\ell(x)u_\ell + g_m(x)u_m + g_e(x)F_e, & x^- \notin \mathcal{S}, \\ x^+ = \Delta(x^-), & x^- \in \mathcal{S}, \end{cases}$$

where the symbols have the meaning explained above.

### 3.2 Coupled Locomotion and Arm Control

This section proposes a controller that manipulates the inputs of the arm and locomotion subsystems to ensure that the biped adapts its dynamic walking pattern

to the external force. It is emphasized that the proposed controller perceives the force applied by the leader on the biped’s arm as an instruction to follow rather than a perturbation to be rejected.

### 3.2.1 Virtual Constraint for the Locomotion Task

Walking gaits are captured by certain outputs being driven to zero. To the continuous dynamics (3.4), we associate the output

$$y_\ell = h_\ell(q) := q_c - h_\ell^{\text{des}} \circ \theta(q) \ , \quad (3.16)$$

where  $q_c := (q_2, q_3, q_4, q_5)^T$  includes the angles of the controllable joints, i.e. relative knee and hip angles. The desired evolution of the controlled joint angles,  $q_c$  in (3.16) is given by  $h_\ell^{\text{des}} \circ \theta(q)$  which is a function of the monotonically increasing forward progression angle

$$\theta(q) = q_1 + q_2 + 0.5q_4 \ , \quad (3.17)$$

that is, the angle between the line connecting the stance leg toe and the hip joint, as shown in Fig. 3.1. For each output,  $h_{\ell,i}^{\text{des}}$ ,  $i = 1, \dots, 4$ , a Beziér polynomial of degree  $n$  is selected as

$$h_{\ell,i}^{\text{des}}(s) = \sum_{k=0}^n a_{i,k}^\ell \frac{n!}{k!(n-k)!} s^k (1-s)^{n-k} \ , \quad (3.18)$$

where  $a_{i,k}^\ell$  are the coefficients of the polynomial corresponding to the  $i^{\text{th}}$  output and  $s(q) = \frac{\theta(q) - \theta^+}{\theta^- - \theta^+}$  with  $\theta^+$  and  $\theta^-$  being the values of  $\theta(q)$  at the beginning and end of a step. It can be noted that  $s \in [0, 1]$  for each step, where  $s = 0$  corresponds to the beginning of the step while  $s = 1$  to the end. We highlight here that the virtual holonomic constraints (3.16) depend exclusively on the configuration variables associated with the locomotion subsystem,  $q_\ell := (q_1, \dots, q_5)^T$ .

### 3.2.2 Impedance Regulation for the Manipulation Task

The manipulation task is encoded in some suitably designed output functions so that the system responds to the interaction force  $F_e$  according to a desired impedance.

In particular, we are interested in providing tunable compliant behavior of the biped’s manipulator. To achieve this, consider the relative position  $p_E$  of the end effector with respect to the shoulder position  $p_S$ , and define the manipulation output as

$$y_m = h_m(q) := (p_E(q) - p_S(q)) - h_m^{\text{des}} \circ \theta(q) , \quad (3.19)$$

where  $h_m^{\text{des}} \circ \theta(q) \in \mathbb{R}^2$  is a vector of Beziér polynomials with coefficients  $a_{i,k}^m$ . These polynomials describe the desired relative position of end effector to shoulder joint, which can be equivalently viewed as the desired configuration of the arm. The impedance relationship, which is enforced by the controller,

$$M_m \ddot{y}_m + \frac{N_m}{\epsilon_m} \dot{y}_m + \frac{K_m}{\epsilon_m^2} y_m = F_e , \quad (3.20)$$

where  $\epsilon_m > 0$  is a parameter, and  $M_m$ ,  $N_m$ , and  $K_m$  are positive definite mass, damping and stiffness matrices, respectively, determining the compliance of the arm; see Fig. 3.2(b). When  $F_e = 0$ , the controller drives the manipulator outputs  $y_m$  to zero at a rate that depends on the gains participating in (3.20), so that the arm follows its nominal motion captured by  $h_m^{\text{des}}$ . In the presence of the external force, i.e., when  $F_e \neq 0$ , the system responds according to (3.20) in a way that, for given  $M_m$ ,  $N_m$ ,  $K_m$ , depends on the parameter  $\epsilon_m$  as follows. When  $\epsilon \neq 0$ , the external force  $F_e$  causes the manipulator to respond by deviating from its nominal motion as determined by (3.20). When  $\epsilon_m \rightarrow 0$  the arm becomes rigid and the interaction force does not affect the evolution of its configuration; in this case (3.20) becomes a position controller that drives  $y_m$  to zero [64]. The implications of the dependence of the interaction between the leader’s force and the biped on the parameter  $\epsilon_m$  will be further explored in Section 3.4.2.

### 3.2.3 Controller Design

The objective of the controller is to achieve both manipulation and locomotion tasks using the available actuators. More specifically, the controller needs to drive the

locomotion outputs (3.16) to zero, and to establish the desired mechanical impedance relationship between the interaction force and manipulation output (3.20). This can be performed by feedback-linearizing the input/output dynamics as follows

$$\begin{bmatrix} \ddot{y}_\ell \\ \ddot{y}_m \end{bmatrix} = L_f^2 h(x) + L_g L_f h(x) \begin{bmatrix} u_\ell \\ u_m \end{bmatrix} + L_{g_e} L_f h(x) F_e ,$$

where  $h(x) := (h_\ell^T(x), h_m^T(x))^T$ ,  $g(x) := (g_\ell(x), g_m(x))$ , and  $L_f^2 h$ ,  $L_g L_f h$  and  $L_{g_e} L_f h$  denote the Lie derivatives of  $h$  along the corresponding vector fields; see [111, Section B.1.5] for relevant definitions. Under the condition that the decoupling matrix  $L_g L_f h$  is invertible and assuming that measurements of the external force are available through a suitable sensor, the control law

$$\begin{bmatrix} u_\ell \\ u_m \end{bmatrix} = L_g L_f h(x)^{-1} \left( \begin{bmatrix} v_\ell(y_\ell, \dot{y}_\ell) \\ v_m(y_m, \dot{y}_m, F_e) \end{bmatrix} - L_f^2 h(x) - L_{g_e} L_f h(x) F_e \right) \quad (3.21)$$

leads to the linear input/output relation

$$\begin{bmatrix} \ddot{y}_\ell \\ \ddot{y}_m \end{bmatrix} = \begin{bmatrix} v_\ell(y_\ell, \dot{y}_\ell) \\ v_m(y_m, \dot{y}_m, F_e) \end{bmatrix} \quad (3.22)$$

where  $v_\ell$  and  $v_m$  are auxiliary control variables.

**Remark 1.** *It is straightforward to show that the decoupling matrix can be written as*

$$L_g L_f h(x) = \begin{bmatrix} J_\ell(q) D^{-1}(q) B_\ell & J_\ell(q) D^{-1}(q) B_m \\ J_m(q) D^{-1}(q) B_\ell & J_m(q) D^{-1}(q) B_m \end{bmatrix}$$

where  $J_\ell(q) := \partial h_\ell(q) / \partial q$  and  $J_m(q) := \partial h_m(q) / \partial q$  are the Jacobians of the locomotion and manipulation outputs, respectively. Using this expression one can deduce that at the kinematic singularities of the locomotion or manipulation, where  $J_\ell$  or  $J_m$  lose rank, the decoupling matrix is not invertible. In addition, there exists other dynamic

singularities associated with the diagonal submatrices and the Schur complement of them; see [57, pp.5-6] for details. One has to be careful so that the desired motions imposed by the corresponding Beziér polynomials as discussed above does not force the system to evolve close to these singularities.

For the locomotion subsystem, selecting

$$v_\ell(y_\ell, \dot{y}_\ell) = -\frac{1}{\epsilon_\ell^2} K_\ell y_\ell - \frac{1}{\epsilon_\ell} N_\ell \dot{y}_\ell \quad (3.23)$$

ensures that the output  $y_\ell$  converges to zero at a rate which depends on the positive definite matrices  $K_\ell$ ,  $N_\ell$  and the positive parameter  $\epsilon_\ell$ . Note that the output  $y_\ell$  can be made to converge to zero in finite time by choosing the controller  $v(y_\ell, \dot{y}_\ell)$  as in [111, Section 5.5.1].

For the manipulation subsystem, choosing auxiliary input as in

$$v_m(y_m, \dot{y}_m, F_e) = M_m^{-1} \left( F_e - \frac{N_m}{\epsilon_m} \dot{y}_m - \frac{K_m}{\epsilon_m^2} y_m \right) \quad (3.24)$$

results in the desired dynamical relationship of (3.20).

### 3.2.4 Effect of Interaction Force on Locomotion

Generally, the vast majority of the locomotion controllers that have been developed thus far have the primary purpose of stabilizing the walking gait, nullifying the effect of exogenous inputs that are interpreted as disturbances to the system. However, in a cooperative object transportation task such as the one which is of interest to us, the controller should accommodate the external inputs interpreting them as a guiding signal; in other words the biped needs to adapt its motion to the externally applied forces rather than trying to reject them. Proceeding along this lines, this section examines the response of biped in closed loop with the controller developed above to the interaction forces.

We first note that, under the influence of the controller of Section 3.2.3, the biped cannot modify its stride length in response to the interaction force  $F_e$ . Indeed, since the controller  $v_\ell(y_\ell, \dot{y}_\ell)$  in (3.23) can be selected to drive the locomotion output to zero before the robot completes the step, the solution of  $(h_\ell(q_\ell^-), p_v(q_\ell^-)) = (0, d)$ , uniquely determines the configuration of the legs  $q_\ell^-$  prior to touchdown, regardless of the configuration of the arm. In addition, since the impact map does not change the configuration variables and is not affected by the interaction force<sup>2</sup>, the leg configuration after touchdown  $q_\ell^+$  remains constant over different steps. Due to the fact that  $\theta$  is solely a function of  $q_\ell$  as (3.17) show, the values  $\theta^+$  and  $\theta^-$  of the angle  $\theta$  at the beginning and the end of the step do not change. Consequently, the stride length of the biped remains constant over different steps, as long as the steps can be completed. Although the interaction force does not affect the stride length of the biped, it still modifies the gait followed by the biped by compelling it to adapt by changing its stride frequency; see Section 3.4.1 for more details. The way that the controller coordinates the underactuated DOF of the system to respond to interaction force holds the key to this adaptive behavior. Note that, while humans have a preferred speed-stride length relationship [32], keeping a constant stride length can be advantageous when traversing over terrains with constrained periodic geometry, such as ascending or descending a staircase for example. In this environment, the biped should preserve a stride length that is compatible with the stair tread; see Section 3.4.3.

### 3.2.5 Closed Loop Hybrid System

Under the influence of the control law (3.21), the system (3.4) takes the closed-loop form

$$\Sigma_{\text{cl}} : \begin{cases} \dot{x} = f_{\text{cl}}^\epsilon(x) + g_{\text{e,cl}}^\epsilon(x)F_e, & x \notin \mathcal{S} \\ x^+ = \Delta(x^-), & x^- \in \mathcal{S}. \end{cases} \quad (3.25)$$

---

<sup>2</sup> The model of impact assumes that impulsive forces govern its dynamics. Interaction force is assumed to be non-impulsive by its nature.

where  $\epsilon = (\epsilon_m, \epsilon_\ell)$ .

The following lemma introduces the coordinate transformation that separates the manipulation and locomotion output dynamics from the remaining dynamics of the system. The lemma will be used in the sequel to bring the system in the standard singular perturbation form [48].

**Lemma 1.** *Suppose that the output function  $h(q) := \begin{bmatrix} h_\ell(q)^\top & h_m(q)^\top \end{bmatrix}^\top$  is smooth and*

- *There exist an open set  $\tilde{\mathcal{Q}} \subset \mathcal{Q}$  such that  $h(q)$  has a vector relative degree (2...2) at every point  $q \in \tilde{\mathcal{Q}}$ , (this implies that the decoupling matrix is invertible);*
- *There exists smooth functions  $\theta(q)$  and  $\gamma(x)$  such that the Jacobian of the map  $\Upsilon : T\tilde{\mathcal{Q}} \rightarrow \mathbb{R}^{14}$  defined by*

$$\Upsilon(x) := \begin{bmatrix} \eta_\ell^\top & \eta_m^\top & \xi^\top \end{bmatrix}^\top \quad (3.26)$$

where

$$\begin{aligned} \eta_\ell &:= \begin{bmatrix} \frac{1}{\epsilon_\ell} h_\ell(q)^\top & L_f h_\ell(x)^\top \end{bmatrix}^\top \\ \eta_m &:= \begin{bmatrix} \frac{1}{\epsilon_m} h_m(q)^\top & L_f h_m(x)^\top \end{bmatrix}^\top \\ \xi &:= \begin{bmatrix} \theta(q) & \gamma(x) \end{bmatrix}^\top \end{aligned} \quad (3.27)$$

is nonsingular at every point  $x \in T\tilde{\mathcal{Q}}$ .

Then the map  $\Upsilon$  qualifies as a valid local coordinate transformation and

$$L_{g_\ell} \gamma(x) = 0, \quad L_{g_m} \gamma(x) = 0 \quad . \quad (3.28)$$

In addition, applying the constructive proof of Frobenius theorem [45] one can find that

$$\gamma(x) = D_1(q)\dot{q}, \quad (3.29)$$

where  $D_1(q)$  denotes the first row of the mass matrix  $D$  in (3.3).

*Proof.* The first part of the statement, namely the validity of the coordinate transformation is a direct consequence of [45, Proposition 5.1.2]. For the second part, with the choice of  $\gamma(x) = D_1(q)\dot{q}$ , one can compute

$$L_{g_m}\gamma = \begin{bmatrix} \frac{\partial\gamma}{\partial q} & \frac{\partial\gamma}{\partial\dot{q}} \end{bmatrix} g_m$$

Substituting  $g_m$  from (3.5) in the last equation we get

$$L_{g_m}\gamma = D_1 D^{-1} B_m = B_{m_1} = 0 \quad (3.30)$$

where  $B_{m_1}$  is the first row of  $B_m$  which is zero due to the fact that the absolute angle  $q_1$  is not actuated. The same computation results in  $L_{g_e}\gamma = 0$ .  $\square$

Defining  $\eta := \begin{bmatrix} \eta_\ell^T & \eta_m^T \end{bmatrix}^T$ , Lemma 1 implies that the closed loop system (3.25) can be written in the form

$$\Sigma_{c2} : \begin{cases} \epsilon_\ell \dot{\eta}_\ell & = A_\ell \eta_\ell & \text{if } (\eta, \xi) \notin \mathcal{S} \\ \epsilon_m \dot{\eta}_m & = A_m \eta_m + G_m F_e \\ \dot{\xi} & = f_\xi(\eta, \xi) + g_\xi(\eta, \xi) F_e \\ \eta_\ell^+ & = \Delta_{\eta_\ell}(\eta^-, \xi^-) & \text{if } (\eta^-, \xi^-) \in \mathcal{S} \\ \eta_m^+ & = \Delta_{\eta_m}(\eta^-, \xi^-) \\ \xi^+ & = \Delta_\xi(\eta^-, \xi^-) \end{cases} \quad (3.31)$$

where  $A_\ell = \begin{bmatrix} 0 & I \\ -K_\ell & -N_\ell \end{bmatrix}$  and  $A_m = \begin{bmatrix} 0 & I \\ -M_m^{-1}K_m & -M_m^{-1}N_m \end{bmatrix}$  are Hurwitz matrices, and  $G_m = \begin{bmatrix} 0 \\ \epsilon_m M_m^{-1} \end{bmatrix}$ .

It is important to mention that the arm's motion according to the impedance (3.20) violates hybrid invariance [111, Theorem 5.2] of the zero dynamics surface

$$\mathcal{Z}' := \{x \in TQ \mid h_\ell(q) = 0, L_{f_{cl}^\epsilon} h_\ell(x) = 0\} ;$$

that is,  $x^- \in \mathcal{Z}' \cap \mathcal{S}$  does not imply that  $x^+ \in \mathcal{Z}'$ . Although there exist methods to recover hybrid invariance as proposed in [69] and [15], their application in our compliant manipulator will yield a 3 DOF HZD, which is still complicated to analyze. However, in the stiff manipulator limit as  $\epsilon_m \rightarrow 0$  in (3.20), the closed-loop system (3.25) can be reduced to a single DOF analytically integrable HZD, which is driven by the external force  $F_e$ , allowing for explicit conclusions to be drawn.

### 3.3 Reduced-order Stiff Manipulator System

The goal of this section is to investigate the effect of interaction force on the locomotion of the biped and to deduce conditions for which the reduced-order biped can complete a step. The reduced-order system corresponds to the case of  $\epsilon_m \rightarrow 0$  in (3.20) in which the control action essentially corresponds to imposing an additional set of virtual holonomic constraints; namely, the manipulator's outputs (3.19) [64]. Physically, this controller results in a "stiff" manipulator, that transmits the interaction force  $F_e$  to the locomotion system directly as if the arm is locked in its equilibrium configuration. In this case, the augmented zero dynamics surface

$$\mathcal{Z} := \{x \in TQ \mid h_\ell(q) = 0, L_{f_{cl}^\epsilon} h_\ell(x) = 0, h_m(q) = 0, L_{f_{cl}^\epsilon} h_m(x) = 0\}$$

can be rendered invariant under the flow of the continuous dynamics and under the map  $\Delta$ , so that the one DOF HZD

$$\Sigma_z : \begin{cases} \dot{z} = f_z(z) + g_{e_z}(z)F_e, & z \notin \mathcal{S} \cap \mathcal{Z} \\ z^+ = \Delta_z(z^-), & z^- \in \mathcal{S} \cap \mathcal{Z} \end{cases}, \quad (3.32)$$

is well defined. In (3.32),  $f_z := f_{\text{cl}}|_{\mathcal{Z}}$  and  $g_{e_z} := g_{\text{ecl}}|_{\mathcal{Z}}$  are the restrictions on  $\mathcal{Z}$  of the closed loop dynamics (3.25), and  $\Delta_z := \Delta|_{\mathcal{S} \cap \mathcal{Z}}$ .

### 3.3.1 Effect of External Force on a Step

Our objective in this section is to examine the influence of the external force over a step and to determine conditions under which a step can be taken. We begin with defining the restricted step map, which takes the state of (3.32) at the beginning of a step to the state at the beginning of the next, provided that the step is completed. To do this we first define the (restricted on  $\mathcal{Z}$ ) time-to-impact function as follows. Suppose that the  $k$ -th step starts at  $t_{k-1} \in [t_0, t_f]$ . Let  $\varphi_{z,k}^{F_e}(t, z_0)$  be the solution of the continuous-time part of (3.32) with initial condition  $\varphi_{z,k}^{F_e}(t_{k-1}, z_0) = z_0$ . The (restricted on  $\mathcal{Z}$ ) time-to-impact function  $T_{I,k}^{F_e} : \mathcal{Z} \rightarrow \mathbb{R} \cup \{\infty\}$ , can then be defined as

$$T_{I,k}^{F_e}(z_0) = \begin{cases} \inf \{t \in [0, +\infty) \mid \varphi_{z,k}^{F_e}(t, z_0) \in \mathcal{S} \cap \mathcal{Z}\}, \\ \quad \text{if } \exists t \text{ such that } \varphi_{z,k}^{F_e}(t, z_0) \in \mathcal{S} \cap \mathcal{Z} \\ \infty, \text{ otherwise.} \end{cases}$$

We now proceed with the definition of the step map. Let  $z^- \in \mathcal{S} \cap \mathcal{Z}$  be a pre-impact initial condition so that the post-impact state  $z^+ = \Delta_z(z^-)$  is such that  $T_{I,k}^{F_e}(z^+) < \infty$  for the values of the external force  $F_e$  over the interval  $[t_{k-1}, t_k]$ , where  $t_k := t_{k-1} + T_{I,k}^{F_e}(z^+)$ . This implies that the model completes the  $k$ -th step. The corresponding step map  $\rho_k : \mathcal{S} \cap \mathcal{Z} \rightarrow \mathcal{S} \cap \mathcal{Z}$  is then defined by

$$\rho_k(z^-) := \varphi_{z,k}^{F_e}(T_{I,k}^{F_e}(\Delta_z(z^-)), \Delta_z(z^-)) . \quad (3.33)$$

The rest of this section is devoted to the derivation of an explicit expression for the step map  $\rho_k$ , which will greatly facilitate the analysis of the effect of the external force  $F_e$  on the stepping pattern of the biped.

In what follows, we restrict our attention to steps for which the angle  $\theta$  used to parameterize the output function (3.16) is a strictly monotonically increasing function

of time; see Fig. 3.1. Intuitively, this assumption allows us to use  $\theta$  to replace time in parameterizing the motion of the model, so that the output (3.16) is a function of the configuration variables only.

Using now the same notation as in the definition of the step map (3.33), the evolution of the angle  $\theta$  with respect to time over the  $k$ -th step is represented as a function  $\vartheta_k : [t_{k-1}, t_k] \rightarrow \mathbb{R}$  defined by the rule  $\vartheta_k(t) = \Pi \circ \varphi_{z,k}^{F_e}(t, z^+)$ , where the mapping  $\Pi$  constructs  $\theta$  from the flow  $\varphi_{z,k}^{F_e}(t, z^+)$ . Based on the discussion above, the function  $\vartheta_k$  is monotonically increasing over the  $k$ -th step, and, as such, it achieves its minimum and maximum values at the end points  $t_{k-1}$  and  $t_k$ . Finally, note that the function  $\vartheta_k$  is a bijection onto its image; that is,  $\vartheta_k^{-1} : [\theta^+, \theta^-] \rightarrow [t_{k-1}, t_k]$  is well defined. We will use this fact to express the portion of the external force  $F_e$  that is acting on the biped over the duration  $[t_{k-1}, t_k]$  of the  $k$ -th step as a function of the angle  $\theta$ ; see Fig. 3.3. In more detail, we define  $F_k : [\theta^+, \theta^-] \rightarrow \mathbb{R}^2$  by

$$F_k(\theta) := F_e \circ \vartheta_k^{-1}(\theta) , \quad (3.34)$$

which, in general, differs among steps, as shown in Fig. 3.3.

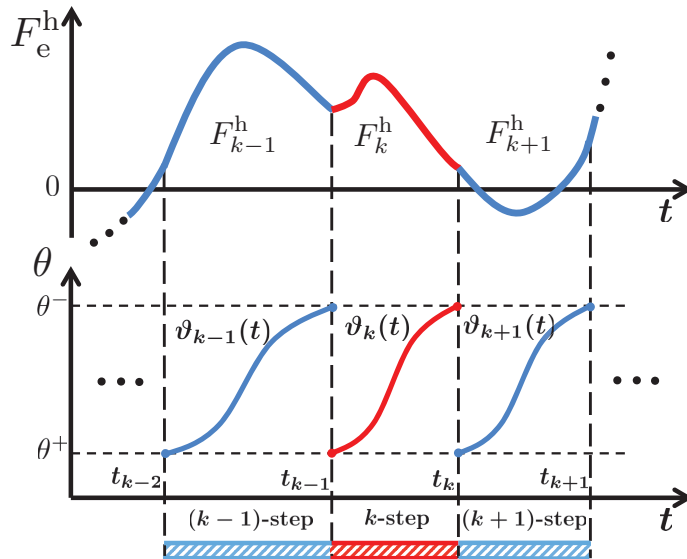


**Figure 3.3:** An example of a force profile. The force over the duration of each step can be expressed as a function of the monotonic angle  $\theta$ .

When the impedance controller renders the manipulator infinitely stiff, i.e.  $\epsilon_m \rightarrow 0$ , and a high-gain control is imposed on the locomotion output, i.e.  $\epsilon_\ell \rightarrow 0$ , then the closed-loop system rapidly converges to its desired configuration, corresponding to the manipulation and locomotion outputs being zero, and it does so irrespectively of the interaction force. On the other hand, the underactuated locomotion part corresponding to the evolution of the  $\theta$  is affected by the externally applied force. To study this better we use singular perturbation. This limiting case can vastly simplify analysis by allowing analytical integration of the corresponding zero dynamics; then, singular perturbation theory can be used to draw conclusions regarding the behavior of the overall system.

Setting  $\epsilon := [\epsilon_\ell \quad \epsilon_m] = 0$  results in  $\eta := [\eta_\ell^T \quad \eta_m^T]^T = 0$  as the unique solution to the first two equations of (3.31) and brings the continuous part of (3.31) in the standard singular perturbation model [48, Section 11.1]. The following Lemma provides the explicit form of the third and sixth equations of (3.31) when  $\eta = 0$ .

**Lemma 2.** *The reduced model of the continuous part of (3.31) when  $\eta = 0$ , takes the form*

$$\dot{\xi} = f_\xi(0, \xi) + g_{e_\xi}(0, \xi)F_e \quad (3.35)$$

where

$$f_\xi(0, \xi) = \begin{bmatrix} \kappa_1(\xi_1)\xi_2 \\ \kappa_2(\xi_1) \end{bmatrix}, \quad g_{e_\xi}(0, \xi) = \begin{bmatrix} 0 \\ \kappa_3(\xi_1) \end{bmatrix}$$

and

$$\begin{aligned} \kappa_1(\xi_1) &= \frac{\partial \theta}{\partial q} \left[ \begin{array}{c} \frac{\partial h_m}{\partial q} \\ \frac{\partial h_\ell}{\partial q} \\ D_1 \end{array} \right]^{-1} \left[ \begin{array}{c} 0 \\ 0 \\ 1 \end{array} \right] \Big|_{\mathcal{Z}}, \\ \kappa_2(\xi_1) &= -G_1 \Big|_{\mathcal{Z}}, \end{aligned}$$

$$\kappa_3(\xi_1) = J_1^T|_{\mathcal{Z}} , \quad (3.36)$$

where  $G_1$  and  $J_1^T$  are the first rows of  $G$  and  $J^T$  respectively, and  $\xi_1$  and  $\xi_2$  are the first and second components of  $\xi$  defined in (3.27). The slow dynamics (3.35) corresponds to the continuous-time part of (3.32).

In addition, the discrete part of (3.32)  $\Delta_z|_{\epsilon=0} : \mathbb{R}^2 \rightarrow \mathbb{R}^2$  in the coordinates (3.27) can be computed as

$$\Delta_z|_{\epsilon=0}(z^-) = [\theta^+ \quad \delta_z \xi_2^-]^T \quad (3.37)$$

where  $\delta_z$  is a constant computed as in [112, Section IV-A].

*Proof.* When  $\eta = 0$  then  $\frac{\partial h_m}{\partial q} \dot{q} = 0$  and  $\frac{\partial h_\ell}{\partial q} \dot{q} = 0$ . Combining these two equations with  $\xi_2 = D_1 \dot{q}$  one gets

$$\begin{bmatrix} \frac{\partial h_m}{\partial q} \\ \frac{\partial h_\ell}{\partial q} \\ D_1 \end{bmatrix}_Z \dot{q} = \begin{bmatrix} 0 \\ 0 \\ \xi_2 \end{bmatrix} \quad (3.38)$$

Noting that  $\dot{\xi}_1 = \frac{\partial \theta}{\partial q} \dot{q}$  one can easily derive the form of  $\kappa_1$  in (3.36). To find the form of  $\kappa_2$  and  $\kappa_3$ , noting that  $L_{g_m} \gamma = 0$  and  $L_{g_\ell} \gamma = 0$  from Lemma 1, direct computation of  $\dot{\xi}_2$  gives

$$\dot{\xi}_2 = L_f \gamma + L_{g_e} \gamma F_e = \left[ \dot{q}^T \frac{\partial D_1^T}{\partial q} \quad D_1 \right] \left( \begin{bmatrix} \dot{q} \\ -D^{-1}[C\dot{q} + G(q)] \end{bmatrix} + \begin{bmatrix} 0 \\ D^{-1}(J^T F_e) \end{bmatrix} \right) \quad (3.39)$$

Then, use

$$C_1(q, \dot{q}) = \dot{q}^T \frac{\partial D_1^T}{\partial q} - \frac{1}{2} \dot{q}^T \frac{\partial D}{\partial q_1}$$

and  $\partial D(q)/\partial q_1 = 0$  as in the proof of [112, Theorem 1] in (3.39) to obtain

$$\dot{\xi}_2 = -G_1 + J_1^T F_e ,$$

Restricting (3.39) on  $\mathcal{Z}$  results in  $\kappa_2$  and  $\kappa_3$  as in (3.36). The derivation of the discrete map of (3.37) is a direct consequence of the arguments in [112, Section IV-A].  $\square$

In the coordinates of Lemma 1, the continuous part of (3.32) can be integrated analytically as follows. Let  $\zeta := \frac{1}{2}(\xi_2^2)$  be an auxiliary variable so that

$$\frac{d\zeta}{d\xi_1} = \frac{\kappa_2(\xi_1) + \kappa_3(\xi_1)F_e(\vartheta_k^{-1}(\xi_1))}{\kappa_1(\xi_1)} . \quad (3.40)$$

Then, integrating (3.40) over the  $k$ -th step gives

$$\zeta^-[k+1] = \zeta^+[k] - v(\theta^-) + w_k(\theta^-) , \quad (3.41)$$

in which  $\zeta^+$  and  $\zeta^-$  are the post- and pre-impact values of  $\zeta$  for the  $k$ -th step, and  $v$  and  $w_k$  are given by

$$v(\xi_1) := - \int_{\theta^+}^{\xi_1} \frac{\kappa_2(\xi)}{\kappa_1(\xi)} d\xi \quad (3.42)$$

$$w_k(\xi_1) := \int_{\theta^+}^{\xi_1} \frac{1}{\kappa_1(\xi)} (\kappa_3(\xi)F_k(\xi)) d\xi , \quad (3.43)$$

where  $F_k$  corresponds to the part of the force  $F_e$  that is acting on the biped over the  $k$ -th step expressed as in (3.34). Notice that the index  $k$  appears explicitly as a subscript of  $w_k$  to emphasize that these functions may differ among steps due to the possibly varying force; see Fig. 3.3. On the other hand, the function  $v$  is independent of the force and it does not change among different steps.

With the help of (3.37), the post-impact value  $\zeta^+[k]$  in (3.41) can be computed as  $\zeta^+[k] = \delta_z^2 \zeta^-[k]$  so that

$$\zeta^-[k+1] = \rho(\zeta^-[k], w_k(\theta^-)) , \quad (3.44)$$

where

$$\rho(\zeta^-, w_k(\theta^-)) := \delta_z^2 \zeta^- - v(\theta^-) + w_k(\theta^-) \quad (3.45)$$

represents the discrete evolution of the hybrid system given by (3.35) and (3.37) as it passes  $\mathcal{S}$ . The discrete dynamics  $\rho$  is a function of the pre-impact value  $\zeta^-$  of  $\zeta$  and the input  $w_k$ , which intuitively can be regarded as the “work” done by the force along a solution restricted to  $\mathcal{Z}$ .

Furthermore, the domain of definition of  $\rho$  associated with the  $k$ -th step can be characterized explicitly as

$$\mathcal{D}_k = \{\zeta^- > 0 \mid \delta_z^2 \zeta^- - M_k \geq 0\} \quad (3.46)$$

where

$$M_k := \max_{\theta^+ \leq \xi_1 \leq \theta^-} [v(\xi_1) - w_k(\xi_1)] \ .$$

This implies that if  $\zeta^- \in \mathcal{D}_k$  the biped takes a well-defined step.

Owing to the availability of an explicit form for the step map (3.45), the underlying mechanism behind the speed adaptation of the biped in the presence of an externally applied force can be revealed. It is observed that  $w_k(\theta^-)$  is the only term that changes with  $k$  in  $\rho$ . The step-to-step partial maps belong to a family of affine functions having a similar slope  $\delta_z^2$ . The fixed point of the step map  $\rho$  associated with  $w_k$  can be computed by

$$\zeta_k^* = -\frac{v(\theta^-) - w_k(\theta^-)}{1 - \delta_z^2} \ , \quad (3.47)$$

and is exponentially stable if, and only if,  $\delta_z^2 < 1$ . Due to the exponential stability of  $\zeta_k^*$ , the initial condition  $\zeta^-[k]$  of the step will be attracted by  $\zeta_k^*$ . Hence, if  $\zeta^-[k] < \zeta_k^*$ , the biped will take a faster step to catch up with  $\zeta_k^*$ , while if  $\zeta^-[k] > \zeta_k^*$  the biped will take a slower step to approach  $\zeta_k^*$ . It should be noted that the fixed point  $\zeta_k^*$  may *never* be realized despite its exponentially stable nature because the map  $\rho$  generally depends on the varying input  $w_k$ . Generally, the step map may not repeat itself as is the case for periodic walking gaits occurring in the absence of interaction forces.

### 3.3.2 Effect of External force on Gait Constraints

While the domain of definition of step map (3.46) determines if the biped can complete a well-defined step, there is a possibility that some of the gait constraints are violated as a result of the applied external force. This section discusses conditions on the external force such that the gait constraints – e.g. actuator limitations and toe-ground interactions – are satisfied. It turns out that these constraints provide an upper bound on the domain of definition of the step map  $\rho_k$ . Let  $u := (u_\ell^T, u_m^T)^T$ , then careful investigation of the terms in (3.21) show that the expression of  $u$  is quadratic in  $\dot{q}$  and linear in  $F_e$  [112, Section IV-B]. When restricted to  $\mathcal{Z}$ , it becomes affine in  $\zeta$ . Considering this with the solution of (3.40), yields an expression for actuator torque over an step of the biped as

$$u(\xi_1, \zeta^-, F_e) = \Lambda_2(\xi_1)F_e + \Lambda_1(\xi_1)\zeta^- + \Lambda_0(\xi_1) \quad (3.48)$$

Since the portion of external force acting during the  $k$ -th step is written as a function of  $\theta$ , the above equation becomes

$$u_k(\xi_1, \zeta^-) = \Lambda_1(\xi_1)\zeta^- + \bar{\Lambda}_{0,k}(\xi_1) \quad (3.49)$$

Thus, the upper bound on  $\zeta^-$  such that the actuator torques do not exceed a maximum value  $u^{\max} \in \mathbb{R}$  is given by

$$\zeta_k^{\max, u} := \zeta^- \quad \text{s.t.} \quad \sup_{\zeta^-} \left( \max_{\theta^+ \leq \xi_1 \leq \theta^-} u_k(\xi_1, \zeta^-) \right) \leq u^{\max} \quad (3.50)$$

which changes among the steps since the force is different for each step. In a similar way, the corresponding upper bound of  $\zeta^-$  that respects the sign of the normal ground reaction force and the friction cone requirement is given by

$$\zeta_k^{\max, F_N} := \zeta^- \quad \text{s.t.} \quad \sup_{\zeta^-} \left( \min_{\theta^+ \leq \xi_1 \leq \theta^-} F_k^N(\xi_1, \zeta^-) \right) \geq 0 \quad (3.51)$$

$$\zeta_k^{\max, \mu} := \zeta^- \quad \text{s.t.} \quad \sup_{\zeta^- \geq \zeta_k^{\max, F_N}} \left( \max_{\theta^+ \leq \xi_1 \leq \theta^-} \left| \frac{F_k^T(\xi_1, \zeta^-)}{F_k^N(\xi_1, \zeta^-)} \right| \right) \leq \mu \quad (3.52)$$

where  $F_k^N$  and  $F_k^T$  are the normal and tangential component of ground reaction force, and  $\mu$  is the static Coulomb friction coefficient. To integrate both constraints together, define

$$\zeta_k^{\max} := \min\{\zeta_k^{\max, u}, \zeta_k^{\max, \mu}\} \quad (3.53)$$

Therefore, the domain of definition of the step map becomes

$$\mathcal{D}_k = \{\zeta^- > 0 \mid \delta_z^2 \zeta^- - M_k \geq 0, \zeta^- \leq \zeta_k^{\max}\} \quad (3.54)$$

### 3.3.3 No Fall Conditions under External Force

When excited by a persistent exogenous force, the biped adapts its motion according to the external force as discussed in Section 3.3.1. It is natural to ask under what conditions the biped will keep taking steps. The answer relies on (3.54), which implies that as long as the state of the biped at the beginning of the step belongs to the domain of definition, the biped will take a well-defined step. One can find a conservative *sufficient* condition on the magnitude of the force under which this condition is achieved. We assume that there exists an exponentially stable limit cycle in the absence of external forcing, corresponding to the fixed point

$$\zeta_0^* = -\frac{v(\theta^-)}{1 - \delta_z^2},$$

where  $0 < \delta_z < 1$ , and the external force is bounded and its bound is denoted by  $F_{\text{sup}} = \sup_{t \in \mathbb{R}_+} \|F_e(t)\| < \infty$ . Then, the robot continues to take steps if

$$\zeta_0^* \geq -\frac{1}{1 - \delta_z^2} w_F(\theta^-) + \frac{1}{\delta_z^2} M \quad (3.55)$$

$$\zeta_0^* \leq \frac{1}{1 - \delta_z^2} w_F(\theta^-) + \zeta^{\max} \quad (3.56)$$

where

$$w_F(\xi_1) := -F_{\text{sup}} \int_{\theta^+}^{\xi_1} \frac{\|\kappa_3(\xi)\|}{|\kappa_1(\xi)|} d\xi ,$$

$$M := \max_{\theta^+ \leq \xi_1 \leq \theta^-} [v(\xi_1) - w_F(\xi_1)] ,$$

and  $\zeta^{\max}$  is the bound respecting gait constraints as in (3.53) and  $v(\xi_1)$  is defined in (3.42). Note that these conditions are conservative since they are based on the supremum of the force. Nevertheless, such conditions couple the underlying unforced gait  $\zeta_0^*$  with the external force through the constants  $M$  and  $\zeta^{\max}$ .

### 3.4 Examples

In all the examples that follow, unforced periodic walking motions are computed first and then the effect of external forcing on such motions is investigated using the results of Section 3.3. To compute such unforced periodic walking motions, the method of Poincaré is employed, with  $\mathcal{S}$  defined by (3.6) being the corresponding Poincaré section. Assume that  $F_e(t) \equiv 0$ , and let  $\mathcal{A}$  be a set that includes all the parameters  $\alpha_{\text{Bez}} \in \mathcal{A}$  introduced by the controller; namely, the Beziér coefficients  $a_{i,k}^\ell$  and  $a_{i,k}^m$  of the corresponding locomotion and manipulation polynomials as in (3.18), defining the locomotion and manipulation outputs (3.16) and (3.19). The Poincaré map  $P : \mathcal{S} \times \mathcal{A} \rightarrow \mathcal{S}$  can then be defined as

$$x[k+1] = P(x[k], \alpha_{\text{Bez}}) , \quad (3.57)$$

and periodic walking motions can be computed by searching for fixed points  $x^* \in \mathcal{S}$  and parameters  $\alpha_{\text{Bez}}^* \in \mathcal{A}$  that satisfy

$$x^* = P(x^*, \alpha_{\text{Bez}}^*)$$

together with additional constraints related to actuator limitations, toe-ground interaction constraints and other specifications similar to [111, Section 3.2]. This procedure can be formulated as a nonlinear constrained optimization problem that can be solved using the *fmincon* function in MATLAB. Exponential stability of the fixed point is ensured by checking that the eigenvalues of the linearization of (3.57) are located within the unit disc centered at the origin. In this chapter, three types of unforced periodic gaits are computed, corresponding to flat ground  $(x_f^*, \alpha_{\text{Bez},f}^*)$ , upstairs  $(x_u^*, \alpha_{\text{Bez},u}^*)$  and downstairs  $(x_d^*, \alpha_{\text{Bez},d}^*)$  walking. Since the zero dynamics is invariant, the unforced periodic gait of the full order dynamics corresponds to the unforced periodic gait of the zero dynamics [68]. In the restricted dynamics, such motion is associated with a fixed point

$$\zeta_0^* = -\frac{v(\theta^-)}{1 - \delta_z^2}, \quad (3.58)$$

of the map (3.45). Exponential stability on the restricted dynamics is reflected by the condition  $\delta_z^2 < 1$ . The leader's intention is represented by the desired trajectories  $p_L(t)$  as described in Section 3.1.2. For flat ground walking, we assume  $p_L(t) = (v_L^x t + p_E^x(q(0)), p_E^y(q(0)))^T$ , where  $v_L^x$  is the constant horizontal speed that the leader intends to impose and  $p_E^x(q(0))$  and  $p_E^y(q(0))$  are the horizontal and vertical components of the initial position of end effector. For the stair traversal case,  $p_L(t) = (v_L^x t + p_E^x(q(0)), v_L^y t + p_E^y(q(0)))^T$ , where  $v_L^y$  is the desired vertical speed of leader.

Based on the impedance parameters of human arm [82], we choose  $K_L = 100I_{2 \times 2}(\text{N/m})$  and  $N_L = 20I_{2 \times 2}(\text{Ns/m})$ , where  $I_{2 \times 2}$  is the  $2 \times 2$  identity matrix. The impedance parameters of the biped's arm (3.20) are chosen to exhibit compliance in following the intended trajectory of the leader [31]; we select  $M_m = I_{2 \times 2}(Kg)$ ,  $K_m = 20I_{2 \times 2}(\text{N/m})$ ,  $N_m = 4I_{2 \times 2}(\text{Ns/m})$ .

In Section 3.4.1, we choose  $\epsilon_m = 0.1$  to render the arm stiff and use the results of Section 3.3 to discuss how unforced motions “adapt” to an externally applied force. In Section 3.4.2, the benefit of impedance controller is discussed by varying the value of  $\epsilon_m$ , and finally in Section 3.4.3, we show the application of the controller in the stair

traversal case, where  $\epsilon_m = 1$  is chosen.

### 3.4.1 Adaptation to the Leader's Change of Speed

Now suppose that the leader holds the biped's hand and walks with a higher speed than that of the biped's unforced motion; see Fig. 3.4(a). In this case, the inner product  $\kappa_3(\xi)\hat{r} > 0$ ; see (3.36) for the interpretation of  $\kappa_3$ . Since  $\kappa_1(\zeta) > 0$  as we verified in simulation, we have that  $w_k(\theta^-) > 0$ . Furthermore, since the function  $v(\theta^-)$  and the constant  $\delta_z$  are independent of the leader's trajectory, from (3.47) and (3.58) one can show that

$$\zeta_k^* = \zeta_0^* + \frac{w_k(\theta^-)}{1 - \delta_z^2}, \quad (3.59)$$

which implies  $\zeta_k^* > \zeta_0^*$ . Intuitively, this fact means that, in response to the increase in the leader's speed, the biped also takes faster steps. When the average speed of the biped reaches that of the leader, then the interaction force starts to decrease – see Fig. 3.4(c) – which will also decrease  $\zeta_k^*$ . Even though the interaction force is decreasing, the biped will continue increasing speed until  $\zeta^-[k-1] > \zeta_k^*$  (first intersection point on Fig. 3.4(e)). This period of time corresponds to the overshoot seen in Fig. 3.4(a). Then, the biped decreases speed until it reaches the speed of leader again. Eventually, the interplay between the leader's trajectory, the interaction force and the fixed point of the  $k$ -th step will make the biped match leader's average speed. Note that when the biped is increasing speed there is a possibility that the gait constraints described in Section 3.3.2 are violated. Inequality (3.56) ensures that these constraints are respected.

Suppose next that the leader is walking with a speed lower than that of the biped's unforced walking gait, so that  $\kappa_3(\xi)\hat{r} < 0$ . Using the same arguments as above, one can conclude that  $\zeta_k^* < \zeta_0^*$ . This means that the biped will take slower steps, and, under certain conditions, it may not have enough energy to complete the step. Equation (3.55) gives the explicit condition which ensures that the biped will continue taking steps. Depending on the underlying unforced motion  $\zeta_0^*$ , this condition also means that there exists a critical average speed of the leader, below which the biped cannot take a step and consequently will not be able to match its speed with that of the

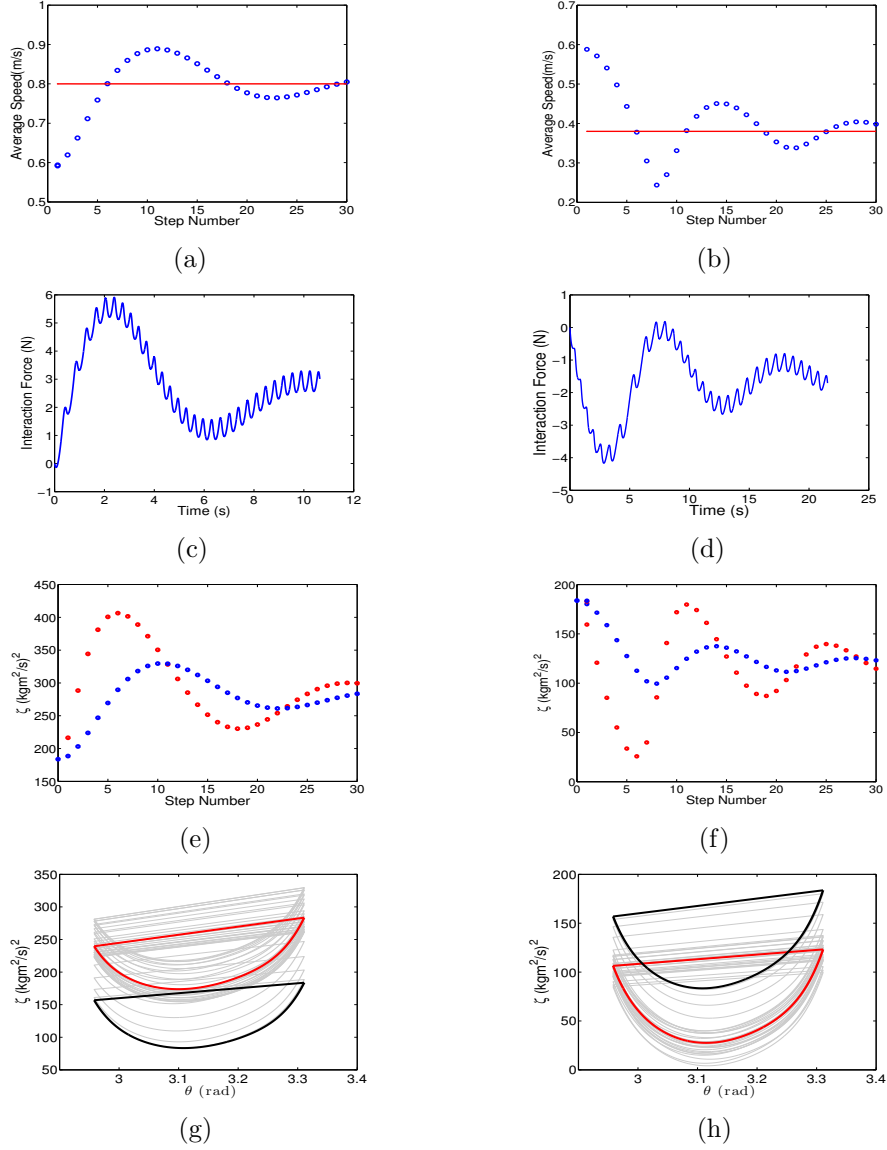


**Figure 3.4: Left:** Biped response when the average speed of the leader is higher than that of the biped. **Right:** Biped response when the average speed of the leader is lower than that of the biped. (a) and (b) Average speed of leader (solid red line) and average speed of biped (blue marker). (c) and (d) Horizontal component of interaction force. (e) and (f) Zero dynamics state at the end of each step  $\zeta^-$  (blue markers) and fixed point of each step  $\zeta_k^*$  as in (3.47) (red markers). (g) and (h) Convergence of limit cycles. Black is the base (unforced) limit cycle, gray is the transitioning and red is the final limit cycle.

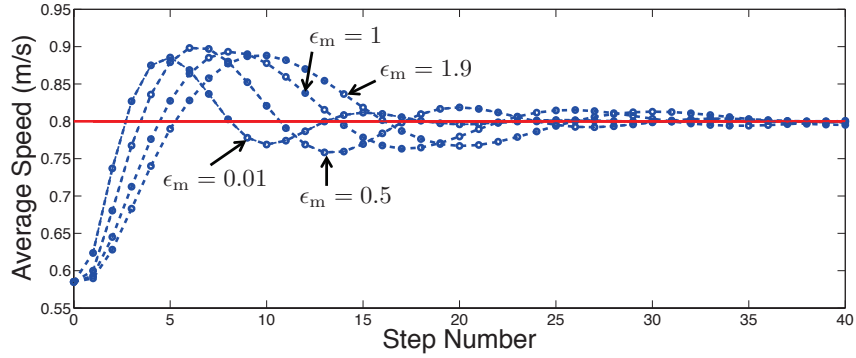
leader. Fig. 3.4(b) shows an example of this case, where the minimum average speed of leader that can be followed by the biped is 0.38 m/s. The procedure of matching leader’s speed can be described by interaction force in Fig. 3.4(d) and fixed point of each step map in Fig. 3.4(f), the same way as was given for previous case.

As was discussed in Section 3.2.4, the stride length of the biped’s walking gait remains constant as its speed changes. This can be seen in the phase portraits of the monotonic variable  $\theta$  depicted in Figs. 3.4(g) and 3.4(h) corresponding to the acceleration and deceleration cases. Clearly, the range of values of  $\theta$  remains the same, while the rate of change of  $\theta$  changes, implying that the stride frequency increases or decreases to generate faster or slower walking motions.

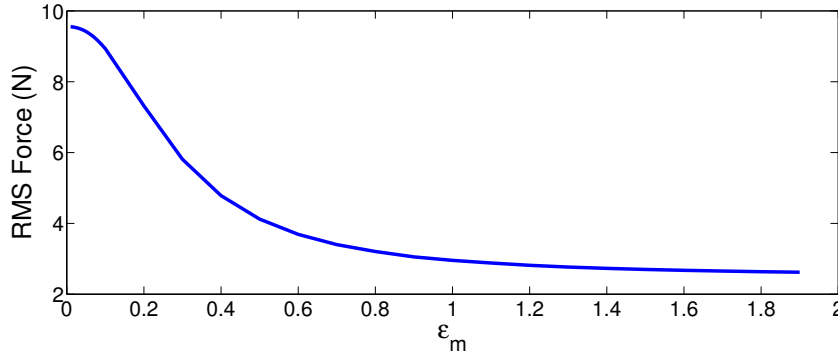
In summary, when the leader walks with a higher speed than that of the biped’s unforced gait, it pushes the biped to take faster steps. In this case, if the gait constraints are not violated; see (3.56), the robot matches the speed of leader. On the other hand, when the leader has a slower walking speed, it forces the biped to take slower steps. In this case, if the biped has enough energy, it catches the speed of leader. In fact, these conditions can be translated to a maximum and minimum walking speed of leader to which the biped is able to adapt.

### 3.4.2 Effectiveness of the Arm’s Impedance Controller

The impedance controller provides safe human-biped interaction, while at the same time it enables the biped to passively track the intended trajectory of the leader. While this property of the impedance controller is beneficial in many ways, in this section we turn our attention to the implications of the arm’s impedance controller on the magnitude of the interaction force that is developed between the biped and the leader. This force is generated by the leader, and it is desirable to keep it as small as possible to avoid excessive effort on the leader’s part. To examine this issue, we focus on a scenario according to which the leader’s intended speed is increased from 0.6m/s to 0.8m/s and different values of  $\epsilon_m$  are used to modify the impedance (3.20) of the robot’s arm.



(a)



(b)

**Figure 3.5:** (a) Speed convergence of the biped (dashed blue line) to intended speed of leader (solid red line) for different impedance values of manipulator. (b) RMS of the interaction force as a function of manipulator impedance.

Figure 3.5(a) shows the convergence of the biped’s speed to that of the leader for different impedance values of manipulator. We can see that compliance in the arm does not substantially change the adaptive response of biped’s locomotion to the leader’s intended speed. The compliance only modifies the settling time; in more detail, as the arm becomes more compliant it takes more steps for the biped to catch the intended speed of the leader.

Figure 3.5(b) shows the root mean square (RMS) of the interaction force until the biped converges within 3% of the leader’s intended speed. In interpreting this figure note that small  $\epsilon_m$  correspond to stiffer manipulators; in the limit  $\epsilon_m \rightarrow 0$  the impedance controller (3.20) reduces to a position controller imposing the constraints (3.19). Clearly, stiffer manipulators result in higher interaction forces that are needed

from the leader so that the biped achieves the leader’s intended speed. In fact, the worst case corresponds to  $\epsilon_m \rightarrow 0$ , illustrating the benefits of impedance controllers over position controllers as in [6]. However, there is a limit on how compliant the manipulator can be, since for  $\epsilon_m > 1.9$  the manipulator reaches its singular configuration.

### 3.4.3 Switching from Flat Ground to Upstairs and Downstairs

The adaptability of the biped’s speed to the leader’s intended velocity carries to the case of walking over stairs of known geometry. However, in this case, the biped needs to be capable of switching from flat ground to upstairs or downstairs walking. To achieve this switching, the one-step transition controller in [111, Section 7.2] is employed, which will be described next.

Let  $\alpha$  and  $\beta$  be two sets of parameters, each including the parameters of the locomotion (3.16) and the manipulation output (3.19), that result in two different unforced periodic motions, one for flat ground walking and one for stair climbing. Suppose that the corresponding controllers  $\Gamma_\alpha$  and  $\Gamma_\beta$  correspond to the zero dynamics surfaces  $\mathcal{Z}_\alpha$  and  $\mathcal{Z}_\beta$  that are invariant under the impact map; i.e.  $\Delta(\mathcal{S} \cap \mathcal{Z}_\alpha) \subset \mathcal{Z}_\alpha$  and  $\Delta(\mathcal{S} \cap \mathcal{Z}_\beta) \subset \mathcal{Z}_\beta$ ; and that there exist exponentially stable periodic orbits  $\mathcal{O}_\alpha \subset \mathcal{Z}_\alpha$  and  $\mathcal{O}_\beta \subset \mathcal{Z}_\beta$ , both transversal to  $\mathcal{S}$ . The objective is to design a transition controller  $\Gamma_{(\alpha \rightarrow \beta)}$ , with the swing phase zero dynamics  $\mathcal{Z}_{(\alpha \rightarrow \beta)}$  connecting the zero dynamics manifolds  $\mathcal{Z}_\alpha$  and  $\mathcal{Z}_\beta$  so that the biped can stably transition from  $\mathcal{O}_\alpha$  to  $\mathcal{O}_\beta$ . More specifically, the transition step maps the state of the biped after the impact  $\Delta(\mathcal{S} \cap \mathcal{Z}_\alpha)$  under controller  $\Gamma_\alpha$ , to the state right before the next impact  $\mathcal{S} \cap \mathcal{Z}_\beta$  under controller  $\Gamma_\beta$ . Mathematically, this requires that  $\Delta(\mathcal{S} \cap \mathcal{Z}_\alpha) \subset \mathcal{Z}_{(\alpha \rightarrow \beta)}$  and  $\mathcal{S} \cap \mathcal{Z}_{(\alpha \rightarrow \beta)} = \mathcal{S} \cap \mathcal{Z}_\beta$ . To achieve these conditions, the parameters of the transition controller  $\alpha \rightarrow \beta$  are

selected as

$$\begin{aligned}
(\alpha \rightarrow \beta)_0 &= \alpha_0 \\
(\alpha \rightarrow \beta)_1 &= \alpha_0 - \frac{\theta_\beta^- - \theta_\alpha^+}{\theta_\alpha^- - \theta_\alpha^+}(\alpha_0 - \alpha_1) \\
(\alpha \rightarrow \beta)_{n-1} &= \beta_n + \frac{\theta_\beta^- - \theta_\alpha^+}{\theta_\beta^- - \theta_\beta^+}(\beta_{n-1} - \beta_n) \\
(\alpha \rightarrow \beta)_n &= \beta_n \\
\theta_{(\alpha \rightarrow \beta)}^+ &= \theta_\alpha^+ \\
\theta_{(\alpha \rightarrow \beta)}^- &= \theta_\beta^-
\end{aligned} \tag{3.60}$$

where  $n$  is the degree of Beziér polynomial as in (3.18), and the numbered index refers to the column of the parameter matrices. Equation (3.60) determines the beginning and ending parameters of the transition controller. The intermediate parameters  $(\alpha \rightarrow \beta)_i$ ,  $i = 2$  to  $i = n - 2$  are computed through numerical optimization, by minimizing the torques during the transition. Note that the transitioning controller connects the zero dynamics manifolds  $\mathcal{Z}_\alpha$  to  $\mathcal{Z}_\beta$  in one step, however convergence to the periodic orbit  $\mathcal{O}_\beta$  does not occur in finite time.

The effect of force on transitioning can be explained by deriving the closed-form expression of the one dimensional transitioning step map  $\rho_{\alpha \rightarrow \beta}$  in a similar manner as the step map in (3.45). The snapshots of walking over the stair case <sup>3</sup> is depicted in Figs. 3.6(a) and 3.6(b). Figures 3.6(c) and 3.6(d) depict the convergence of the biped's speed to the leader's intended speed for both cases of transitioning from flat ground to upstairs and downstairs walking. Both components of the interaction force are plotted in Figs. 3.6(e) and 3.6(f), indicating that the leader does not need to make an excessive effort to guide the motion of the biped.

As a final remark, note that the adaptation mechanism of the biped's speed – i.e., keeping the stride length constant and changing the stride frequency – is beneficial to walking over stairs with known geometry since the biped can accelerate or decelerate

---

<sup>3</sup> In these results, the stair geometry is specified by  $\omega = 20\text{cm}$  and height  $d = 10\text{cm}$ , where  $\omega$  and  $d$  are depicted in Fig. 3.2(a).

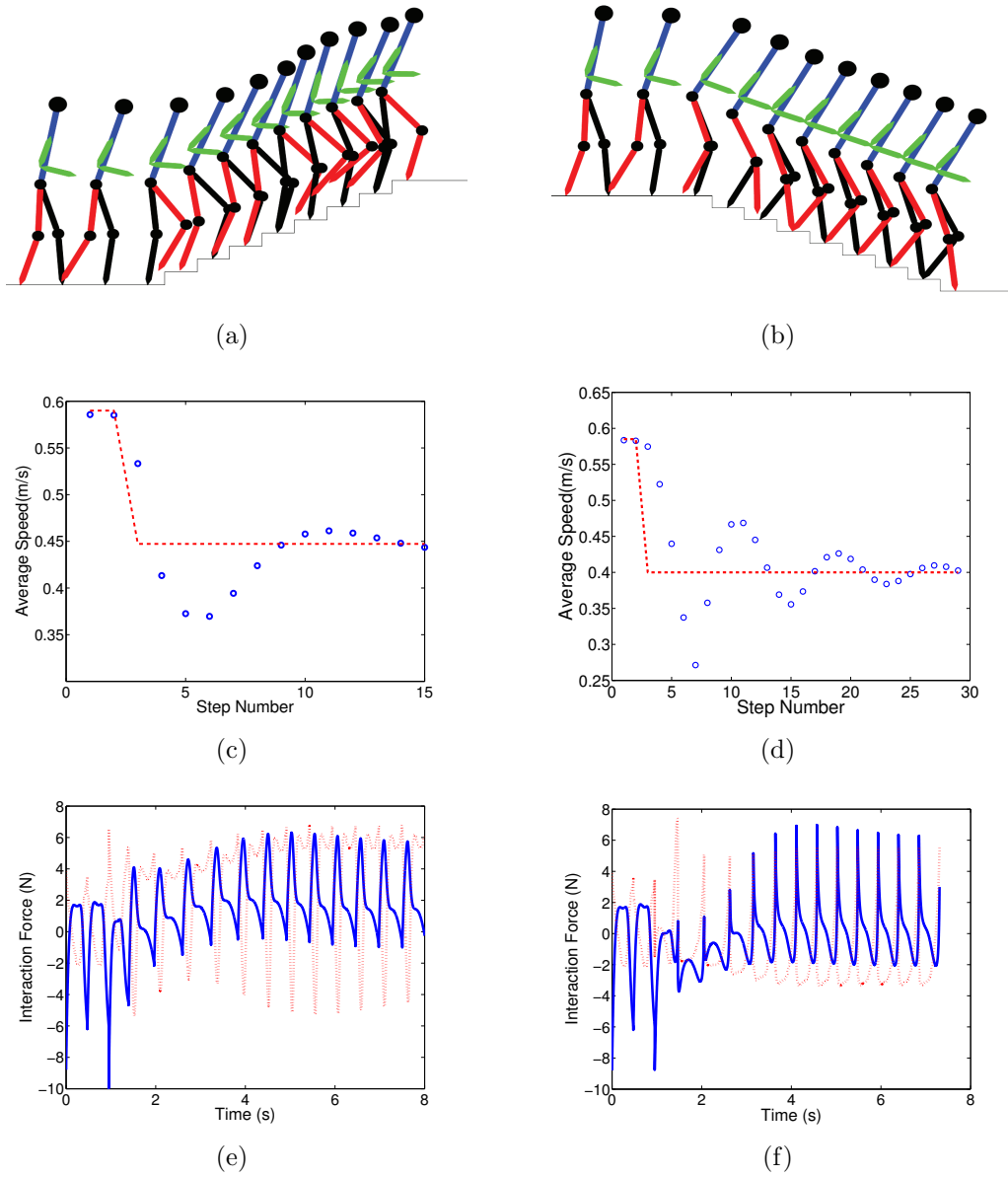


**Figure 3.6:** **Left:** Simulation results when transitioning from flat ground to upstairs. **Right:** Transitioning from flat ground to downstairs. (a) and (b) Snapshots of walking. Black and red links correspond to the stance and swing foot respectively. (c) and (d) Average walking speed of the biped (blue markers) and desired speed of leader (red line). (e) and (f) Interaction force. Solid blue is the horizontal component and dashed red is the vertical component.

while maintaining its foot placement, thereby avoiding hitting the edges of stair profile.

### 3.5 Discussion

This chapter provided a framework for cooperation of a bipedal robot with a leading co-worker in a planar setting; see Fig. 3.7. At the high level, the leading co-worker plans an intended trajectory  $p_L$  which is not directly accessible to the robot. The robot perceives the leader’s intention as an interaction force which is applied on its end effector on the basis of the location of the end effector. At the low level, the locomotion controller generates limit-cycle walking gaits that can be shaped by the interaction force. Essentially, the locomotion controller adjusts the speed of the robot in response to the change in leader’s speed. The result of this chapter takes the first step towards integrating high-level cooperative tasks with low-level locomotion controllers to enable a bipedal robot help a human carry an object over a distance that engages the robot’s locomotion system.

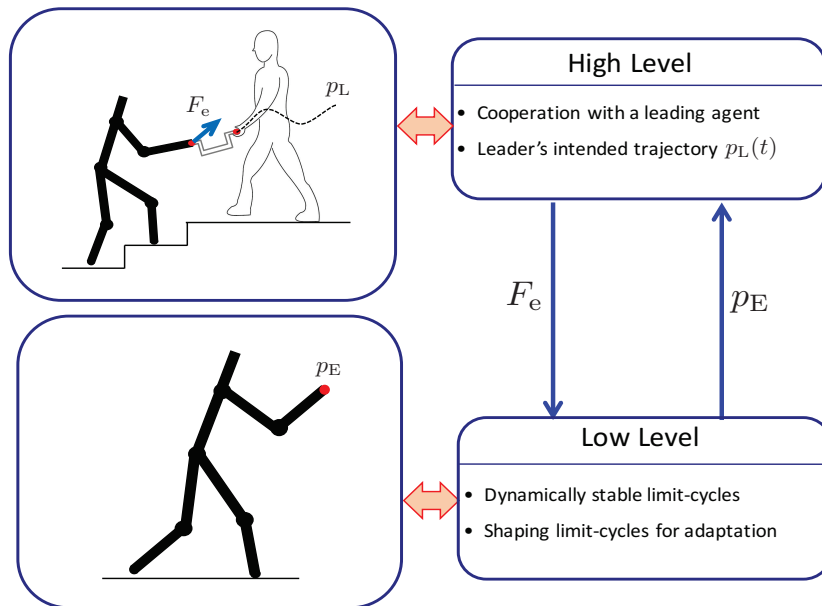


**Figure 3.7:** The hierarchical components for a cooperation task. The leading co-worker plans a trajectory  $p_L$  (high-level) and guides the robot to follow it by applying a suitable force  $F_e$  at the biped’s end effector.

## Chapter 4

### BIPED-LEADER COOPERATIVE TASK: 3D MODEL

This chapter extends the previous results to a more complex model of cooperation suitable for 3D workspaces. The complexity arises from the fact that in 3D spaces, the biped has to adapt its heading angle as well as its speed in response to the leader’s intention. With this adaptation, the biped can leverage the leader’s knowledge regarding the environment and the task and allow the collaborator to effectively walk the biped along an obstacle-free path. Section 4.1 describes the hybrid dynamics of the 3D walking robot in the presence of an external force. Section 4.2 presents the controller design that enables the biped to adapt its locomotion behavior to the interaction force, and at the same time exhibit compliance in its arm. Section 4.3 discusses certain key properties of the closed-loop system that are important in realizing adaptable locomotion in the presence of the interaction force. Section 4.4 provides examples of biped-leader cooperative tasks in which the biped tracks the intended trajectory of the leader in an environment with obstacles *without* any explicit knowledge of the leader’s intentions or the environment. Finally, Section 4.5 summarizes the contributions of this chapter and relates it to the chapters that follow. The results of this chapter have appeared in [72].

#### 4.1 Walking under Interaction Forces

##### 4.1.1 Three-Dimensional Model

We consider a fairly generic model of a three-dimensional (3D) bipedal walker as shown in Fig. 4.1. The model is composed of a torso, a manipulator that is connected to the torso through a two-DOF revolute shoulder joint, and two identical legs, each connected to the torso via a two-DOF revolute hip joint. In our model, we consider

only one manipulator system to simplify numerical computations. The manipulator consists of an upper arm and a forearm that are connected at the elbow joint with one DOF. The legs are composed of two links, the thigh and the shin, which are connected through a one-DOF revolute knee joint. We assume that the stance foot acts as a pivot with three rotational DOFs corresponding to the yaw  $q_1$ , pitch  $q_2$ , and roll  $q_3$  angles; see Fig. 4.1. In total, during the single support phase, the model has twelve degrees of freedom  $q := (q_1, \dots, q_{12})^T \in \mathcal{Q}$ , where  $\mathcal{Q}$  contains physically reasonable configurations of the system. Seven actuators – four located at the hip joints, two at the knee joints and one at the roll joint of the foot – provide the input torques for the locomotion part, and three actuators – two at the shoulder joint and one at the elbow joint – provide the input torques for the manipulation part. Note that the roll joint of the foot is actuated so that the external force does not destabilize the lateral motion of the biped. For this actuation to be physically realizable we assume that the foot has non-zero size and is mass-less, which is common in the literature [29, 30]. The physical parameters of the 3D model are provided in Table 4.1.

**Table 4.1:** Mechanical Parameters of the 3D Bipedal Model

Model Parameter	Units	Label	Value
Mass	kg	$m_1$	0.875
		$m_2$	0.875
		$m_3$	5.5
		$m_4$	0.3
		$m_5$	0.3
Length	m	$W$	0.15
		$L_1$	0.275
		$L_2$	0.275
		$L_3$	0.3
		$L_4$	0.15
		$L_5$	0.15

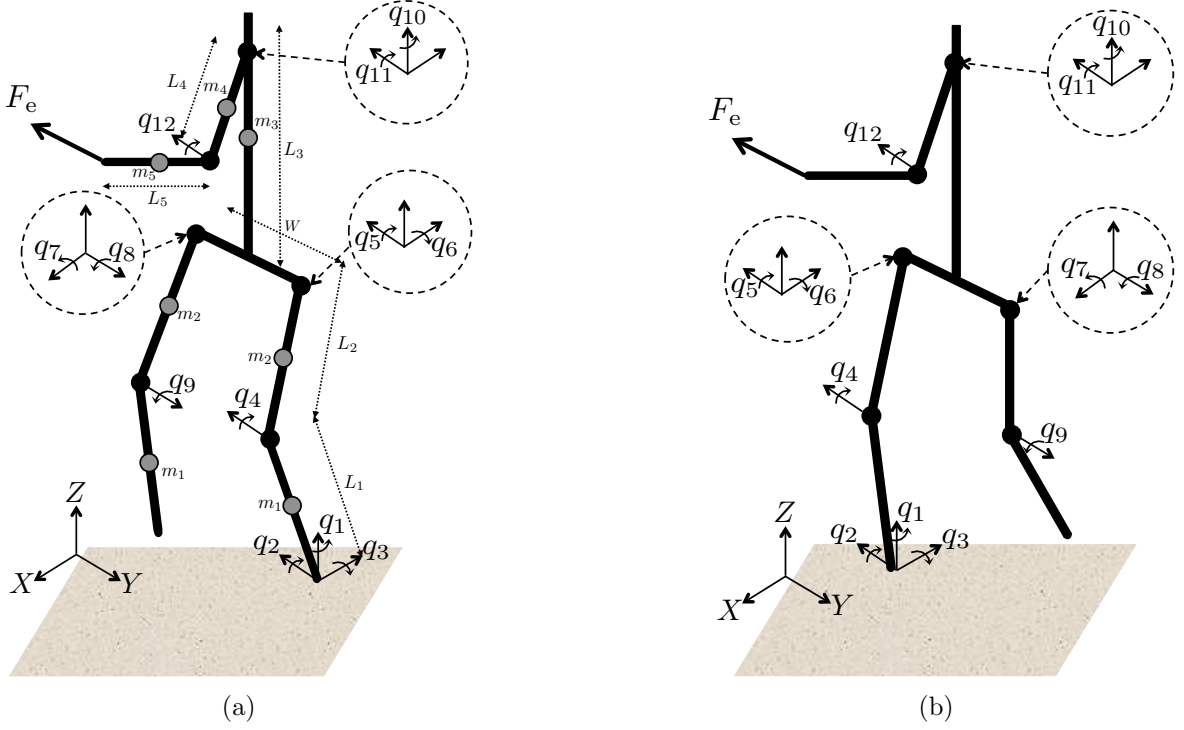


**Figure 4.1:** (a) 3D biped model with a choice of generalized coordinates when supported on leg 1. (b) 3D biped model with a choice of generalized coordinates when supported on leg 2. Each link has a length and a mass that is modeled by point mass located at the center of the link. The values of these parameters are given in Table 4.1.

#### 4.1.2 Swing Phase

Due to the nontrivial length of the hip joint, the equations of motion during the support on leg 1 and leg 2 are different. The dynamics of the biped in the continuous phase supported on leg 1 can be written as

$$D(q)\ddot{q} + C(q, \dot{q})\dot{q} + G(q) = B_\ell u_\ell + B_m u_m + J_E^T(q)F_e, \quad (4.1)$$

where  $D(q)$  is the mass matrix,  $C(q, \dot{q})\dot{q}$  contains the centrifugal and Coriolis forces and  $G(q)$  contains the gravitational forces. The matrices  $B_\ell$  and  $B_m$  distribute the locomotion inputs  $u_\ell$  and manipulation inputs  $u_m$  to the configuration variables  $q$ . Finally,  $J_E(q) := \partial p_E(q) / \partial q$ , where  $p_E$  is the position of biped's end-effector on which

the interaction force  $F_e$  acts; see Fig. 4.1. Defining the state vector  $x_i := (q^T, \dot{q}^T)^T$ , where the subscript  $i \in 1, 2$  denotes the support leg number, the swing phase dynamics (4.1) on leg 1 can be transformed to state-space model as

$$\dot{x} := f_1(x) + g_{\ell,1}(x)u_{\ell,1} + g_{m,1}(x)u_{m,1} + g_{e,1}(x)F_e, \quad (4.2)$$

where the vector fields  $f_1$ ,  $g_{\ell,1}$ ,  $g_{m,1}$ ,  $g_{e,1}$  are defined accordingly. The swing phase dynamics when the support is on leg 2 can be obtained in a similar manner by using a hip width of  $-W$  in place of  $W$ , when the kinematic equations are derived.

### 4.1.3 Double Support Phase

When the swing leg touches the ground, the biped enters the instantaneous double support phase. The double support phase is composed of two sub-phases, the impact model and the relabeling. Analogously to the planar case of Section 3.1.3, the impact model can be derived. However, the relabeling in 3D model involves the solution of an inverse kinematic problem, which is described as follows. Let  $R_{\text{sh}}$  be the rotation matrix describing the orientation of the shin of leg 2, and  $\omega_{\text{sh}}$  be the vector containing the angular velocities of shin of leg 2, right after the impact. Now we need to compute the corresponding  $q_1$ ,  $q_2$  and  $q_3$  that result in the same orientation and angular velocity of shin of leg 2, in the beginning of the swing phase on leg 2 support. Using the new generalized coordinates describing the support on leg 2, an expression for  $R^{\text{sh}}$  can be obtained

$$R^{\text{sh}} = \begin{bmatrix} c_1 c_2 c_3 - s_1 s_3 & -c_1 c_2 s_3 - s_1 c_3 & -c_1 s_2 \\ s_1 c_2 c_3 + c_1 s_3 & -s_1 c_2 s_3 + c_1 c_3 & -s_1 s_2 \\ s_2 c_3 & -s_2 s_3 & c_2 \end{bmatrix}, \quad (4.3)$$

where  $c_i := \cos(q_i)$  and  $s_i := \sin(q_i)$  for  $i = 1, 2, 3$ . Note that (4.3) has the same form as the rotation matrix for Euler transformation [98, Section 2.5.1]. Solving this equation

gives

$$\begin{aligned}
q_1^+ &= \text{atan2}(R_{2,3}^{\text{sh}}, R_{1,3}^{\text{sh}}) , \\
q_2^+ &= \text{atan2}(R_{3,3}^{\text{sh}}, \sqrt{1 - (R_{3,3}^{\text{sh}})^2}) , \\
q_3^+ &= \text{atan2}(R_{3,2}^{\text{sh}}, -R_{3,1}^{\text{sh}}) ,
\end{aligned}$$

where  $\text{atan2}$  is the two argument arctangent function. The joint velocities  $\dot{q}_1^+$ ,  $\dot{q}_2^+$  and  $\dot{q}_3^+$  are obtained as

$$\begin{bmatrix} \dot{q}_1^+ \\ \dot{q}_2^+ \\ \dot{q}_3^+ \end{bmatrix} = \begin{bmatrix} c_3 c_2 & -s_3 & 0 \\ -s_3 c_2 & -c_3 & 0 \\ -s_2 & 0 & 1 \end{bmatrix} \omega^{\text{sh}} . \quad (4.4)$$

The remaining angles in the legs, i.e.  $q_4$  to  $q_9$ , simply exchange their roles and the angles in the arm  $q_{10}$  to  $q_{12}$  remain the same. The combined result of the impact and the relabeling for support on leg 1 can be described by a map  $\Delta_1$  taking the final state  $x_1^-$  of support on leg 1 to the initial state  $x_2^+$  of support on leg 2. , i.e.

$$x_2^+ = \Delta_1(x_1^-) .$$

The complete walking motion of the biped can be expressed as a hybrid nonlinear system with impulse effects

$$\Sigma: \begin{cases} \dot{x}_1 = f_1(x) + g_{\ell,1}(x)u_{\ell,1} + g_{m,1}(x)u_{m,1} + g_{e,1}(x)F_e, & x_1^- \notin \mathcal{S}_1, \\ x_2^+ = \Delta_1(x_1^-), & x_1^- \in \mathcal{S}_1, \\ \dot{x}_2 = f_2(x) + g_{\ell,2}(x)u_{\ell,2} + g_{m,2}(x)u_{m,2} + g_{e,2}(x)F_e, & x_2^- \notin \mathcal{S}_2, \\ x_1^+ = \Delta_2(x_2^-), & x_2^- \in \mathcal{S}_2, \end{cases} \quad (4.5)$$

where the switching surfaces are defined as

$$\mathcal{S}_1 := \{(q^T, \dot{q}^T)^T \in TQ \mid p_1^y(q) = 0, \dot{p}_1^y(q, \dot{q}) < 0\} , \quad (4.6)$$

and

$$\mathcal{S}_2 := \{(q^T, \dot{q}^T)^T \in TQ \mid p_2^v(q) = 0, \dot{p}_2^v(q, \dot{q}) < 0\} \quad , \quad (4.7)$$

and  $p^v$  and  $\dot{p}^v$  refer to the height and vertical velocity of the swing leg.

## 4.2 Coupled Locomotion and Arm Control

This section proposes a controller that manipulates the inputs of the arm and locomotion subsystems to ensure that the biped adapts its dynamic walking pattern to the external force. The procedure is developed for one continuous phase and is similar to the one described in planar case in Section 3.2, so the exposition here will be brief and only the differences will be highlighted.

### 4.2.1 Virtual Constraints for the Locomotion Task

The walking motions are realized by assigning output functions to the actuated joints of the legs and designing the controller to drive the outputs to zero. To the continuous dynamics (4.2), we associate the output

$$y_\ell = h_\ell(q) := q_a - h_\ell^{\text{des}}(\theta(q)) \quad , \quad (4.8)$$

where  $q_a := (q_3, \dots, q_9)^T$  includes the controlled variables in the legs and  $h_\ell^{\text{des}}$  denotes the desired evolution as a function of the monotonic quantity  $\theta(q) = -q_2 - q_4/2$ , which corresponds to the angle of the line connecting the foot of the support leg with the corresponding hip joint. The function  $h_d$  is designed using Beziér polynomials of degree 3; see (3.18) for the expression of the Beziér polynomials. The Beziér parameters are determined such that in the beginning and end of a step, on the nominal orbit, the output (4.8) is identically zero. However, when the system is off the nominal orbit, there is no guarantee that the output (4.8) remains zero under the effect of impact map. In other words, the output (4.8) is not capable of rendering the zero dynamics invariant under the impact map.

As in [14], we render the evolution of the system hybrid invariant by augmenting the output with a correction term  $h_c(\theta, \alpha_c)$  as

$$y_{\ell,c} = h_{\ell,c}(q, \alpha_c) = q_a - h_\ell^{\text{des}}(\theta) - h_c(\theta, \alpha_c) . \quad (4.9)$$

The correction output  $h_c$  is chosen to be three times continuously differentiable function of  $\theta$  that satisfies

$$\begin{cases} h_c(\theta^+, \alpha_c) = y_{\ell,i} \\ \frac{\partial}{\partial \theta} h_c(\theta^+, \alpha_c) = \frac{\dot{y}_{\ell,i}}{\dot{\theta}^+} \\ h_c(\theta, \alpha_c) = 0, \quad 0.5\theta^+ + 0.5\theta^- \leq \theta \leq \theta^- \end{cases} \quad (4.10)$$

where  $y_{\ell,i}$  is the initial value of the uncorrected output in the beginning of the step computed by (4.8). For  $\theta^+ \leq \theta \leq 0.5\theta^+ + 0.5\theta^-$ , we choose a fifth order polynomial that ensures the continuity of position, velocity and acceleration at the connecting point  $\theta = 0.5\theta^+ + 0.5\theta^-$ . The vector of coefficients  $\alpha_c$  is updated on a step-to-step basis so that the initial error with respect to the uncorrected output is smoothly rejected by the middle of the step. Compared to a PD controller with high gains, the correction output requires less torques to attenuate the error.

#### 4.2.2 Impedance Regulation for the Manipulation Task

Similarly to Section 3.2.2, we select the manipulation output as

$$y_m = h_m(q) := p_E(q_m) - h_m^{\text{des}} \circ \theta(q) , \quad (4.11)$$

where  $p_E \in \mathbb{R}^3$  is the position vector of end-effector with respect to a local frame attached to the shoulder,  $q_m := (q_{10}, q_{11}, q_{12})^T$  contains the arm configuration variables and  $h_m^{\text{des}} \circ \theta(q)$  is a vector of Beziér polynomials of degree 3 that describes the desired relative position of the end effector to the shoulder joint, which can be equivalently viewed as the desired configuration of the arm. Note that the arm has three DOFs

that are all slaved to provide compliance along the three axes of the global frame. The goal of the impedance controller is to enforce a mechanical impedance relation between the manipulation output and the interaction force as

$$M_m \ddot{y}_m + \frac{N_m}{\epsilon_m} \dot{y}_m + \frac{K_m}{\epsilon_m^2} y_m = F_e , \quad (4.12)$$

where  $\epsilon_m > 0$  is a parameter, and  $M_m$ ,  $N_m$ , and  $K_m$  are positive definite mass, damping and stiffness matrices, respectively, determining the compliance of the arm. In the absence of an external force, (4.12) implies that the error  $y_m$  converges to zero at a rate specified by the matrices  $M_m$ ,  $N_m$ , and  $K_m$  and the parameter  $\epsilon_m$ , so that the arm settles at its desired configuration captured by  $h_m^{\text{des}}$ .

### 4.2.3 Controller Design

The controller design is identical to Section 3.2.3. To drive the locomotion output (4.9) to zero and simultaneously establish the desired impedance dynamics (4.12) in the arm, we select the control law

$$u = \Gamma(x, F_e) = L_g L_f h(x)^{-1} [v(x, F_e) - L_f^2 h(x) - L_{g_e} L_f h(x) F_e] , \quad (4.13)$$

where  $u := (u_\ell^T, u_m^T)^T$ ,  $h(x) := (h_{\ell,c}^T, h_m^T)^T$  and

$$v(x, F_e) := \begin{bmatrix} v_\ell(y_{\ell,c}, \dot{y}_{\ell,c}) \\ v_m(y_m, \dot{y}_m, F_e) \end{bmatrix} = \begin{bmatrix} -\frac{1}{\epsilon_\ell^2} K_\ell y_{\ell,c} - \frac{1}{\epsilon_\ell} N_\ell \dot{y}_{\ell,c} \\ M_m^{-1} (F_e - \frac{N_m}{\epsilon_m} \dot{y}_m - \frac{K_m}{\epsilon_m^2} y_m) \end{bmatrix} \quad (4.14)$$

The system (4.5) under the influence of the control law (4.13) takes the form

$$\Sigma: \begin{cases} \dot{x} = f_{\text{cl}}^{\alpha_c}(x) + g_{\text{cl}}^{\alpha_c}(x) F_e, & x^- \notin \mathcal{S}, \\ x^+ = \Delta(x^-), & x^- \in \mathcal{S}, \end{cases} \quad (4.15)$$

where the closed loop vector fields  $f_{\text{cl}}$ ,  $g_{\text{cl}}$  can be defined accordingly. For simplicity, only one swing phase and impact is considered in (4.15). Note that these vector fields

depend on the parameter  $\alpha_c$  of the correction term  $h_c$  of (4.10) that is updated at the beginning of each step.

### 4.3 Effect of External Force on Locomotion

This section discusses certain key properties of the closed-loop system (4.15) that are important in realizing adaptable locomotion in the presence of the interaction force.

#### 4.3.1 Effect of External Force on Stepping Pattern

An important property of the controller in Section 4.2 is that the step length and step width of the biped are not affected by the external force. To see this, let  $q_\ell := (q_2, \dots, q_9)^T$  denote the configuration of legs excluding the yaw angle  $q_1$ . The locomotion output  $h_\ell$  in (4.9) and the height of swing leg  $p^v$  depend only on  $q_\ell$ . Since the correction output in (4.10) accounts for the induced initial error by the interaction force and rejects it before the robot completes a step, the solution of  $(h_{\ell,c}(q_\ell^-), p^v(q_\ell^-)) = (0, 0)$  uniquely determines the locomotion configuration prior to impact  $q_\ell^-$ . As a result, the step length which only depends on  $q_\ell^-$  remains constant over different steps.

The property that the stride length cannot be changed in response to the interaction force does *not* mean that the motion of the biped remains unaffected. In fact, as will be shown in Section 4.4 below, the biped reacts to the external force by adapting its stride frequency to accelerate or decelerate as well as adapting its heading angle in order to catch up with the intention of the leading co-worker. This adaptability is essentially a consequence of the way the controller deals with the two degrees of underactuation in the bipedal model considered.

#### 4.3.2 Effect of External Force on Symmetry under Yaw Rotation

A second property that is important, particularly in steering, is the symmetry of the unforced Poincaré map with respect to yaw rotations and the associated symmetry breaking upon the application of an external force at the bipeds end effector. The

formal definition of Poincaré map is first presented and then the symmetry property is described.

Let  $\varphi_1(t, x_1^+)$  and  $\varphi_2(t, x_2^+)$  be the maximal unforced solutions of the two continuous phases in (4.5), initialized at  $x_1^+$  and  $x_2^+$  respectively. The time-to-impact function  $T_I : T\mathcal{Q} \rightarrow \mathbb{R}_+$  for the two continuous phases can then be defined as  $T_{I,1}(x) = \inf\{t \geq 0 \mid p_1^y \circ \varphi_1(t, \Delta_2(x)) = 0\}$  and  $T_{I,2}(x) = \inf\{t \geq 0 \mid p_2^y \circ \varphi_2(t, \Delta_1(x)) = 0\}$ . Note that the time-to-impact functions are independent of the yaw angle  $q_1$ , since the height of the swing foot  $p^y$  does not depend on  $q_1$ . The partial map  $P_{21} : \mathcal{S}_2 \rightarrow \mathcal{S}_1$  that sends the state of the biped before the impact of leg 2 one step ahead is defined as

$$P_{21}(x_2) = \varphi_1(T_{I,1}(x_2), \Delta_2(x_2)) \quad , \quad (4.16)$$

and similarly the partial map  $P_{12} : \mathcal{S}_1 \rightarrow \mathcal{S}_2$  can be defined as

$$P_{12}(x_1) = \varphi_2(T_{I,2}(x_1), \Delta_1(x_1)) \quad . \quad (4.17)$$

To study the unforced periodic solutions of the closed loop system (4.15), we define the Poincaré return map  $P : \mathcal{S}_2 \rightarrow \mathcal{S}_2$  as the composition of the two partial maps,  $P := P_{12} \circ P_{21}$ , that takes the state  $x_2[k]$  one stride (two steps) ahead; i.e.

$$x_2[k+1] = P(x_2[k]) \quad . \quad (4.18)$$

The following Proposition is based on observations in [93], and it shows that restricting the choice of feedback controllers (4.13) so that they do not depend on the yaw angle  $q_1$  results in a symmetry property of the Poincaré map.

**Proposition 1.** *Let  $q_1$  denote the yaw angle and  $\tilde{x} := (x_2, \dots, x_{18})^T$  and define the group action*

$$\Psi_g(x) = (q_1 + g, \tilde{x}^T)^T \quad . \quad (4.19)$$

*Then, if the control law (4.13) is independent of the yaw angle  $q_1$ , the Poincaré map*

$P$  is equivariant under the action of  $\Psi_g$ , i.e.

$$P \circ \Psi_g(x) = \Psi_g \circ P(x) . \quad (4.20)$$

As a result, the Poincaré map can be written as

$$P(x) = \begin{bmatrix} q_1 + P^{(q_1)}(\tilde{x}) \\ \tilde{P}(\tilde{x}) \end{bmatrix} , \quad (4.21)$$

where  $q_1 + P^{(q_1)}$  and  $\tilde{P}$  are the projections of  $P$  onto  $q_1$  and  $\tilde{x}$ , respectively.

*Proof.* Equation (4.20) is proved in [93, Proposition 3]. We briefly mention that the kinetic and potential energies of the Lagrangian model are invariant under  $\Psi_g$ , the group of rotations around the Z-axis of the world frame, while the impact map is equivariant under  $\Psi_g$ . Since the control law is independent of the yaw angle, then the closed-loop vector fields are also equivariant under  $\Psi_g$ . As a result, the Poincaré map which is derived by sampling the solution of the model at time to impact, will be equivariant under  $\Psi_g$ . As it was mentioned earlier, the time to impact is itself invariant under  $\Psi_g$ . To prove (4.21), note that for any  $x = [q_1, \tilde{x}^T]^T$ , (4.19) and (4.20) imply

$$P([q_1, \tilde{x}^T]^T) = P \circ \Psi_{q_1}([0, \tilde{x}^T]^T) = \Psi_{q_1} \circ P([0, \tilde{x}^T]^T) = \begin{bmatrix} q_1 + \Pi_{q_1} \circ P([0, \tilde{x}^T]^T) \\ \Pi_{\tilde{x}} \circ P([0, \tilde{x}^T]^T) \end{bmatrix}$$

for any arbitrary  $q_1$ , where  $\Pi_{q_1}$  and  $\Pi_{\tilde{x}}$  project the state onto its  $q_1$  and  $\tilde{x}$  components, respectively. Defining  $P^{(q_1)}(\tilde{x}) := \Pi_{q_1} \circ P([0, \tilde{x}^T]^T)$  and  $\tilde{P}(\tilde{x}) := \Pi_{\tilde{x}} \circ P([0, \tilde{x}^T]^T)$ , which are independent of  $q_1$ , completes the proof.  $\square$

Note that our choices of locomotion (4.9) and manipulation outputs (4.11) are independent of yaw angle  $q_1$  and hence the control law (4.13) in the absence of external force will also be independent of  $q_1$ . So the condition of Proposition 1 is satisfied for the unforced case and the Poincaré map is equivariant under  $\Psi_g$ .

Computing the linearization of the Poincaré map  $A := \frac{\partial P(x)}{\partial x} \Big|_{x=x^*}$  from (4.21), one can observe that the first column of  $A$  is equal to  $(1, 0, \dots, 0)^T$ . Consequently,  $A$  will always have an eigenvalue equal to 1, and hence the fixed point is not exponentially stable. In this case, if all the eigenvalues of the linearization of the second component of Poincaré map  $\tilde{A} := \frac{\partial \tilde{P}(x)}{\partial \tilde{x}} \Big|_{\tilde{x}=\tilde{x}^*}$  in (4.21) are located within the unit disc centered at the origin, the fixed point  $x$  is said to be exponentially stable “modulo yaw”. Physically, this means that if we perturb the nominal heading angle  $q_1^*$  by the amount  $\delta q_1$ , the biped will continue taking steps in the new heading direction  $q_1^* + \delta q_1$ .

It is important to emphasize that the presence of the external force  $F_e$  breaks the symmetry discussed above. This is because the term  $J_E(q)$  in (4.1) depends on the yaw angle  $q_1$ . As a result, the application of  $F_e$  can be used to induce turning on the biped, enabling the leader to change the heading angle of the biped to a new desired one by applying a suitable force. Note that once the biped settles at the desired direction, then the external force is no longer required to maintain the new direction. It should be mentioned here that a similar conclusion does not hold for the case where the leader wants to change the bipeds speed, which depends on  $\tilde{x}$ . In this case, the leader needs to keep applying a force to maintain the desired speed, since if the force is removed, the exponential stability of the fixed point  $\tilde{x}^*$  of  $\tilde{P}$  will bring the speed of the biped back to its nominal unforced value.

### 4.3.3 Effect of External Force on Zero Dynamics

As it was mentioned earlier, the adaptive behavior of the biped to the interaction force in the form of speed and heading angle modifications, results from the underactuated nature of the biped. In this section we discuss how the two degrees of underactuation respond to the interaction force, through the derivation of swing phase zero dynamics. The control law (4.13) renders the zero dynamics surface

$$\mathcal{Z} := \{x \in TQ \mid h_{\ell,c}(q, \alpha_c) = 0, L_{f_{cl}} h_{\ell,c}(x, \alpha_c) = 0\} ,$$

attractive and invariant under the flow of the swing phase dynamics and the impact map. Note that unlike the planar case, the motion of the biped's arm due to the assigned impedance dynamics (4.12) does not break the hybrid invariance of  $\mathcal{S}$ , since the correction output  $h_c$  accounts for the initial error in the locomotion output (4.8) that is induced by the motion of the arm, and rejects the error before the next impact occurs. As a result, a five-DOF *Forced Hybrid Zero Dynamics (FHZD)* emerges from the closed loop dynamics (4.15). The FHZD is

$$\Sigma_z : \begin{cases} \dot{z} = f_z^{\alpha_c}(z) + g_z^{\alpha_c}(z)F_e, & z \notin \mathcal{S} \cap \mathcal{Z} \\ z^+ = \Delta_z(z^-), & z^- \in \mathcal{S} \cap \mathcal{Z} \end{cases}, \quad (4.22)$$

where  $z := (q_z^T, \dot{q}_z^T)^T$  with  $q_z := (q_1, \theta, q_{10}, q_{11}, q_{12})^T$  represent proper coordinates on  $\mathcal{Z}$ . In (4.22),  $f_z^\beta := f_{\text{cl}}^\beta|_{\mathcal{Z}}$  and  $g_z^\beta := g_{\text{cl}}^\beta|_{\mathcal{Z}}$  are the restrictions on  $\mathcal{Z}$  of the closed-loop dynamics (4.15), and  $\Delta_z := \Delta|_{\mathcal{S} \cap \mathcal{Z}}$ . Note that the high dimensionality of the FHZD precludes us from deriving closed-form solutions. However, we are still able to derive the explicit form of the continuous dynamics of the HZD, which will be described next.

Let  $q_a := (q_3, \dots, q_9)^T$  denote the controlled variables of the legs. Then,

$$q = \tau_q \begin{bmatrix} q_z \\ q_a \end{bmatrix} \quad (4.23)$$

where  $\tau_q$  is a constant  $12 \times 12$  invertible matrix given by

$$\tau_q := \begin{bmatrix} 1 & 0 & 0 & 0 & 0 & 0 & 0 & 0 & 0 & 0 & 0 & 0 \\ 0 & -1 & 0 & 0 & 0 & 0 & -0.5 & 0 & 0 & 0 & 0 & 0 \\ 0 & 0 & 0 & 0 & 0 & 1 & 0 & 0 & 0 & 0 & 0 & 0 \\ 0 & 0 & 0 & 0 & 0 & 0 & 1 & 0 & 0 & 0 & 0 & 0 \\ 0 & 0 & 0 & 0 & 0 & 0 & 0 & 1 & 0 & 0 & 0 & 0 \\ 0 & 0 & 0 & 0 & 0 & 0 & 0 & 0 & 1 & 0 & 0 & 0 \\ 0 & 0 & 0 & 0 & 0 & 0 & 0 & 0 & 0 & 1 & 0 & 0 \\ 0 & 0 & 0 & 0 & 0 & 0 & 0 & 0 & 0 & 0 & 1 & 0 \\ 0 & 0 & 0 & 0 & 0 & 0 & 0 & 0 & 0 & 0 & 0 & 1 \\ 0 & 0 & 1 & 0 & 0 & 0 & 0 & 0 & 0 & 0 & 0 & 0 \\ 0 & 0 & 0 & 1 & 0 & 0 & 0 & 0 & 0 & 0 & 0 & 0 \\ 0 & 0 & 0 & 0 & 1 & 0 & 0 & 0 & 0 & 0 & 0 & 0 \end{bmatrix} \quad (4.24)$$

Substituting  $\ddot{q}$  in (4.1) with  $\tau_q \begin{bmatrix} \ddot{q}_z \\ \ddot{q}_a \end{bmatrix}$  gives

$$D(q)\tau_q \begin{bmatrix} \ddot{q}_z \\ \ddot{q}_a \end{bmatrix} + H(q, \dot{q}) = \begin{bmatrix} 0_{2 \times 10} \\ I_{10 \times 10} \end{bmatrix} u + J_E^T(q) F_e, \quad (4.25)$$

where  $H(q, \dot{q}) := C(q, \dot{q})\dot{q} + G(q)$  and  $u := (u_\ell^T, u_m^T)^T$ . The first two lines of (4.25) can be written as

$$D_{11}(q)\ddot{q}_z + D_{12}(q)\ddot{q}_a + H_1(q, \dot{q}) = J_{E,1}(q)F_e, \quad (4.26)$$

where  $D_{11}$  is the  $2 \times 5$  upper left sub-matrix of  $D(q)\tau_q$ ,  $D_{12}$  is the  $2 \times 7$  upper right sub-matrix of  $D(q)\tau_q$ , and  $H_1$  and  $J_{E,1}$  denote the first two rows of  $H(q, \dot{q})$  and  $J_E^T(q)$  respectively. Considering that on the zero dynamics, the locomotion output (4.9) is

identically zero, we have  $q_a = \bar{h}(\theta, \alpha_c) := h_\ell^{\text{des}}(\theta) + h_c(\theta, \alpha_c)$ . Then the expressions for  $q_a$ ,  $\dot{q}_a$  and  $\ddot{q}_a$  can be obtained <sup>1</sup> and by substituting in (4.26) and using (4.23) results in

$$D_{11}(q_z)\ddot{q}_z + D_{12}(q_z)\left(\frac{\partial\bar{h}}{\partial\theta}\ddot{\theta} + \frac{\partial^2\bar{h}}{\partial\theta^2}\dot{\theta}^2\right) + H_1(q_z, \dot{q}_z) = J_{E,1}(q_z)F_e, \quad (4.27)$$

which are two out of the five equations needed to describe the swing phase zero dynamics. The other three differential equations result from the impedance dynamics in the arm. Note that the manipulation output (4.11) depends on the arm configuration  $q_m$  and the monotonic variable  $\theta$ , and hence is a function of  $q_z$ . Obtaining the expressions for  $y_m$ ,  $\dot{y}_m$  and  $\ddot{y}_m$  from (4.11) and substituting the results in the desired impedance dynamics (4.12) yields

$$M_m \frac{\partial h_m}{\partial q_z} \ddot{q}_z + M_m \psi_m(q_z, \dot{q}_z) \dot{q}_z + \frac{N_m}{\epsilon_m} \frac{\partial h_m}{\partial q_z} + \frac{K_m}{\epsilon_m^2} h_m = F_e. \quad (4.28)$$

where  $\psi_m(q_z, \dot{q}_z) := \frac{d}{dt}\left(\frac{\partial h_m(q_z)}{\partial q_z}\right)$ . Combining (4.27) and (4.28), the five DOF swing phase zero dynamics can be obtained as

$$D_z(q_z)\ddot{q}_z + H_z(q_z, \dot{q}_z) = J_z(q_z)F_e \quad (4.29)$$

where

$$D_z := \begin{bmatrix} D_{11}(q_z) + \begin{bmatrix} 0_{2 \times 1} & D_{12}(q_z) \frac{\partial \bar{h}}{\partial \theta} & 0_{2 \times 3} \end{bmatrix} \\ M_m \frac{\partial h_m}{\partial q_z} \end{bmatrix}$$

$$H_z := \begin{bmatrix} H_1(q_z, \dot{q}_z) + D_{12}(q_z) \frac{\partial^2 \bar{h}}{\partial \theta^2} \dot{\theta}^2 \\ M_m \psi_m(q_z, \dot{q}_z) \dot{q}_z + \frac{N_m}{\epsilon_m} \frac{\partial h_m}{\partial q_z} + \frac{K_m}{\epsilon_m^2} h_m \end{bmatrix}, \quad J_z(q_z) := \begin{bmatrix} J_{E,1}(q_z) \\ I_{3 \times 3} \end{bmatrix}$$

The explicit form of the zero dynamics is important in our application. First, it is clearly seen from (4.27) that the evolution of the unactuated DOF's  $q_1$  and  $\theta$  are affected by the external force. Physically, this means that the biped changes its heading

---

<sup>1</sup> Since  $\alpha_c$  remains constant throughout the step, we can treat it as a parameter and the dependence of  $\bar{h}$  on  $\alpha_c$  will be suppressed.

angle as well as its speed in response to external force. Second, the dynamics of  $q_1$  and  $\theta$  in (4.27) are coupled, implying that a speed change in the direction of motion of the biped may change the heading angle as well. The choice of the locomotion output plays an important role in the dynamics of (4.27) and influences this coupling behavior. Therefore, if a desired response to an external force is sought, one can optimize the parameters of the locomotion output accordingly; this topic will be further discussed in Section 4.4.2. Third, in the absence of perturbations, the evolution of the biped can be obtained by integration of the reduced system (4.28), significantly reducing the computational time compared to integrating the full-order system (4.1),.

#### 4.4 Examples

In this section, details regarding the implementation of the controller are discussed and the method is evaluated in simulation to steer a 3D biped amidst obstacles based on the external force generated during the execution of a collaborative task. We first need to compute unforced walking motions which correspond to fixed points of the Poincaré map (4.18) defined as  $x_2^* = P(x_2^*)$ . Particularly, we are interested in unforced straight walking motions that are symmetric along the X-axis of the world frame; see Fig. 4.1. For the periodic walking motion to be symmetric, it is required that the duration of the steps be equal, i.e.  $T_{1,1} = T_{1,2} = T_1$ , and in addition for all  $0 \leq t \leq T_1$

$$\varphi_1(t, x_1^+) = E_s \varphi_2(t, x_2^+) , \quad (4.30)$$

where  $\varphi_1$  and  $\varphi_2$  are the maximal unforced solutions of the two continuous phases in (4.5), and

$$E_s = \begin{bmatrix} F_s & 0_{12 \times 12} \\ 0_{12 \times 12} & F_s \end{bmatrix}, \quad F_s = \text{diag}(-1, 1, -1, 1, 1, -1, -1, 1, 1, -1, 1, 1) . \quad (4.31)$$

As a result, the search for the fixed point of the Poincaré map can be reduced to finding  $x_2^*$  that satisfies

$$E_s x_2^* = P_{21}(x_2^*) , \quad (4.32)$$

where  $P_{21}$  is the partial map in (4.16). Additional constraints related to actuator saturation, foot-ground interaction and other specifications similar to [111, Section 3.2] should also be considered when searching for the fixed point.

In Sections 4.4.1 and 4.4.2 below, we focus on the effect of force on locomotion. To do so, we stiffen the arm dynamics in response to the force by selecting relatively high gains for the impedance controller; in more detail, we select  $\epsilon_m = 0.1$ ,  $M_m = I_{3 \times 3}(Kg)$ ,  $K_m = 20I_{3 \times 3}(N/m)$ ,  $N_m = 4I_{3 \times 3}(Ns/m)$ , where  $I_{3 \times 3}$  is the  $3 \times 3$  identity matrix. In cooperation scenarios in Sections 4.4.3 and 4.4.4, we allow the arm to exhibit compliance to the interaction force by selecting  $\epsilon_m = 0.5$ .

#### 4.4.1 An Example of Periodic Gait under External Force

Following the procedure above, a symmetric periodic gait along the X-axis was computed. The walking gait has a step length of 0.12 m, a period of 0.52 s, and an average walking speed of 0.23 m/s. Now suppose that a constant external force along the X direction is applied on the end-effector of the biped. As the red markers in Fig. 4.2(a) indicate, the biped responds to this force by taking faster steps and it eventually converges to a new constant speed. However, the center of mass trajectory of the biped deviates from the X direction; see red line in Fig. 4.2(b). This is not surprising, as  $F_{e,x}$  affects the dynamics of the heading angle  $q_1$  despite the fact that it is perfectly aligned with the direction of the unforced motion; this is evident by (4.27). Clearly, this behavior is undesirable in a cooperation task. It implies that if the leader intends to accelerate or decelerate the biped along the direction of motion, it will also need to apply possibly large forces in the Y direction to keep the biped walking straight. The next section proposes a way to minimize this effect by seeking a new optimized periodic gait.

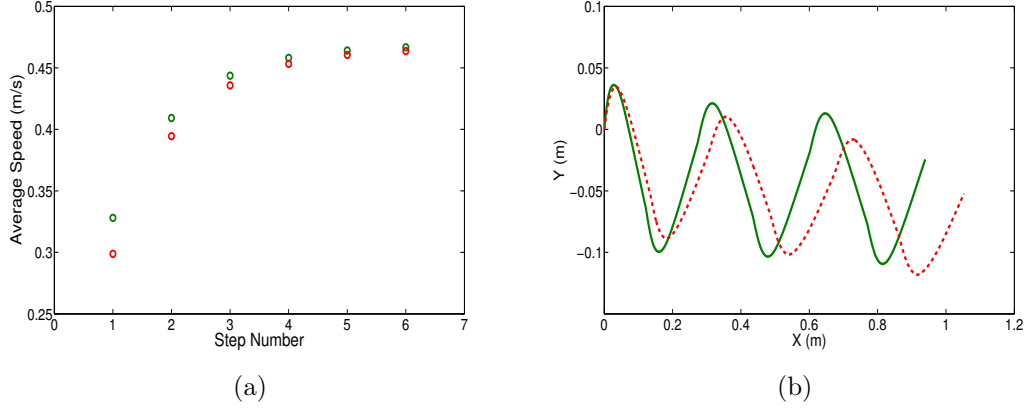


**Figure 4.2:** Comparison of the behavior of two periodic gaits in response to the external force  $F_e = (5, 0, 0)^T N$ . (a) Average speed (b) Trajectory of biped's COM. The green color refers to the periodic gate that minimizes (4.33); i.e. the change in the heading angle of biped is less sensitive to the external force in the X direction.

#### 4.4.2 Optimized Periodic Gait with Respect to External Force

The existence of an external force applied at the end effector calls for additional specifications to be considered when computing unforced periodic motions. To reduce the effect of  $F_{e,x}$  on the heading angle, we consider the cost function

$$\left| \frac{\partial P^{(q_1)}(x)}{\partial F_{e,x}} \right|_{x=x^*} \quad (4.33)$$

in the optimization process described in Section 4.4. Initializing the optimization process from the previous fixed point, a new periodic motion is computed that minimizes the cost function in (4.33). The new walking gait has a step length of 0.13 m, a period of 0.48 s, and an average walking speed of 0.27 m/s. It is interesting to note that the new periodic gait has similar locomotion pattern compared to the previous one, but the nominal motion of the arm is significantly different. The green markers in Fig. 4.2(a) show that the biped increases its speed in response to the horizontal external force, while Fig. 4.2(b) indicates that the biped has smaller deviation from the X direction compared to the previous gait. This behavior is beneficial in a cooperation task, since

the leader does not need to apply excessive force in the Y direction to enforce its walking motion along the X direction.

#### 4.4.3 Straight Walking with Leader

We will now examine the response of the periodic gait computed in Section 4.4.2 to the interaction force that is generated by the cooperation model in Section 3.1.2. To simulate the cooperative task, the intention of the leader is translated to the interaction force through an impedance model

$$F_e = K_L y_L + N_L \dot{y}_L \quad , \quad (4.34)$$

where

$$y_L = h_L(t) := p_L(t) - p_E(q(t)) \quad . \quad (4.35)$$

and  $K_L$  and  $N_L$  are the corresponding stiffness and damping matrices of the leader,  $p_E(q(t))$  is the current position vector of biped's end-effector, and  $p_L(t)$  is the location at which the leader intends to drive it; see Section 3.1.2 for more details. The impedance parameters of the leader are selected as  $K_L = 10I_{3 \times 3}$  N/m and  $N_L = 2I_{3 \times 3}$  Ns/m.

To investigate how the biped adapts to changes in the intended speed of the leader, two cases are considered. In the first case, the leader starts walking in the X direction with a speed greater than that of the biped; see Fig. 4.3(a). In accordance to (4.34), the interaction force shown in Fig. 4.3(c) increases, forcing the biped to take faster steps. When the biped reaches the intended speed, the interaction force stops growing and becomes periodic, eventually causing the biped to converge to a new forced limit cycle that corresponds to the increased speed as shown in Fig. 4.4(a) and 4.4(c). Note that the biped almost aligns its direction of motion with that of the leader as it is evident in Fig. 4.3(e). In the second case, the leader's intended speed decreases, thereby resulting in a negative force that opposes the biped's motion; see Fig. 4.3(d). The biped responds to this interaction by taking slower steps and matching its speed

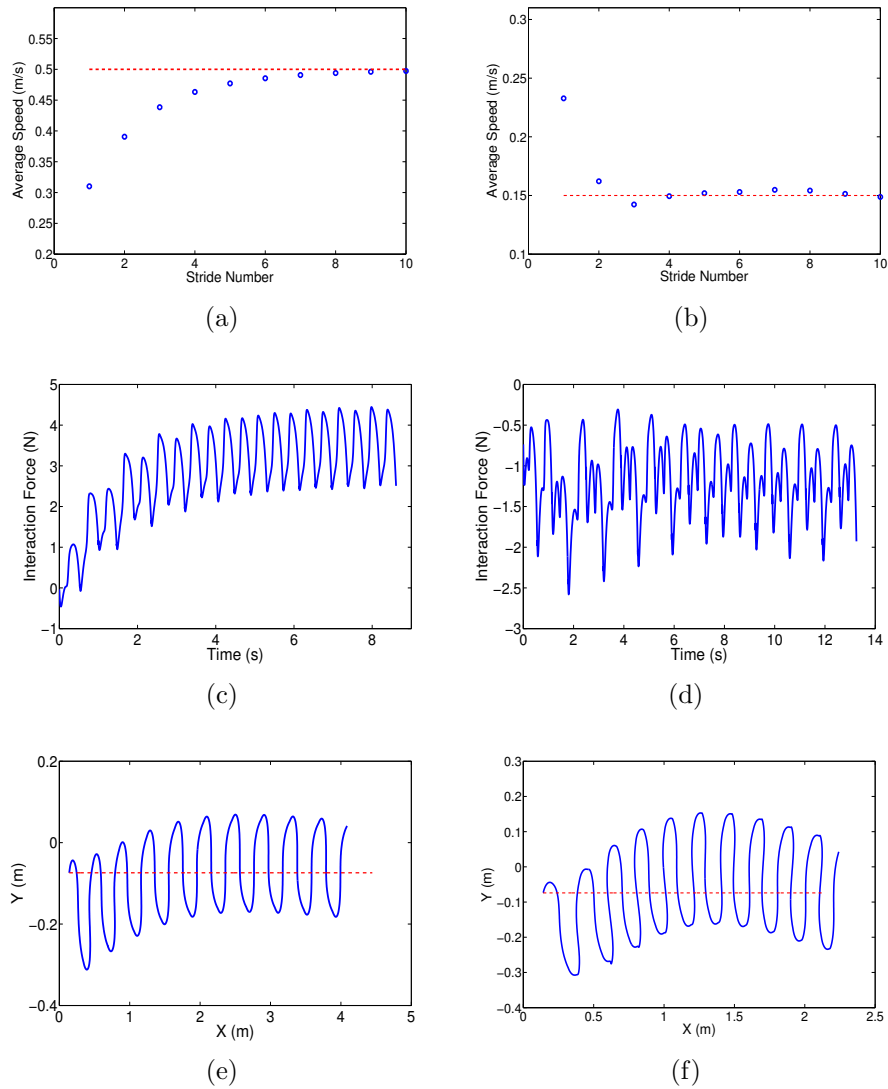


**Figure 4.3: Left:** Response of a 3D biped when the leader walks along the X direction with higher average speed than that of the biped. **Right:** Response of a 3D biped when the leader walks along the X direction with lower average speed than that of the biped. (a) and (b) Intended average speed of leader (dashed red line) and average speed of biped (blue marker). (c) and (d) Component of interaction force in the X direction. (e) and (f) Intended trajectory of leader (dashed red line) and trajectory of biped's end effector (solid blue line) in the X-Y plane.

to that intended by the leader as shown in Fig. 4.3(b), without deviating much from the intended direction of leader as shown in Fig. 4.3(f).

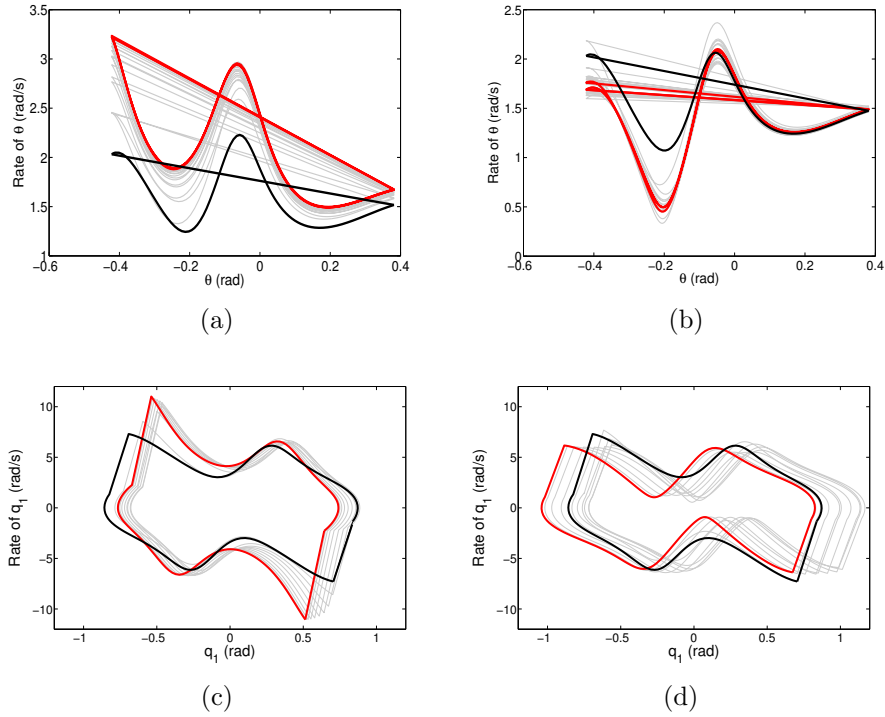


**Figure 4.4: Left:** Response of a 3D biped when the leader walks along the X direction with higher average speed than that of the biped. **Right:** Response of a 3D biped when the leader walks along the X direction with lower average speed than that of the biped. (a) and (b) Convergence of limit cycles in terms of  $\theta$  and  $\dot{\theta}$ . (c) and (d) Convergence of limit cycles in terms of  $q_1$  and  $\dot{q}_1$ . Black is the base (unforced) limit cycle, gray is the transitioning and red is the final forced limit cycle.

Note that as we can see from Figs. 4.4(a) and 4.4(b) that correspond to the acceleration and deceleration cases, the range of values of  $\theta$  remains the same, while the rate of change of  $\theta$  changes. This observation verifies the discussion in Section 4.3 that the stride length of the biped remains constant as its speed changes. On the other hand, as it is shown in Figs. 4.4(c) and 4.4(d), the interaction force changes the evolution of both heading angle  $q_1$  and its derivative  $\dot{q}_1$ , while the overall direction of biped's motion almost remains in the X direction; the direction the biped was walking in the absence of force.

#### 4.4.4 Steering the Biped to a Goal Region

We now consider a scenario in which a leading collaborator – possibly a human – intends to move an object with the help of a bipedal robot to a desired location in the workspace of Fig. 4.5(a). The leader plans an obstacle-free trajectory  $p_L(t)$  for the object so that all the specifications of the task are fulfilled. The biped needs to adapt its motion to the leader’s intended trajectory, the explicit form of which is unknown. However, it turns out that the interaction force developed as a result of the leader’s intentions can provide sufficient information to steer the biped accordingly. In the simulations that follow, care is taken so that actuator saturation and friction cone limitations are respected throughout the motion of the biped.

Figures 4.5(b) and 4.5(c) present the interaction force and average speeds of the biped and the leader, respectively. As expected, the biped perceives the leader’s acceleration as an increase in the X component of the force, and its left turning as an increase in the Y component; see Fig. 4.5(b). As the biped turns, its average speed converges to that of the leader, as shown in Fig. 4.5(c). After the narrow passage between the two obstacles of Fig. 4.5(a), the biped is guided to walk with the same speed and direction it started. As a result, the biped converges to a new forced limit cycle that is almost identical to the unforced one, as Fig. 4.5(d) and 4.5(e) show.

It is natural to ask under what conditions the biped adapts its motion in response to the interaction force. Unlike the planar case, we cannot derive such conditions analytically in the 3D case due to the high-dimensional FHZD (4.22). Nevertheless, we observe in simulation that – similarly to the planar case – the biped fails when the moment of the interaction force around the stance ankle either prevents the robot to complete a step, or results in a violation of the actuation and ground contact constraints. The former occurs when the leader’s speed is much lower than that of the unforced motion of the biped or when the leader makes sharp turns, while the latter failure happens when the leader’s speed is much greater than that of the unforced motion.

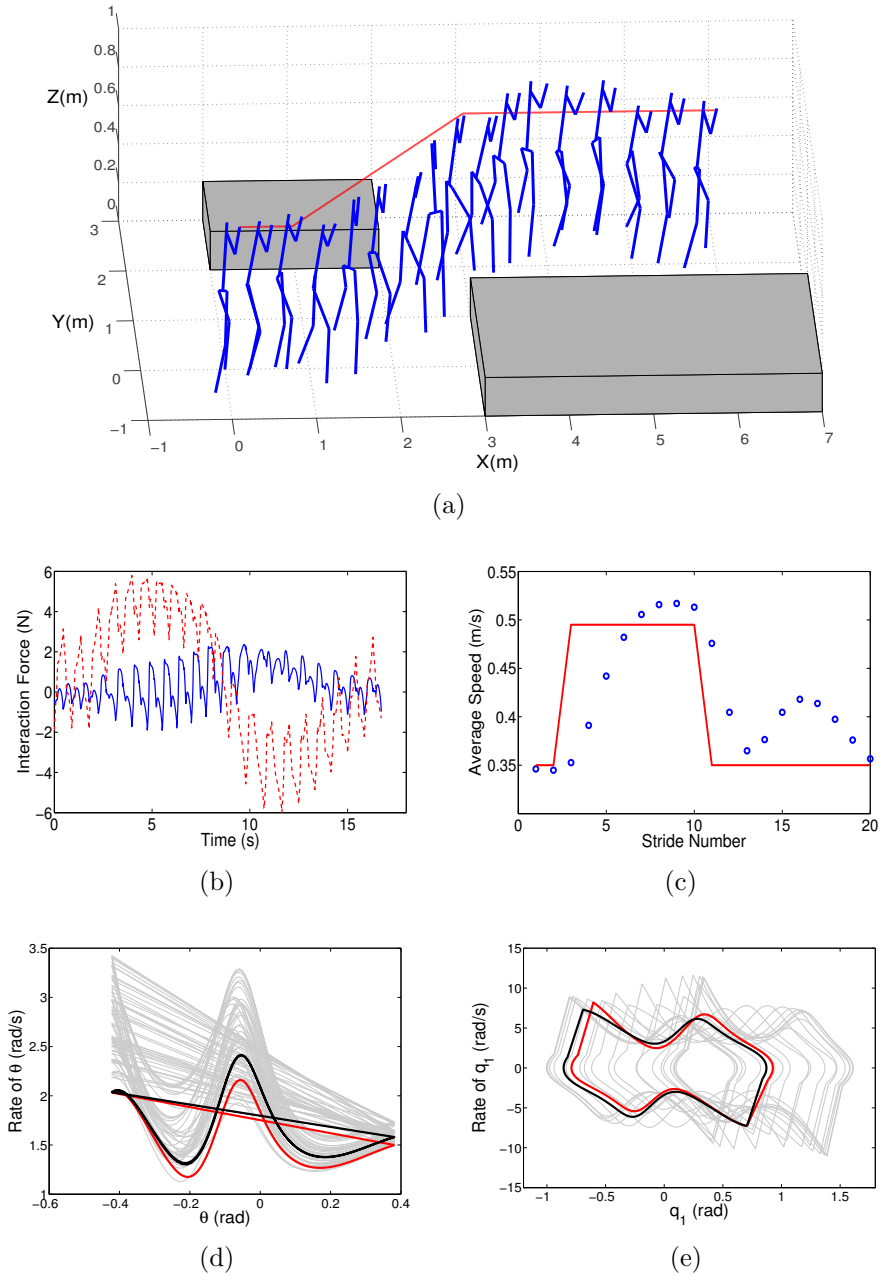


**Figure 4.5:** (a) Biped-leader cooperation in an environment with obstacles. The intended trajectory of the leader is denoted as red line. (b) X component (blue) and Y component (dashed red) of the interaction force. (c) Intended average speed of the leader (red) and average speed of the biped (blue). (d) Convergence of limit cycles in terms of  $\theta$  and  $\dot{\theta}$ . (e) Convergence of limit cycles in terms of  $q_1$  and  $\dot{q}_1$ . Black is the base (unforced) limit cycle, red is the final forced limit cycle and gray correspond to transition.

## 4.5 Discussion

This chapter proposed a framework for cooperation of a bipedal robot with a leading co-worker in 3D spaces; see Fig. 4.6. At the high level, the leading collaborator, who has knowledge of the environment, chooses an obstacle-free trajectory  $p_L$ , which is a signal exogenous to the biped’s dynamics. Through the interaction of the robot with the leader, the trajectory is then transformed to a force  $F_e$  that is applied on the robot’s end effector. This force acts as a command signal for the robot with the purpose of guiding its motion along the desired trajectory. At the low level, the locomotion controller generates limit-cycle gaits that are capable of adapting to interaction force. Essentially, the controller modifies the speed and heading angle of the robot in response to a high-level descending signal, which in the scenario examined in Chapters 3 and 4 represents the interaction force between the biped and the external collaborator in a collaborative object transportation task. In the following chapter, this exogenous high-level command signal will be the output of motion planning algorithm, the purpose of which is to steer the biped to a goal location while avoiding any obstacles that exist in the workspace.

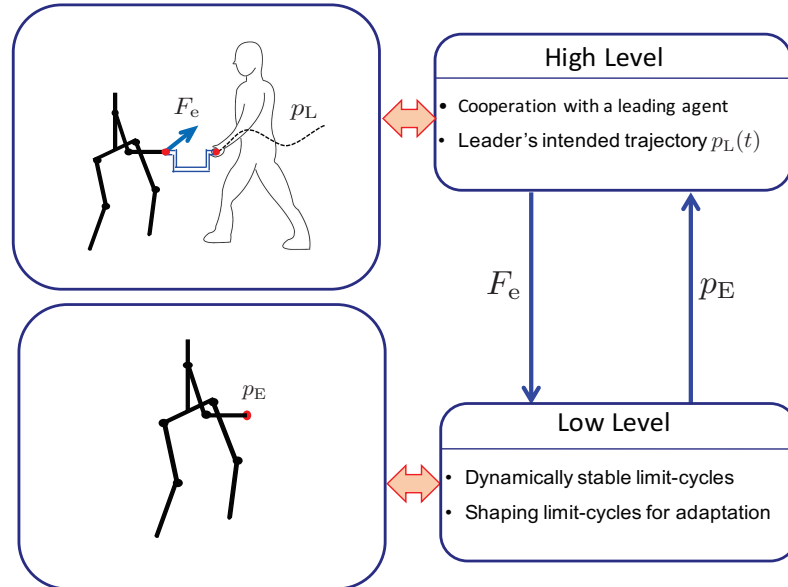


**Figure 4.6:** The hierarchical components for a cooperation task in 3D space. The leading co-worker plans a trajectory  $p_L$  and guides the robot to follow it by applying a suitable force at the biped’s end effector.

## Chapter 5

### A SWITCHED SYSTEM APPROACH TO MOTION PLANNING OF LIMIT CYCLE ROBOTIC SYSTEMS WITH APPLICATION TO 3D BIPEDAL WALKERS

This chapter presents a framework for autonomous navigation of a 3D bipedal robot in an environment cluttered by obstacles. The autonomous navigation problem differs from what we studied in the previous chapters in that the motion of the robot is guided by a high-level motion planning algorithm instead of a leading co-worker. In both cases, a descending command signal is applied to the biped, which must adapt its motion to this signal to achieve the desired task; however, the nature of this signal is different. In this chapter, instead of the continuous time leader's intended trajectory that is communicated to the biped through the interaction force, the descending signal is a sequence of limit-cycle motion primitives that must be composed to navigate the biped in its workspace. It should be emphasized that the method proposed in this chapter can be used to plan motions in other robotics systems, which like legged robots, exhibit periodic motions, such as flying robots with flapping wings [17], turtle-like robots [91] and quadrupedal robots [50]. The structure of this chapter is as follows. Section 5.1 describes the motion planning problem for general robotic systems that admit exponentially stable motion primitives in the form of limit cycles. In Section 5.2, the concatenation of motion primitives is formulated as a discrete-time switched system with multiple equilibria, and stability guarantees for the motion sequence are provided by analytical bounds on the dwell time of the switching signal. These bounds distill stability limitations of the system dynamics, and when communicated to the motion planner, ensure that the suggested plan stably brings the robot to the desired goal region. The stability analysis of the switched system also gives a compact trapping set

in the state-space within which the solution evolves, thus providing a way to compute bounds on the deviation of the robot from the nominal plan. Section 5.3 demonstrates this method on a 3D biped model with a hybrid zero dynamics based controller. Note that the dimensional reduction inherent to the hybrid zero dynamics method facilitates the computation of estimates of the basin of attraction of each motion primitive using sums-of-squares programming, thus allowing the analytical computation of dwell-time bounds. Finally, Section 5.4 summarizes the contributions of this chapter. The results of this chapter have appeared in [71, 107].

## 5.1 Problem Formulation

We are interested in motion planning of robotic systems that exhibit periodic motions. As in dynamic legged systems, these periodic motions can be represented as fixed points of Poincaré maps

$$x[k + 1] = P_p(x[k]) \ . \quad (5.1)$$

As a limit cycle is realized, the periodic motion of the robot’s joints results in its center of mass (COM) moving in the workspace. The motion of COM can be characterized as a net change in the robot’s coordinates in  $SE(3)$ , and is considered as the output  $H_p(x)$  of the system

$$w[k] = H_p(x[k]) \ .$$

We assume that each  $P_p(x)$  is locally exponentially stable with the fixed point  $x_p^*$ , and  $p \in \mathcal{P}$  is an index from a finite index set  $\mathcal{P}$  corresponding to different behaviors of the system. A motion primitive can be defined as a pair  $\mathcal{G}_p(x) = \{P_p(x), H_p(x)\}$ . The planner endowed with the collection  $\mathbb{M} = \{\mathcal{G}_p(x), p \in \mathcal{P}\}$  is tasked to output a suitable sequence of motion primitives based on a high-level logic to achieve a desired objective. In this context, the planner sequentially composes motion primitives resulting in a switching signal  $\sigma : \mathbb{Z}_+ \rightarrow \mathcal{P}$  that maps the discrete-time  $k$  to the corresponding motion primitive  $p = \sigma(k)$  to be executed in the current step. In general, the computation

of the motion primitive  $\mathcal{G}_p(x)$  would require evaluating the corresponding sub-system  $P_p(x)$ . This would slow down the planning process considerably, since the maps  $P_p(x)$  are not in general analytically available and may only be obtained by numerical integration. To speed up the planning, one can admit a limited set of actions available to the planner that corresponds to a discrete set of fixed points  $x_p^*$ , namely *nominal motion primitives* defined by  $\mathcal{G}^*(x_p^*) := \mathcal{G}(x_p^*) = \{P_p(x_p^*), H_p(x_p^*)\}$ , which essentially reduce to the output  $H_p(x_p^*)$ . The fact that the planning algorithm has a discrete collection of actions  $\{H_p(x_p^*), p \in \mathcal{P}\}$  available significantly reduces the time required to compute feasible plans.

## 5.2 Stable switching among multiple equilibria

Switching among systems with a common exponentially stable equilibrium may result in unstable behavior [60]. Certain constraints imposed on the switching signal, such as slow switching can alleviate this behavior, as illustrated in [60]. However, (5.1) differs from the switched systems studied in [60] in that the individual maps  $\{P_p, p \in \mathcal{P}\}$  do *not* share a common equilibrium. Thus, the solution of (5.1) is not expected to converge to any one of the equilibrium points under switching. The main results of this section provide conditions that ensure the system's solution remains trapped in a compact set that includes the equilibrium points. This compact set can be explicitly characterized as the union of sub-level sets of Lyapunov functions, and its size is essential in estimating the drift that arises when using the nominal motion primitives for planning.

### 5.2.1 Set Constructions

We work in an open connected set  $\mathcal{D}$  over which  $P_p$  is well defined for all  $p \in \mathcal{P}$ . It is assumed that  $x_p^* \in \mathcal{D}$  for all  $p \in \mathcal{P}$ ; that is, all fixed points are contained in  $\mathcal{D}$ .

**Definition 1.** A continuous function  $V_p : \mathcal{D} \rightarrow \mathbb{R}$  is an exponential Lyapunov function, if for all  $x \in \mathcal{D}$

$$\chi_{p,1}(\|x - x_p^*\|) \leq V_p(x) \leq \chi_{p,2}(\|x - x_p^*\|) , \quad (5.2)$$

$$V_p(x[k+1]) \leq \epsilon V_p(x[k]) , \quad (5.3)$$

where  $\chi_{p,1}, \chi_{p,2}$  are class- $\mathcal{K}$  functions and  $0 < \epsilon < 1$ .

Owing to the local and discrete nature of the system, the evolution of the state can jump out of  $\mathcal{D}$  in one step, resulting in the Lyapunov function  $V_p(x[k+1])$  of (5.3) not to be well defined. Certain constructions as outlined in the proof of [35, Theorem 13.2], are necessary to ensure that the sub-level sets  $\mathcal{D}_p$  of the Lyapunov functions are well defined and positively invariant. All our future constructions will be restricted within the intersection  $\underline{\mathcal{D}} := \bigcap_{p \in \mathcal{P}} \mathcal{D}_p$  of the positively invariant sets, and we require  $\underline{\mathcal{D}}$  to satisfy the following requirement:

- $\underline{\mathcal{D}} \neq \emptyset$ , and
- $x_p^*$  is an interior point of  $\underline{\mathcal{D}}$  for all  $p \in \mathcal{P}$ ,

Now we turn our attention towards set constructions motivated from [2] which are essential in presenting the main results of this section. For each  $p \in \mathcal{P}$ , let

$$\mathcal{N}_p(\kappa) := \{x \in \mathcal{D} : V_p(x) \leq \kappa\} , \quad (5.4)$$

and let the union of these sets over all  $p \in \mathcal{P}$  be

$$\mathcal{N}(\kappa) := \bigcup_{p \in \mathcal{P}} \mathcal{N}_p(\kappa) , \quad (5.5)$$

which is not necessarily connected. Next, define

$$\omega_p(\kappa) := \max_{x \in \mathcal{N}(\kappa)} V_p(x) , \quad (5.6)$$

and let  $\omega_{\max}(\kappa)$  and  $\omega_{\min}(\kappa)$  be the maximum and minimum of  $\omega_p(\kappa)$  over the finite index set  $\mathcal{P}$ , respectively. Let

$$\mathcal{M}_p(\kappa) := \{x \in \mathcal{D} : V_p(x) \leq \omega_p(\kappa)\} . \quad (5.7)$$

We require that  $\mathcal{M}_p(\kappa) \subset \underline{\mathcal{D}}$  for all  $p \in \mathcal{P}$ , and complete our constructions by defining

$$\overline{\mathcal{M}}(\kappa) := \bigcup_{p \in \mathcal{P}} \mathcal{M}_p(\kappa) , \quad \underline{\mathcal{M}}(\kappa) := \bigcap_{p \in \mathcal{P}} \mathcal{M}_p(\kappa) . \quad (5.8)$$

Note that

$$\mathcal{N}(\kappa) \subset \underline{\mathcal{M}}(\kappa) , \quad (5.9)$$

and that the set  $\overline{\mathcal{M}}(\kappa)$  is connected. See Fig. 5.1 for a schematic of the set-constructions.

With these set constructions, we are ready to state the main result of this section, which guarantees that a solution of (5.1) that starts in  $\underline{\mathcal{M}}(\kappa)$  will stay in  $\overline{\mathcal{M}}(\kappa)$  for all future time steps, provided that a bound on the dwell time of the switching signal  $\sigma$  is respected.

### 5.2.2 Stability of the switched system with dwell-time

Let  $\sigma : \mathbb{Z}_+ \rightarrow \mathcal{P}$  be a switching signal with  $p = \sigma(k)$ , and let  $\{k_1, k_2, \dots\}$  be the corresponding switching times. The dwell time  $N_d \geq 1$  represents the minimum number of steps between two successive switches in  $\sigma$ ; i.e.,  $\sigma(k_i + k) = \sigma(k_i)$  for all  $k < N_d$ . The class of signals that satisfy the  $N_d$  dwell-time constraint is denoted by  $\mathcal{L}_d[N_d]$ . With the definition of dwell-time, we are ready to state the main result of this section.

**Theorem 1.** *Consider (5.1) and assume that for each  $p = \sigma(k) \in \mathcal{P}$  there exists a function  $V_p : \mathcal{D} \rightarrow \mathbb{R}$  that satisfies the conditions of Definition 1. Let  $\mu(\kappa) > 1$  be such that*

$$\frac{V_{p_i}(x)}{V_{p_j}(x)} \leq \mu(\kappa), \quad \forall p_i, p_j \in \mathcal{P}, \quad \forall x \in \mathcal{D} \setminus \mathcal{N}(\kappa) . \quad (5.10)$$

Assume further that the dwell time  $N_d \in \mathbb{Z}_+$  of the switching signal  $\sigma$  satisfies

$$N_d \geq \frac{\log\left(\mu(\kappa) \frac{\omega_{\max}(\kappa)}{\omega_{\min}(\kappa)}\right)}{\log(1/\epsilon)}. \quad (5.11)$$

Then, for every initial condition in the set  $\underline{\mathcal{M}}(\kappa)$ , the solution of (5.1) remains in  $\overline{\mathcal{M}}(\kappa)$ .

*Proof.* Consider an arbitrary switching signal  $\sigma : \mathbb{Z}_+ \rightarrow \mathcal{P}$  with switching times  $\{k_1, k_2, \dots\}$ . Without loss of generality, assume that the system starts at  $k = 0$  and let  $x[0] \in \underline{\mathcal{M}}(\kappa)$ . This implies that  $x[0] \in \mathcal{M}_p(\kappa)$  for all  $p \in \mathcal{P}$  so that  $x[0] \in \mathcal{M}_{\sigma(0)}(\kappa)$ . Thus,

$$V_{\sigma(0)}(x[0]) \leq \omega_{\sigma(0)}(\kappa), \quad (5.12)$$

and by (5.3),  $V_{\sigma(0)}(x[k]) \leq \omega_{\sigma(0)}(\kappa)$  for all  $0 \leq k \leq k_1$ , implying that  $x[k] \in \mathcal{M}_{\sigma(0)}(\kappa) \subset \overline{\mathcal{M}}(\kappa)$  for all  $0 \leq k \leq k_1$ .

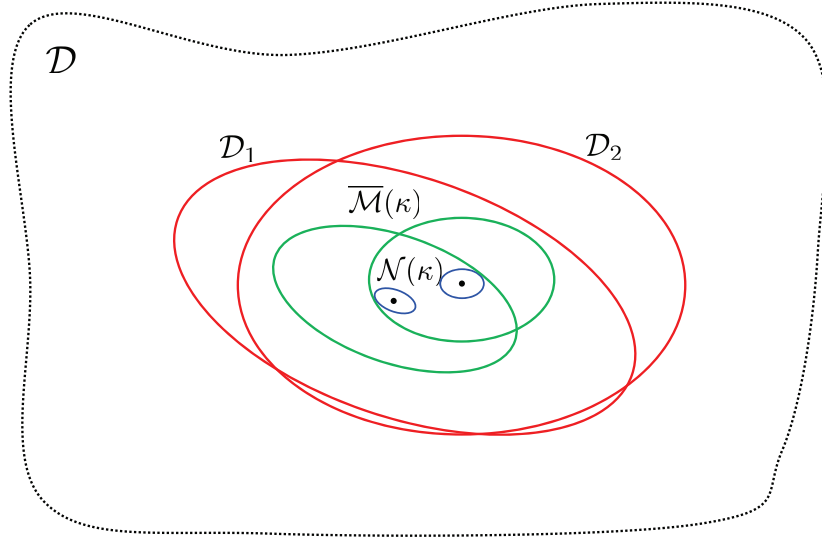


**Figure 5.1:** Schematic of the set construction for two discrete systems with different equilibria. The open domain  $\mathcal{D}$  of the discrete maps is represented by the black dotted outer boundary. The largest positive invariant sub-level sets  $\mathcal{D}_1$  and  $\mathcal{D}_2$  in the domain  $\mathcal{D}$  are represented by red.  $\overline{\mathcal{M}}(\kappa)$  is represented by green, and  $\mathcal{N}(\kappa)$  is represented by blue. The  $\overline{\mathcal{M}}(\kappa)$  construction lies entirely within  $\mathcal{D}_1 \cap \mathcal{D}_2$ .

Note that, at the switching time  $k_1$ , the state  $x[k_1] \in \overline{\mathcal{M}}(\kappa)$ , and we distinguish the following cases:

*Case I:*  $x[k_1] \in \underline{\mathcal{M}}(\kappa)$ . Then, arguing as above we have that  $V_{\sigma(k_1)}(x[k_1]) \leq \omega_{\sigma(k_1)}(\kappa)$ , and thus  $x[k] \in \mathcal{M}_{\sigma(k_1)}(\kappa) \subset \overline{\mathcal{M}}(\kappa)$  over the interval  $k_1 \leq k \leq k_2$ .

*Case II:*  $x[k_1] \in \overline{\mathcal{M}}(\kappa) \setminus \underline{\mathcal{M}}(\kappa)$ . In fact, we will show by contradiction that this case is not possible due to the condition (5.11) imposed on the dwell time. By (5.9),  $\mathcal{N}(\kappa) \subset \underline{\mathcal{M}}(\kappa)$  and thus the fact that  $x[k_1] \notin \underline{\mathcal{M}}(\kappa)$  implies that  $x[k_1] \notin \mathcal{N}(\kappa)$ . Then, (5.10) can be used to obtain  $V_p(x[k_1]) \leq \mu V_{\sigma(0)}(x[k_1])$  for all  $p \in \mathcal{P}$ , which by (5.3) results in  $V_p(x[k_1]) \leq \mu \epsilon^{k_1} V_{\sigma(0)}(x[0])$  for all  $p \in \mathcal{P}$ . Then, since  $k_1 \geq N_d$  by the definition of the dwell time, we obtain

$$V_p(x[k_1]) \leq \mu \epsilon^{N_d} V_{\sigma(0)}(x[0]) \quad \forall p \in \mathcal{P} . \quad (5.13)$$

In view of (5.11), we have  $\mu \epsilon^{N_d} \leq \omega_{\min}(\kappa)/\omega_{\max}(\kappa)$ , and by using (5.12) and (5.13) we obtain

$$V_p(x[k_1]) \leq \frac{\omega_{\min}(\kappa)}{\omega_{\max}(\kappa)} \omega_{\sigma(0)}(\kappa) \leq \omega_{\min}(\kappa) \quad \forall p \in \mathcal{P} , \quad (5.14)$$

which implies that for any  $p \in \mathcal{P}$  that is “switched in” at  $k_1$ ,  $x[k_1] \in \mathcal{M}_p(\kappa)$ . Thus,  $x[k_1] \in \underline{\mathcal{M}}(\kappa)$ , which contradicts the initial assumption that  $x[k_1] \in \overline{\mathcal{M}}(\kappa) \setminus \underline{\mathcal{M}}(\kappa)$ , essentially guaranteeing that Case II does not emerge.

Hence, for any  $x[0] \in \underline{\mathcal{M}}(\kappa)$ , we have shown that  $x[k] \in \overline{\mathcal{M}}(\kappa)$  over the interval  $0 \leq k \leq k_1$ . Then, the constraint (5.11) on the dwell time ensures that  $x[k_1] \in \underline{\mathcal{M}}(\kappa)$  so that  $x[k] \in \overline{\mathcal{M}}(\kappa)$  over the interval  $k_1 \leq k \leq k_2$ . Propagating this construction to future time steps proves the result.  $\square$

An immediate consequence of Theorem 1 is the following Corollary that will be useful for our planning purposes.

**Corollary 1.** *Under the assumptions of Theorem 1, for every initial condition in the set  $\mathcal{N}(\kappa)$ , the solution of (5.1) will remain in  $\overline{\mathcal{M}}(\kappa)$  for all future times.*

Theorem 1 has some important implications for planning. First, it constraints the switching signal in a way that the stability limitations imposed by the different dynamics of motion primitives do not destabilize the overall motion. Second, the constraint (5.11) can readily be integrated in the planning algorithm due to its analytically explicit form so that descending commands from the high-level planner respect the dynamics of the low-level platform. Third, Theorem 1 provides a means of regulating the size of the compact set within which the state of (5.1) evolves, by adjusting the parameter  $\kappa$ .

When planning with nominal motion primitives, the size of the compact set can be used to estimate the deviation of the robot from the nominal plan; as will be shown in Section 5.3.6.1 below. Reducing the size of the compact set ensures smaller deviations from the nominal plan, at the expense of more stringent constraints on the switching signal, which in turn reduces the flexibility of the planner in providing a path that respects the geometry of the workspace.

### 5.3 Application to 3D Bipedal Walking

We will now explore some of the implications of Theorem 1 in the context of the 3D bipedal model of Fig. 5.2 walking under the influence of an HZD control law. It should be emphasized that the dimensional reduction afforded by HZD, greatly facilitates the set constructions of Theorem 1 and the verification of the basins of attraction of the corresponding gait primitives via established SOS techniques.

#### 5.3.1 A Model of 3D Bipedal Walking

We consider a model similar to the one used in Section 4.1.1; as shown in Fig. 5.2 the only difference is that the arm is removed for simplicity. We assume that the stance foot acts as a pivot with three rotational DOFs corresponding to the yaw  $q_1$ , pitch  $q_2$ , and roll  $q_3$  angles; see Fig. 5.2. In total, during the single support phase, the model has nine degrees of freedom  $q := (q_1, \dots, q_9)^T \in \mathcal{Q}$ , where  $\mathcal{Q}$  contains physically reasonable

configurations of the system. Seven actuators – four located at the hip joints, two at the knee joints and one at the roll joint of the foot – provide the input torques.

As in Section 4.1.1, due to the nontrivial length of the hip joint, the equations of motion during the left and right leg support phases are different. In what follows, we briefly describe the model for the left leg support phase; the equations for the right leg are similar. The swing-phase dynamics of the biped during left leg support can be written as

$$D(q)\ddot{q} + C(q, \dot{q})\dot{q} + G(q) = Bu \quad , \quad (5.15)$$

where  $D(q)$  is the mass matrix,  $C(q, \dot{q})\dot{q}$  contains the centrifugal and Coriolis forces and  $G(q)$  contains the gravitational forces. The matrix  $B$  distributes the inputs  $u$  to the configuration variables  $q$ . Defining  $\hat{x} := (q^T, \dot{q}^T)^T$ , the model can be written as

$$\dot{\hat{x}} = f(\hat{x}) + g(\hat{x})u \quad , \quad (5.16)$$

where  $\hat{x} \in T\mathcal{Q} := \{(q^T, \dot{q}^T)^T \mid q \in \mathcal{Q}, \dot{q} \in \mathbb{R}^9\}$  and the vector fields  $f$  and  $g$  are defined accordingly.

The continuous evolution of the swing dynamics (5.16) is interrupted when the swing leg hits the ground; i.e., when the state crosses the surface

$$\mathcal{S} := \{\hat{x} \in T\mathcal{Q} \mid p^v(q) = 0, \dot{p}^v(\hat{x}) < 0\} \quad , \quad (5.17)$$

where  $p^v$  denotes the vertical position of the foot of the swing leg. As in [93], the impact is assumed instantaneous and purely plastic, and can be modeled as a discrete map  $\Delta : \mathcal{S} \rightarrow T\mathcal{Q}$ , as

$$\hat{x}^+ = \Delta(\hat{x}^-) \quad . \quad (5.18)$$

The derivation of the map  $\Delta$  also involves the transformation of coordinates from left leg support to right leg support; see Section 4.1.3 for more details.

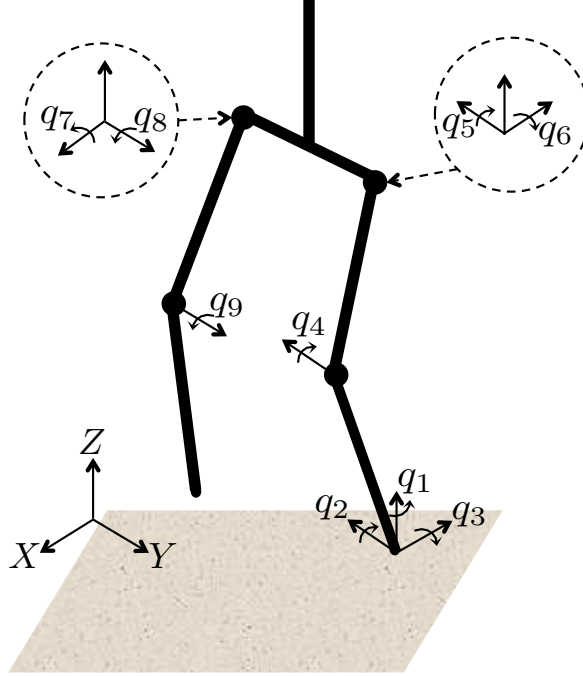


**Figure 5.2:** Robot model with a choice of generalized coordinates when supported on left leg.

### 5.3.2 Equivariance-Preserving Control Law

This section exploits the structure of the Poincaré map to extract a family of exponentially stable motion primitives, which are then concatenated by a planning algorithm to achieve desired objectives, such as reaching a goal position in the biped’s workspace while avoiding obstacles on the way.

We begin by assuming the availability of a family of locally Lipschitz feedback control laws  $\Gamma_p : T\mathcal{Q} \rightarrow \mathbb{R}^7$ ,

$$u = \Gamma_p(\hat{x}) \tag{5.19}$$

indexed by  $p \in \mathcal{P}$ , where  $\mathcal{P}$  is a finite index set corresponding to controllers that enable straight-line and turning motions. Such controllers can be designed using a variety of methods, including [29, 37, 93, 94]; for concreteness, in Section 5.3.3 below we will use HZD to design  $\Gamma_p$ . The dynamics of the biped in closed loop with the control law

(5.19) can be expressed in the form of a system with impulse effects,

$$\Sigma_p : \begin{cases} \dot{\hat{x}} = f_p(\hat{x}), & \hat{x} \notin \mathcal{S} \\ \hat{x}^+ = \Delta(\hat{x}^-), & \hat{x}^- \in \mathcal{S} \end{cases}, \quad (5.20)$$

where  $f_p(\hat{x}) := f(\hat{x}) + g(\hat{x})\Gamma_p(\hat{x})$ , for  $p \in \mathcal{P}$ . To study periodic solutions of  $\Sigma_p$ ,  $p \in \mathcal{P}$ , we use the Poincaré return map  $\hat{P}_p : \mathcal{S} \rightarrow \mathcal{S}$  that transfers the state  $\hat{x}[k]$  one step ahead; i.e.

$$\hat{x}[k+1] = \hat{P}_p(\hat{x}[k]) . \quad (5.21)$$

Restricting the choice of feedback controllers (5.19) so that they do not depend on the yaw angle  $q_1$  results in a symmetry property of the Poincaré map that was established in Proposition 1. As a result, the Poincaré map can be written as

$$\hat{P}_p(\hat{x}) = \begin{bmatrix} q_1 + P_p^{(q_1)}(x) \\ P_p(x) \end{bmatrix}, \quad (5.22)$$

where  $q_1 + P_p^{(q_1)}$  and  $P_p$  are the projections of  $\hat{P}_p$  onto  $q_1$  and  $x$ , respectively.

The structure of the Poincaré map allows the extraction of motion primitives suitable for navigation purposes in workspaces cluttered by obstacles. Intuitively, these motion primitives correspond to cyclic locomotion patterns – that is, limit cycles – which result in a net change of the heading angle. In more detail, such motions can be computed by seeking a fixed point  $x_p^*$  of

$$x[k+1] = P_p(x[k]) , \quad (5.23)$$

i.e.,  $x_p^* = P_p(x_p^*)$ , with  $P_p$  defined by the decomposition of the Poincaré map (5.22). Associated with a fixed point of a Poincaré map  $P_p(x)$ , is a change in the heading angle  $s_p(x) = P_p^{(q_1)}(x)$ , and a change in the position of the center of mass which can be computed as the length  $l_p(x)$  and angle  $o_p(x)$  of the COM displacement vector. We can consider these functions as the output of the system (5.23), i.e.,  $H_p(x) :=$

$$(s_p(x), l_p(x), o_p(x))^T.$$

A motion primitive can now be defined as a pair  $\mathcal{G}_p(x) = \{P_p(x), H_p(x)\}$ . If all the eigenvalues of the linearization  $A_p := \frac{\partial P_p(x)}{\partial x} \Big|_{x=x_p^*}$  of  $P_p$  about the fixed point  $x_p^*$  in (5.23) are located within the unit disc centered at the origin, the fixed point  $x_p^*$  is locally exponentially stable, and so is the corresponding motion primitive  $\mathcal{G}_p$ . The basin of attraction of the fixed point  $x_p^*$  can then be defined as

$$\text{BoA}(x_p^*) = \left\{ x \in \mathcal{S} \mid \lim_{k \rightarrow \infty} P_p^k(x) = x_p^* \right\}, \quad (5.24)$$

where  $P_p^k$  denotes the composition of  $P_p$  with itself  $k$  times when it is defined. In Section 5.3.5.1 below, we characterize the basin of attraction associated with a fixed point  $x_p^*$  using sums-of-squares programming.

Switching between different motion primitives  $\mathcal{G}_p$  is equivalent to switching among different fixed points  $x_p^*$  of (5.23). A motion plan consists of a concatenation of these motion primitives, and can be treated as a switching signal  $\sigma : \mathbb{Z}_+ \rightarrow \mathcal{P}$  that maps the stride number  $k$  to the  $p$ -th Poincaré map, giving rise to the discrete switched system of the form (5.1).

### 5.3.3 HZD Based Controller Design

The controller is developed within the HZD framework as was discussed in Section 4.2.1; thus the exposition here will be terse. We emphasize that the dimensional reduction inherent to the HZD method, greatly facilitates the application of SOS programming for the verification of the basins of attraction of the motion primitives and the set construction in Section 5.2.1. To the continuous dynamics (5.16), associate the output functions

$$y = h(q) := q_a - h^{\text{des}}(\theta(q)), \quad (5.25)$$

where  $q_a := (q_3, \dots, q_9)^T$  includes the controlled variables and  $h^{\text{des}}$  denotes the desired evolution as a function of the monotonic quantity  $\theta(q) = -q_2 - q_4/2$ , which corresponds

to the angle of the line connecting the foot of the support leg with the corresponding hip joint. As in Section 4.2.1,  $h^{\text{des}}$  is designed using Beziér polynomials.

To render the evolution of system, hybrid invariant, we augment the output (5.25) with correction polynomials  $h_c(\theta, \alpha_c)$ , i.e.,

$$\bar{y} = \bar{h}(q, \alpha_c) := q_a - h^{\text{des}}(\theta) - h_c(\theta, \alpha_c) \quad , \quad (5.26)$$

where  $\alpha_c$  is a vector of coefficients that are chosen to smoothly reject the initial error with respect to the (uncorrected) output (5.25) by the middle of the step; see Section 4.2.1 for details.

To induce turning on a straight walking gait, we augment the output (5.26) with polynomials  $h_s$ , i.e.,

$$\tilde{y} = \tilde{h}_p(q, \alpha_c, \beta_p) := q_a - h^{\text{des}}(\theta) - h_c(\theta, \alpha_c) - h_s(\theta, \beta_p) \quad , \quad (5.27)$$

where  $\beta_p$  is the vector parameters determined in a way that does not interfere with the design of  $h_c$  that renders the zero dynamics surface  $\mathcal{Z}$  associated with the original output (5.25) hybrid invariant. More specifically,  $h_s$  satisfies

$$\left\{ \begin{array}{l} h_s(\theta, 0) = 0 \\ h_s(\theta^+, \beta_p) = 0 \\ \frac{\partial}{\partial \theta} h_s(\theta^+, \beta_p) = 0 \\ h_s(0.5\theta^+ + 0.5\theta^-, \beta_p) = \beta_p \\ h_s(\theta, \beta_p) = 0, \quad 0.1\theta^+ + 0.9\theta^- \leq \theta \leq \theta^- \end{array} \right.$$

Then, selecting the control inputs according to

$$u = \Gamma_p(x) := L_g L_f \tilde{h}_p(x)^{-1} \left[ v(\tilde{y}, \dot{\tilde{y}}) - L_f^2 \tilde{h}_p(x) \right] \quad , \quad (5.28)$$

where  $v$  is an auxiliary controller that renders the surface

$$\tilde{\mathcal{Z}}_p := \{(q, \dot{q}) \in T\mathcal{Q} \mid \tilde{h}_p(q, \alpha_c, \beta_p) = 0, L_f \tilde{h}(x, \alpha_c, \beta_p) = 0\}$$

attractive and hybrid invariant under the flow of the system  $\Sigma_p$  defined by (5.20); the controller  $v$  can be designed as in (3.23). It is important to emphasize that the control law (5.28) does *not* depend on the yaw angle  $q_1$  due to the fact that the output (5.27) is independent of  $q_1$ . Then, by Proposition 1 the closed-loop Poincaré map is equivariant under yaw rotations.

The hybrid invariance of  $\tilde{\mathcal{Z}}_p$  ensures that the restriction  $\hat{\rho}_p := \hat{P}_p|_{\mathcal{S} \cap \tilde{\mathcal{Z}}_p}$  of the Poincaré map  $\hat{P}_p$  on the surface  $\mathcal{S} \cap \tilde{\mathcal{Z}}_p$  is well defined, and that  $\hat{z} = (q_1, \dot{q}_1, \dot{\theta})^T$  is a valid set of coordinates on  $\mathcal{S} \cap \tilde{\mathcal{Z}}_p$ . Furthermore, as a result of equivariance the restricted Poincaré map can be decomposed as

$$\begin{bmatrix} q_1[k+1] \\ z[k+1] \end{bmatrix} = \begin{bmatrix} q_1[k] + \rho_p^{(q_1)}(z[k]) \\ \rho_p(z[k]) \end{bmatrix} =: \hat{\rho}_p(\hat{z}[k]) . \quad (5.29)$$

where  $z = (\dot{q}_1, \dot{\theta})^T$ . Before we turn our attention to computing motion primitives, the following remark is in order.

**Remark 2.** *We will assume that switching between primitives occurs only at the beginning of a stride. This assumption is typical in motion planning scenarios [30], and, while it does not significantly restrict the flexibility of the planner, it allows us to take advantage of the dimensional reduction afforded by HZD in a way that greatly simplifies the planning problem. In this case, switching from one primitive to another excites the uncorrected outputs (5.25) only when the stride begins; i.e.,  $y_i$  and  $\dot{y}_i$  are non-zero. The correction polynomials  $h_c$  in (5.27) account for this excitation, and, by construction, they ensure that after the middle of the stride, the surface  $\tilde{\mathcal{Z}}_p$  coincides with the zero dynamics surface  $\mathcal{Z}$  associated with the original output (5.25). Hence, at the end of the stride, the state is on  $\mathcal{S} \cap \tilde{\mathcal{Z}}_p = \mathcal{S} \cap \mathcal{Z}$ , independent of the perturbation introduced*

by the switching. As a result, HZD greatly facilitates planning by ensuring that, despite switching, the discrete evolution of the system always occurs on  $\mathcal{S} \cap \mathcal{Z}$ , allowing the use of the restricted Poincaré map (5.29) for planning.

The dimensional reduction and the equivariance property allow the definition of low-dimensional motion primitives

$$\mathcal{R}_p(z) = \{\rho_p(z), H_p^z(z)\} \text{ ,} \quad (5.30)$$

for the reduced order system

$$z[k + 1] = \rho_p(z[k]) \text{ ,} \quad (5.31)$$

and  $H_p^z(z)$  is the output function expressed in terms of  $z$ .

### 5.3.4 Generating Motion Primitives

The HZD controller described above can be used to produce limit-cycle motion primitives that correspond to straight and turning walking motions. Searching for the fixed point  $x_p^*$  and the parameters  $\beta_p$  that satisfy

$$\begin{aligned} x_p^* &= P_p(x_p^*) \text{ ,} \\ s_p &= P_p^{(q_1)}(x_p^*) \text{ ,} \end{aligned} \quad (5.32)$$

results in a motion primitive with a net change  $s_p$  in the heading angle. Various design specifications such as actuators saturation and foot-ground interactions are incorporated as additional constraints in the computation of the fixed point as in [111, Section 3.2] and [14].

For feasible switching between two gaits, it is required that the fixed points lie within the basin of attraction of one another. Furthermore, it is desirable that the computed fixed points are in close proximity with each other. Indeed, imposing this requirement provides a number of advantages in motion planning. First, it results in

greater overlap among the regions of attraction. Second, it reduces the dwell time requirement for stability of the switched system, thus enhancing flexibility. Third, it reduces the transient response when the biped switches between primitives, thereby reducing the deviation from the nominal plan.

Initially, the majority of the fixed points that we computed had very small basins of attraction; see Section 5.3.5.1 for estimating basins of attraction. The simulation results showed that the fixed points failed to tolerate small negative perturbation on  $\dot{\theta}$ . To remedy this problem and to find gaits with improved perturbation tolerance, an additional constraint on the minimum value of  $\dot{\theta}$  during the cycle was added to the process of searching for a fixed point. The resulting fixed points yielded considerably bigger basins of attraction.

Next, to compute a family of turning fixed points in the vicinity of a straight-line motion primitive, the following method has been adopted. Note that the method can replace the computationally expensive nonlinear optimization problem that is typically used to search for fixed points. In more detail, we assume that the straight line motion primitive  $\mathcal{R}_0 = (\rho_0, H_0^z)$  is available. To achieve turning, we consider the output ((5.27) which depends on the parameter array  $\beta$ . The corresponding reduced-order Poincaré map can be decomposed as follows

$$\begin{bmatrix} q_1[k+1] \\ z[k+1] \end{bmatrix} = \begin{bmatrix} q_1[k] + \rho_0^{(q_1)}(z[k], \beta) \\ \rho_0(z[k], \beta) \end{bmatrix}. \quad (5.33)$$

Defining  $\delta z[k] = z[k] - z_0^*$  and  $\delta q_1[k] = q_1[k] - q_1[k-1]$ , the linearization of (5.33) about the straight line fixed point  $z_0^*$ , and about nominal value of the parameter  $\beta^* = 0$  gives

$$\begin{bmatrix} \delta q_1[k+1] \\ \delta z[k+1] \end{bmatrix} = \begin{bmatrix} A_{q_1} \delta z[k] + G_{q_1} \beta \\ A_z \delta z[k] + G_z \beta \end{bmatrix}, \quad (5.34)$$

where  $A_{q_1}$  and  $G_{q_1}$  are the Jacobian matrices of  $\rho_0^{(q_1)}$  with respect to the state  $z$  and the parameter  $\beta$ , and  $A_z$  and  $G_z$  are the Jacobian matrices of  $\rho_0$  with respect to  $z$  and

the parameter  $\beta$ . To find a turning fixed point in the closed proximity of the straight line fixed point, it is desirable to steer the biped's heading by the angle  $s$ , without affecting the locomotion-specific state  $z$ . This can be achieved by the control law

$$\begin{bmatrix} G_{q_1} \\ G_z \end{bmatrix} \beta = \begin{bmatrix} s \\ 0 \end{bmatrix} \Leftrightarrow \beta = G^{-R} \begin{bmatrix} s \\ 0 \end{bmatrix}, \quad (5.35)$$

where  $G^{-R}$  is the right pseudo-inverse of  $G := \begin{bmatrix} G_{q_1} \\ G_z \end{bmatrix}$ . It should be noted that the solution  $\beta$  of (5.35) is the minimum norm  $\beta$  thereby ensuring minimal modification of the outputs (5.27) to induce turning. When the controller of (5.35) is applied on the biped that is walking straight, we observe that it turns approximately by  $s$  and it converges to a new fixed point that is in the close proximity of the straight walking fixed point  $z_0^*$ .

For the purpose of illustrating the method, we choose a gait basis set  $\mathbb{G} = \{\mathcal{R}_0, \mathcal{R}_1, \mathcal{R}_2\}$ , consisting of three motion primitives; namely,  $\mathcal{R}_0$  for straight line motion,  $\mathcal{R}_1$  for clockwise (CW) turning by  $45^\circ$ , and  $\mathcal{R}_2$  for counterclockwise (CCW) turning by  $45^\circ$ . The sharp turning primitives in  $\mathbb{G}$  enable the biped to navigate through narrow spaces, as will be shown in Section 5.3.6.

### 5.3.5 Stable Composition of Gait Primitives

In this section we use sum-of-squares (SOS) programming to estimate the basin of attraction of the reduced motion primitives, made available by the dimensional reduction inherent in HZD method. We then use the SOS results to carry out the set construction required by Theorem 1, and compute the dwell time for stable motion planning.

#### 5.3.5.1 Estimation of Basin of Attraction

As it was mentioned in Remark 2, switching between motion primitives preserves hybrid invariance of the zero dynamics, resulting in the reduced-order Poincaré map

$\hat{\rho}_p$  defined by (5.29). As a result of equivariance, we only need to focus on the two-dimensional system  $\rho_p$  in (5.31) to evaluate the basin of attraction of the reduced motion primitives. In what follows, we explain the procedure for one such motion primitive; i.e., for a fixed  $p$ . For simplicity, the corresponding fixed point is translated to origin.

We first numerically estimate the domain of definition by ensuring that  $\rho_p$  is defined on sampled boundary points of a closed disc around the origin. We then densely propagate the disc in the radial direction and repeat the process to obtain the maximum radius  $r_p$  of the ball  $\mathcal{B}_{r_p}(0)$  over which  $\rho_p$  is well defined. Next, we restrict our attention to estimation of the basin of attraction in the form of a sub-level set  $\{z \in \mathcal{B}_{r_p}(0) \mid V_p(z) \leq \eta\}$  that lies inside the domain of definition. We use quadratic Lyapunov functions  $V_p(z) := z^T S_p z$  where  $S_p$  is a positive definite matrix that is obtained from the solution of the discrete Lyapunov equation associated with the linearization of (5.31). To verify (5.3), we formulate a SOS feasibility program as in [81]:

$$\begin{aligned} & \max \eta \\ & \text{s.t } \eta < \lambda_{\min}(S_p)r_p^2 \\ & \quad b_p(z) \text{ is SOS} \\ & \quad \epsilon V_p(z[k]) - V_p(z[k+1]) - b_p(z[k])(\eta - V_p(z[k])) \text{ is SOS} \end{aligned}$$

where  $\lambda_{\min}(S_p)$  is the minimum eigenvalue of  $S_p$ , and  $b_p(z)$  is a positive definite polynomial of  $z$ ; see [81]. The first condition guarantees that the computed estimate of the basin of attraction is restricted inside the domain of definition. Note that  $\epsilon$  is the rate of convergence, and as the construction of Theorem 1 requires, will be selected to be the same for all motion primitives. Finally, we obtain polynomial approximation of  $\rho_p$  –amenable to SOS algorithms– in the neighborhood of the fixed point using Taylor series up to second-order terms.

The value of  $\eta_{\max}$ , beyond which the solution is not feasible, is then computed

based on a sequence of SOS feasibility programs. The procedure is performed for every motion primitive in  $\mathbb{G}$ . The outcome is  $\eta_0 = 0.11$ ,  $\eta_1 = 0.15$  and  $\eta_2 = 0.08$  for  $\mathcal{R}_0$ ,  $\mathcal{R}_1$ ,  $\mathcal{R}_2$ , respectively. The resulting estimates of the basins of attraction are shown as dashed ellipses in Fig. 5.3. Clearly, all the fixed points lie in the intersection of basins of attraction.

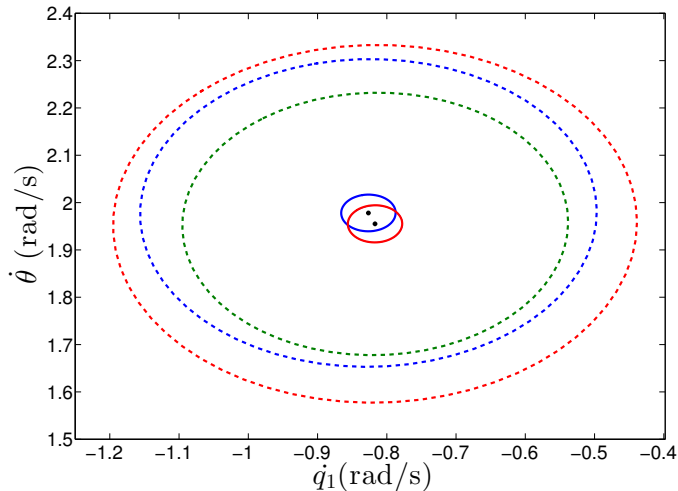


**Figure 5.3:** Estimates of the basin of attraction for each of the motion primitives in  $\mathbb{G}$  (dashed ellipses), and computation of  $\overline{\mathcal{M}}(\kappa)$  (union of solid ellipses), which is entirely inside the intersection of basin of attractions. The colors blue, red and green correspond to the primitives  $\mathcal{R}_0$ ,  $\mathcal{R}_1$  and  $\mathcal{R}_2$  respectively. Note that the fixed points of  $\mathcal{R}_1$  and  $\mathcal{R}_2$  and their corresponding  $\mathcal{M}(\kappa)$  sets are almost coinciding. The set  $\overline{\mathcal{M}}(\kappa)$  of (5.8) corresponds to  $\kappa = 0.0002$  resulting in the dwell time  $N_d = 1$ .

### 5.3.5.2 Computation of Minimum Dwell Time for Stability

Here we apply Theorem 1 to find the bound on the switching frequency among the motion primitives, which guarantees that the evolution of the switched system remains within the desired safe region  $\overline{\mathcal{M}}(\kappa)$ . The SOS results verified that the quadratic functions  $V_p(z) := z^T S_p z$  meet the requirements of Definition 1 for all the motion primitives  $p$  with the same value of  $\epsilon = 0.12$ . For maximal flexibility in the motion planning stage, it is favorable to have the ability to switch at every stride, implying that  $N_d = 1$  is the desired value of the lower bound on the dwell time. To verify the feasibility

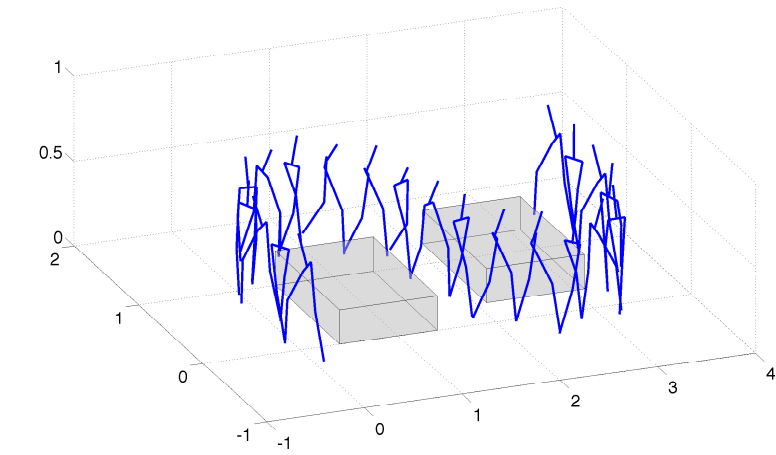
of the desired dwell time, with the knowledge of  $\epsilon = 0.12$  from the SOS program of Section 5.3.5.1, we must determine if there exists a  $\kappa$  that satisfies the conditions of Theorem 1. This is done by numerically computing  $\omega_{\max}(\kappa)$ ,  $\omega_{\min}(\kappa)$  using (5.6), and  $\mu(\kappa)$  using (5.10), and verifying that  $N_d = 1$  satisfies (5.11). As a result, the solution of the switched system that starts within the set  $\mathcal{N}(\kappa)$  defined by (5.5) never leaves the set  $\overline{\mathcal{M}}(\kappa)$ , which corresponds to the union of the solid ellipses in Fig. 5.3. The plotted  $\overline{\mathcal{M}}(\kappa)$  in Fig. 5.3 corresponds to  $\kappa = 0.0002$ .

With  $N_d = 1$  the biped is guaranteed to remain stable as it switches at every stride. Figure 5.4 shows an example of stable motion primitive composition. During the entire walking sequence, we plot the input torques and ground reaction forces and verify that switching between motion primitives does not result in violation of gait constraints. For instance, the evolution of stance and swing hip torques are shown in Fig. 5.4, which confirms that the torques are within the actuator’s saturation limit.

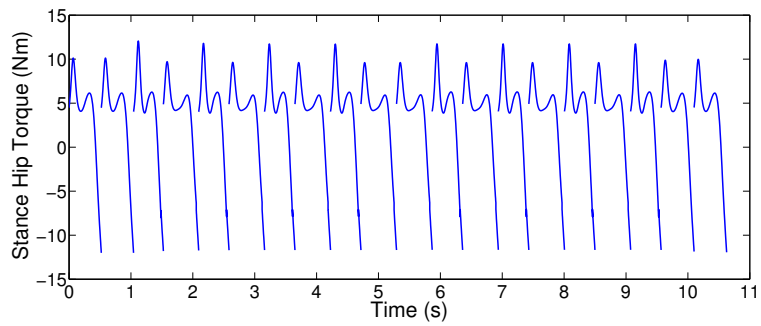
### 5.3.6 Planning with Motion Primitives

We now use the collection of motion primitives  $\mathbb{G} = \{\mathcal{R}_p(z), p \in \mathcal{P}\{0, 1, 2\}\}$  in conjunction with a high-level planning algorithm to construct feasible paths taking the biped from an initial position to a desired final one while avoiding any obstacles on the way. In what follows,  $p^{\text{cm}}$  represent the  $X$  and  $Y$  coordinates of the CoM of the biped in the global frame and  $\Theta$  the heading angle of the biped with respect to the global positive  $X$ -axis. A Rapidly Exploring Random Tree (RRT) [58] is employed to find feasible paths. Each node of the associated tree holds information about  $p^{\text{cm}}$ ,  $\Theta$ , the low-level state of the biped  $z$ , the index of its parent node, and the primitive index  $p \in \mathcal{P}$  that was applied on the parent node. In addition, the number of strides since the last primitive switch on the path is available in the tree to check the dwell time condition (5.11) which the planner must respect.

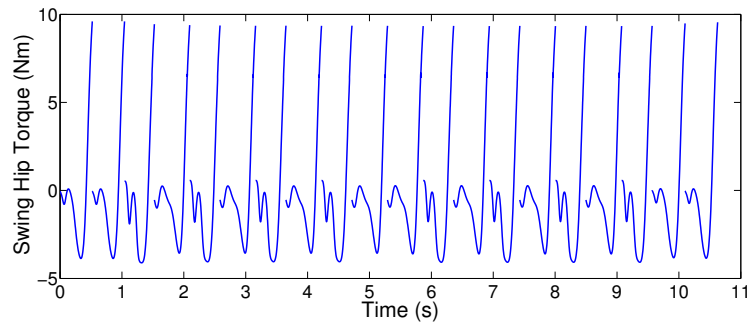
The tree node  $j$  such that  $p_j^{\text{cm}}$  has the least euclidean distance from a randomly chosen point  $(X_r, Y_r)$  in the free space among all other nodes, is expanded for each



(a)



(b)



(c)

**Figure 5.4:** An example of stable composition of motion primitives. The sequence is  $(\mathcal{R}_0, \mathcal{R}_1, \mathcal{R}_1, \mathcal{R}_1, \mathcal{R}_1, \mathcal{R}_2, \mathcal{R}_2, \mathcal{R}_2, \mathcal{R}_2, \mathcal{R}_0)$ . (a) animation of the walking sequence. (b) Evolution of stance hip torque corresponding to joint  $q_5$ . (c) Evolution of swing hip torque corresponding to joint  $q_8$ .

$p \in \mathcal{P}$  to obtain the successive node as

$$\begin{aligned} p_{j+1}^{\text{cm}} &= p_j^{\text{cm}} + R(\Theta_j)L_p(z_j) , \\ \Theta_{j+1} &= \Theta_j + s_p(z_j) , \\ z_{j+1} &= \rho_p(z_j) , \end{aligned} \tag{5.36}$$

where

$$R(\Theta) := \begin{bmatrix} \cos(\Theta) & -\sin(\Theta) \\ \sin(\Theta) & \cos(\Theta) \end{bmatrix}, L_p(z) := \begin{bmatrix} l_p(z) \cos(o_p(z)) \\ l_p(z) \sin(o_p(z)) \end{bmatrix}.$$

If  $p_{j+1}^{\text{cm}}$  is not in the free space, then the corresponding node is pruned. The tree generation continues until  $p_{j+1}^{\text{cm}}$  is within a specified distance of the goal position or until a maximum number of iterations is reached.

In the absence of perturbations, the robot will accurately track the motion plan since the planner has the knowledge of the robot's dynamics  $\rho_p(z)$ . However, the planner is required to evaluate the corresponding Poincaré map  $\rho_p$  at  $z$  as in (5.31). This necessitates the numerical integration of (5.31), which despite its reduced dimension, would be computationally cumbersome. To accelerate the planning process considerably, we trade-off accuracy for reduced computation by using nominal motion primitives as actions available to the planner as detailed below.

### 5.3.6.1 Nominal Motion Primitives

The nominal motion primitives (NMPs) are defined as the motion primitives evaluated at the discrete set of fixed points, i.e.

$$\mathcal{R}_p^*(z_p^*) := \mathcal{R}_p(z_p^*) = \{\rho_p(z_p^*), H_p^z(z_p^*)\} . \tag{5.37}$$

It is important to emphasize the difference between  $\mathcal{R}_p(z)$  in (5.30) and  $\mathcal{R}_p^*(z_p^*)$  in (5.37). In the former, the planner has knowledge of the dynamics in the sense that it

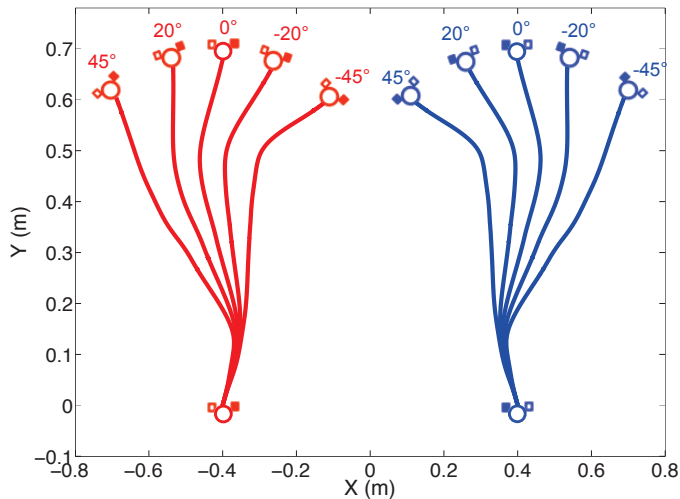


**Figure 5.5:** Nominal motion primitives for a family of primitives. The number on each arc shows the change in the heading angle. Blue corresponds to turning when support is on the left leg and red when support is on the right leg.

can predict the state at the end of the execution of the  $p$ -th primitive with knowledge of the *current* state  $z$ . In the latter, the planner only knows the nominal evolution associated with the fixed points that give rise to the corresponding nominal motion primitives. Hence, if the biped’s initial state does not coincide with a fixed point, the actual evolution of the biped while executing a primitive will deviate from the one expected by the planner. Indeed, each NMP corresponds to a path realized in the biped’s workspace as it follows a limit cycle; see Fig. 5.5 for examples of walking arcs corresponding to NMPs. A discrete set of NMPs is made available to the planning algorithm which concatenates them to effectively capture the net change in the position of the center of mass (CoM) and in the heading direction of the biped as it moves along the limit-cycle of each NMP. For the motion primitives in  $\mathbb{G}$ , these quantities are given in Table 5.1. The nominal motion primitives have also been called nominal walking arcs in the literature; see [30].

When planning with NMPs, each node of the RRT holds information of  $p^{\text{cm}}$  and  $\Theta$  only, without requiring the knowledge of the state  $z$ . Therefore, the nodes expansion

**Table 5.1:** Selected Nominal Motion Primitives

Primitive	$l(z^*)$ [m]	$o(z^*)$ [deg]	$s(z^*)$ [deg]
Straight	0.6789	0	0
CW	0.6710	-25.05	-45
CCW	0.6558	26.21	45

of the RRT (5.36) reduces to

$$\begin{aligned}
 p_{j+1}^{\text{cm}} &= p_j^{\text{cm}} + R(\Theta_j)L_p(z_j^*) , \\
 \Theta_{j+1} &= \Theta_j + s_p(z_j^*) .
 \end{aligned}$$

The availability of a discrete collection of actions  $\{H_p^z(z_p^*), p \in \mathcal{P}\}$  to the motion planner significantly reduces the computational time for generating plans. However, as was mentioned above, the fixed point  $z_p^*$  corresponding to the applied action may not coincide with the actual state of the system  $z$  at the execution of an action  $H_p(z_p^*)$ , thereby causing the system to drift from the suggested plan. Due to the concatenation of the actions with different fixed points, this problem arises even under nominal conditions, i.e. in the absence of externally applied perturbations.

Theorem 1 provides a way to derive an upper bound on the deviation of the biped from the nominal path, based on the size of the set  $\overline{\mathcal{M}}(\kappa)$ . As a direct result of the Theorem, the value of the Lyapunov function of the active subsystem  $\sigma(k)$  is bounded by  $V_{\sigma(k)}(x[k]) \leq \omega_{\sigma(k)}(\kappa)$ . Using (5.2), the deviation of system's solution from the fixed points is given by

$$\|x[k] - x_{\sigma(k)}^*\| \leq \chi_{\sigma(k),1}^{-1}(\omega_{\sigma(k)}(\kappa)) . \quad (5.38)$$

With the choice of quadratic Lyapunov function  $V_p(z) := z^T S_p z$ , equation (5.38) takes

the form

$$\|z[k] - z_{\sigma(k)}^*\| \leq \sqrt{\frac{\omega_{\sigma(k)}(\kappa)}{\lambda_{\min}(S_{\sigma(k)})}} . \quad (5.39)$$

We now need to relate the deviation of the state  $z$  from the fixed point  $z^*$  to the deviation of the biped from the nominal path. First, note that the global position and heading angle of the biped at step  $k$  can be written as

$$\begin{aligned} p^{\text{cm}}[k+1] &= p^{\text{cm}}[k] + m_{\sigma(k)}(\Theta[k], z[k]) , \\ \Theta[k+1] &= \Theta[k] + s_{\sigma(k)}(z[k]) , \end{aligned} \quad (5.40)$$

where  $m_{\sigma(k)}(\Theta[k], z[k]) := R(\Theta[k])L_{\sigma(k)}(z[k])$ . Let  $\Theta^*[k]$  and  $p^{\text{cm}*}[k]$  denote the nominal heading angle and nominal path that are computed by (5.40) when  $z[k] = z_{\sigma(k)}^*$ , i.e. the plan that is computed based on nominal motion primitives. Define  $\delta z[k] := z[k] - z_{\sigma(k)}^*$ ,  $\delta\Theta[k] := \Theta[k] - \Theta^*[k]$  and  $\delta p^{\text{cm}}[k] := p^{\text{cm}}[k] - p^{\text{cm}*}[k]$ , then on linearizing (5.40) around the point  $(\Theta[k], z_{\sigma(k)}^*)$  we obtain

$$\begin{aligned} \delta p^{\text{cm}}[k+1] &= \delta p^{\text{cm}}[k] + B_{\sigma(k)}\delta\Theta[k] + C_{\sigma(k)}\delta z[k] , \\ \delta\Theta[k+1] &= \delta\Theta[k] + D_{\sigma(k)}\delta z[k] , \end{aligned} \quad (5.41)$$

where  $B_{\sigma(k)} := \frac{\partial m_{\sigma(k)}(\Theta, z)}{\partial \Theta} \Big|_{(\Theta[k], z_{\sigma(k)}^*)}$ ,  $C_{\sigma(k)} := \frac{\partial m_{\sigma(k)}(\Theta, z)}{\partial z} \Big|_{(\Theta[k], z_{\sigma(k)}^*)}$ ,  $D_{\sigma(k)} := \frac{\partial s_{\sigma(k)}(z)}{\partial z} \Big|_{z_{\sigma(k)}^*}$ . Note that the Euclidean norms  $\|B_{\sigma(k)}\|$  and  $\|C_{\sigma(k)}\|$  are independent of  $\Theta$ , since  $R(\Theta)$  in the definition of  $m$  is a rotation matrix that preserves the length. As a result, they do not depend on the path and can be computed a priori for each motion primitive. Applying (5.41) in the interval  $[0, k+1]$  and using Euclidean norm inequalities and

(5.39), we derive an upper bound on the deviation from the nominal plan as,

$$\begin{aligned}
\|\delta p^{\text{cm}}[k+1]\| &\leq |\delta p^{\text{cm}}[0]| + \|B_{\sigma(0)}\| \delta\Theta[0] + \sum_{i=1}^k \|C_{\sigma(i)}\| \sqrt{\frac{\omega_{\sigma(i)}(\kappa)}{\lambda_{\min}(S_{\sigma(i)})}} \\
&\quad + \sum_{i=0}^k \|B_{\sigma(i)}\| \left( \delta|\Theta[0]| + \sum_{j=0}^{i-1} \|D_{\sigma(j)}\| \sqrt{\frac{\omega_{\sigma(j)}(\kappa)}{\lambda_{\min}(S_{\sigma(j)})}} \right) \\
\delta\Theta[k+1] &\leq \delta\Theta[0] + \sum_{i=0}^k \|D_{\sigma(i)}\| \sqrt{\frac{\omega_{\sigma(i)}(\kappa)}{\lambda_{\min}(S_{\sigma(i)})}}.
\end{aligned} \tag{5.42}$$

Note that the bound given by (5.42) is conservative since it considers the worst case scenario where the state evolves on the boundary of the set  $\overline{\mathcal{M}}(\kappa)$ . Nevertheless, it has important implications in motion planning. It relates the deviation from nominal path to the size of the set  $\overline{\mathcal{M}}(\kappa)$  through the parameter  $\kappa$ , and to the low-level controller design through the terms  $\|B_{\sigma(i)}\|$ ,  $\|C_{\sigma(i)}\|$  and  $\|D_{\sigma(i)}\|$ . Reducing  $\kappa$  improves the tracking performance of the biped at the expense of deteriorating its maneuverability by increasing the dwell time; i.e., by increasing the number of steps that must be taken by the biped before the planner can switch to a new primitive. The terms  $\|C_{\sigma(i)}\|$ ,  $\|D_{\sigma(i)}\|$  and  $\|E_{\sigma(i)}\|$  can be viewed as performance indices of a motion primitive; smaller values of these terms imply better performance. These indices can be incorporated as a constraint in the optimization problem, when one searches for a periodic gait.

If the initial error of the CoM position and heading angle are zero, i.e.  $\delta p^{\text{cm}}[0] = 0$  and  $\delta\Theta[0] = 0$ , applying (5.42) for the first stride yields

$$\|\delta p^{\text{cm}}[1]\| \leq \|C_{\sigma(0)}\| \sqrt{\frac{\omega_{\sigma(0)}(\kappa)}{\lambda_{\min}(S_{\sigma(0)})}} \tag{5.43}$$

Since the drift depends on the primitive being active during the first stride, we take the average drift per CoM displacement over the three motion primitives in  $\mathbb{G}$  as

$$error \leq \frac{1}{3} \sum_{p=0}^2 \frac{\|C_p\|}{l_p} \sqrt{\frac{\omega_p(\kappa)}{\lambda_{\min}(S_p)}} \tag{5.44}$$

Equation (5.44) can be used to compute a lower bound on the dwell time that guarantees that the drift per stride of the biped is less than a specified value. This can be done in the following manner. For a given *error*, we compute the value of  $\kappa$  such that (5.44) is satisfied. Then, we use (5.11) to compute the corresponding value of dwell time. To reduce the bound on the tracking error, it is desirable to reduce  $\omega_p(\kappa)$  by reducing  $\kappa$ . This in turn increases the dwell time bound of (5.11) and reduces the flexibility of the planner. Table 5.2 shows the computed values of dwell time for a range of given allowable drifts. Note that the drift can not be set arbitrarily small, since there is a lower limit on the value of  $\omega_p(\kappa)$  which can be computed when  $\kappa = 0$ ; see (5.6). In our example, the lower limit on the drift was found to be 3.9%.

**Table 5.2:** Dwell Time Values Based on Allowable Drift

<i>error</i> [%]	$\kappa[\times 10^{-3}]$	$N_d$
10	1.8	1
6	0.2	1
4.5	0.015	2
4	0.005	3

For the purposes of illustration, we consider the environments of Fig. 5.6, in which the bipedal model of Fig. 5.2 starts at an initial position and is required to reach the designated goal while avoiding obstacles in the workspace. Based on the discussion in Section 5.3.5.2, the planner is allowed to switch primitives at every stride. If an allowable drift per stride is specified, we will choose the dwell time based on Table 5.2. With this knowledge, the RRT planner constructs a number of nominal paths, that are all stable. Out of all these paths, we pick the one that has the smallest estimate of final drift, computed by (5.42). The selected nominal path is shown as red circles in Fig. 5.6.

Consider the environment shown in Fig. 5.6(a) which is relatively tight given the

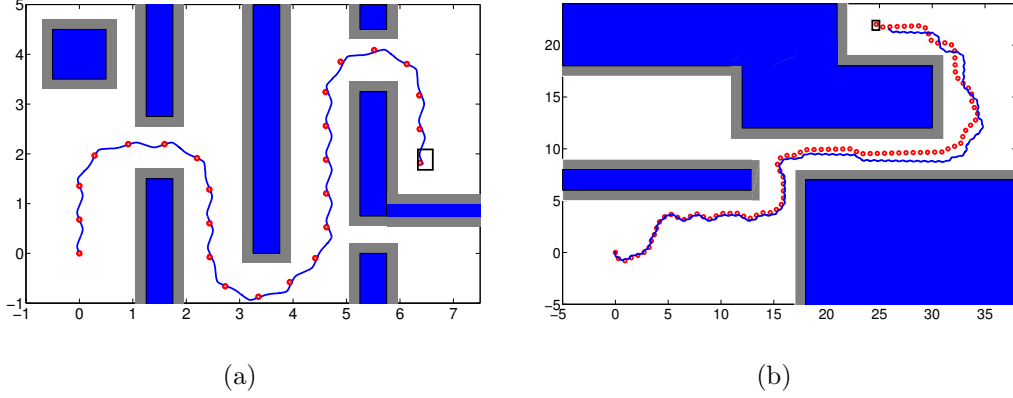


**Figure 5.6:** Two walking environments. The nominal plans using NMP are shown as red circles and the simulated trajectories of biped’s CoM are indicated by blue lines. In the environment (a), the biped takes 24 strides to reach the goal (marked by black rectangle) and the final drifting error is 6.3 cm. In the environment (b), the biped takes 90 strides to reach the goal and the final error is 1.20 m.

dimensions of the biped. Given, for example, a requirement that the drift per stride should not exceed 6% of the COM displacement, we pick the dwell time  $N_d = 1$ , based on Table 5.2. Due to the enhanced flexibility offered to the planner, which is able to switch primitives at every stride and owing to the sharp turns that can be realized by the turning primitives, the biped reaches the goal in 24 strides with a small drifting error, approximately equal to 6.3cm. If a more stringent condition is imposed on the drift, the dwell time should be increased. However, in this example for  $N_d > 1$ , the planner is not able to find a path, since its flexibility is restricted by the dwell time.

Now consider the environment shown in Fig. 5.6(b), which is wider than environment of Fig. 5.6(a). With the prescribed allowable drift per stride, i.e.  $error = 6\%$ , the planner constructs a path with  $N_d = 1$ . The biped takes 90 strides to reach the goal, and the final drift is approximately equal to 1.20m; see Fig. 5.6(b). Yet, this represents a considerable improvement with respect to [30], in which the biped drifts 2.59m away from the goal by the end of plan. Furthermore, the analytically tractable procedure offered by Theorem 1 and the dimensional reduction afforded by the HZD couple the relevant parameters  $error$  and  $\kappa$  in an explicit way, which can be used to

quantify the interplay between the geometry of the environment and the error in the execution of a plan. If a smaller allowable drift of  $error = 4.5\%$  or  $error = 4\%$  is required, the planner must comply with a stricter condition on dwell time, i.e.  $N_d = 2$  and  $N_d = 3$ , respectively. On the nominal path with  $N_d = 2$ , the biped took 94 strides to reach the goal, and the final drift was reduced to 0.93m. Similarly, on the nominal path with  $N_d = 3$ , the biped took 98 strides and the final drift was further slightly reduced to 0.89m. Note that for  $N_d > 3$ , the flexibility of the planner is reduced to the extent that it can not provide a path. The reader is encouraged to see [107] for details of a method that substantially reduces the drift by providing the planner with the analytical approximation of the dynamics and the output of the system.

## 5.4 Discussion

This chapter proposed a framework for autonomous navigation of 3D bipedal robots in environment cluttered with obstacles; see Fig. 5.7. At the low level, the locomotion controller generates gait primitives in the form of dynamically-stable limit cycles which are then composed by a high-level planning algorithm with the purpose of navigating the biped to a goal location while avoiding obstacles. We then formulated the composition of gait primitives as a switched dynamical system, and we derived an analytical condition that guarantees the stability of the robot by restricting the switching frequency between motion primitives. This condition distills the stability limitations in system dynamics, and when communicated to motion planner, results in the generation of a path that stably brings the robot to the desired goal region. The similarity between Fig. 5.7 and Figs. 3.7 and 4.6 of Chapters 3 and 4, respectively, is suggestive of the similarities between the tasks studied in this thesis. Indeed, the only difference is that the descending signal in Fig. 5.7 is a switching sequence that governs the composition of multiple motion primitives while in Figs. 3.7 and 4.6, the descending signal is a continuous-time force signal that represents the intentions of the leader and “deforms” the underlying limit-cycle walking motion. In both cases, the low-level locomotion controller accommodates the requests of the high-level planner,

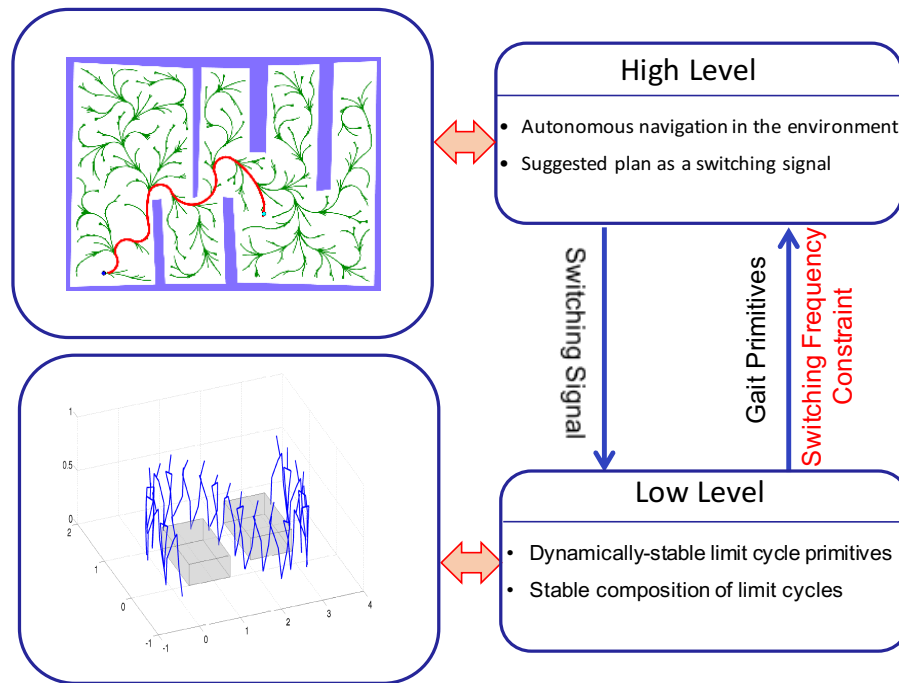


**Figure 5.7:** The hierarchical components for motion planning. Based on the gait primitives and the dwell time constraint, the high-level planner constructs an obstacle-free path, which is then sent to the low-level locomotion controller for execution.

be it a leading collaborator (e.g. a human) exerting a force or a motion planning algorithm suggesting a plan.

## Chapter 6

### CONCLUSION AND FUTURE WORK

#### 6.1 Conclusion

To assist humans, bipedal robots must be capable of operating in human-centric environments. This thesis focuses on integrating high-level tasks with low-level locomotion controllers to enable bipedal robots to cooperate with a leading collaborator and to autonomously navigate in a cluttered environment.

We begin by addressing leader-follower cooperative tasks such as cooperative object transportation over a distance that requires the biped to move using its legs. In such tasks, the biped's manipulator interacts with a leading collaborator in a way that the robot's motion is guided by the collaborator's intentions. In this scenario, the biped can rely on the leader's knowledge of environment in order to avoid the obstacles on the way, and to be steered to the goal region. The proposed approach combines impedance control on the robot's arm with motion control on the robot's legs to ensure (i) compliance of the manipulator as it interacts with its environment and (ii) adaptability of the locomotion system in response to the corresponding interaction forces. In the planar setting, analytic conditions were derived to ensure that the biped is able to continue taking steps under external forcing. With these conditions satisfied, the proposed controller allows the biped to adjust its stepping pattern by altering its stride frequency, while maintaining a constant stride length; a property that is useful especially when walking over stairs is needed. In the 3D setting, on top of the aforementioned adjustments, the biped also adapts its heading angle in response to the interaction force. This capability allows the biped to follow the intended path that the leader enforces.

In applications where the robot has to autonomously navigate the environment without the help of a leader, this thesis presented a motion planning framework that provides *a priori* conditions that ensure that the biped will not fall as it navigates among obstacles in its workspace. In essence, our framework allows the biped to reason about the space in which it operates while ensuring that locomotion stability is maintained. The framework relies on the extraction of motion primitives in the form of exponentially stable limit cycles which are then concatenated by a planning algorithm with the purpose of navigating the robot through a cluttered environment. Stable operation on the nominal path is guaranteed by constraining the frequency of the switching signal. The analytic nature of this constraint, which relates dwell time to the size of the region where the system evolves, provides a way to estimate the deviation of the biped from the nominal plan. We show our development on a 3D bipedal walking model under the influence of an HZD controller, and emphasize the significance of the dimensional reduction offered by such controllers in establishing certificates of stability of the motion primitives using SOS programming.

To summarize, this thesis examined two scenarios in which external signals are used to deliberately modify the basic locomotion pattern of dynamically walking bipeds. In the first case, the external signal is in the form of a continuous-time force that encodes the intended trajectory of a leading collaborator while in the second case the external signal is a sequence of motion primitives that need to be combined to realize an obstacle-free path of the biped in a space cluttered by obstacles. In both cases, the control system needs to modify the basic locomotion pattern of the biped either by “deforming” a basic limit cycle or by “composing” a number of basic limit cycles through descending commands from a higher-level algorithm. This higher-level logic must respect the constraints that are imposed by the low-level dynamics of the platform. Hence, our work in this thesis, provides a first step toward bridging the gap between high-level motion planning algorithms and low-level locomotion controllers with dynamically rich behaviors in the form of periodic (limit cycle) motion primitives.

## 6.2 Future Work

### 6.2.1 Prioritizing between Adaptive Response and Obstacle Avoidance

In Chapter 3 and 4, a framework for cooperation between a biped and a leader was presented that allowed the biped to follow the intended trajectory of the leader through the corresponding interaction force. In this setting, the biped solely relies on the leader's decision-making capabilities to prevent collision with obstacles. This can be problematic when the leader does not promptly communicate its intention or when the biped does not precisely follow the command.

To reconcile this issue, one possible solution is to add a high-level planner with knowledge of the environment, and use it to prioritize between command following and obstacle avoidance. Roughly speaking, when the biped gets critically close to an object, the controller should give priority to avoiding the obstacle rather than adapting to the leader's intentions. As the biped moves away from the obstacle, the controller should be switched back to the adaptive mode, giving authority to the leader to guide the motion of biped.

In Chapter 5, we presented a motion planning framework that allowed the robot to avoid obstacles in the absence of external forcing. However, the application of external force affects the motion of the biped and it may cause the biped to deviate from the suggested safe path. To resolve this issue, one solution is to add two more actuators on the pitch and yaw joints of the stance leg (fully actuated) in order to completely reject the effect of force on biped's motion and to enforce a suitable corrective action, regardless of the leader's commands. Once the biped is safe from collision, the extra actuators can be switched off to allow adaptive response to interaction force. The results of Chapter 5 still hold for the fully actuated phase, that is, the biped stably executes the obstacle free path if the switching signal satisfies the dwell time constraint. We only need to recompute motion primitives for the new model which is fully actuated.

### 6.2.2 Improving Adaptive Response

As it was mentioned in Chapter 3 and 4, the adaptive response of biped to interaction force is a consequence of the way the controller deals with the underactuated nature of the bipedal model. The quality of this adaptive behavior depends on the base (unforced, periodic) motion, and therefore optimizing this fundamental motion as was done in Section 4.4.2, can improve the response of the biped to the intended trajectory of the leader. An alternative solution is to produce a library of periodic motions, each optimized for a specific task, and to switch among them in a suitable manner. For instance, in the planar case, multiple motion primitives can be generated that correspond to different nominal speeds. Assume that the biped is walking with a constant speed and the leader suddenly increases its speed. The biped responds to the interaction force by gradually increasing its speed. However, as was mentioned in Chapter 3, the actuators may hit their saturation limit. In this situation, the controller can be switched to a new primitive, one that better matches the speed of the leader. Since the switched controller is optimized for the higher speed, the actuators torque will remain within their operation range. Furthermore, switching to higher-speed primitives (i.e. to limit cycles that have been computed for higher speeds) instead of “deforming” a limit cycle that corresponds to a lower speed, will decrease leader’s effort for enforcing its command. The same approach can be applied to the 3D case. A library of periodic motions corresponding to different nominal speeds and different turning angles can be generated. If the natural response of the biped to the leader’s change of direction is not satisfactory, the biped can switch to a new turning primitive that brings it closer to the intended trajectory of the leader.

The main challenge of this approach is to decide which controller is more suitable for adaptation to leader’s unknown intention. An adaptive supervisory control scheme [106] that chooses the controller based on the measurement of interaction force and biped’s state seems to be an appropriate approach for this problem.

### 6.2.3 Experimental Validation

Perhaps the most important future perspective is to implement the framework developed in this thesis on a humanoid robot. Figure 6.1 shows the humanoid biped HUBO that is carrying an object in physical collaboration with a human. To implement our framework, we would need to account for the geometry of the humanoid and consider a more elaborate model with more degrees of freedom. Several experiments have to be performed to identify the parameters of the model that best fits the experimental data. Furthermore, the simulation will need to consider a more realistic model for leg ground interactions and to account for actuator limitations. Experimentally validating the work proposed in this thesis is currently underway.



**Figure 6.1:** A human carrying an object with the humanoid robot HUBO (photo courtesy of Prof. P. Oh, Drexel University).

## BIBLIOGRAPHY

- [1] Wikipedia, <https://en.wikipedia.org/wiki/asimo>.
- [2] T. Alpcan and T. Basar. A stability result for switched systems with multiple equilibria. *Dynamics of Continuous, Discrete and Impulsive Systems Series A: Mathematical Analysis*, 17:949–958, 2010.
- [3] A. D. Ames. First steps toward automatically generating bipedal robotic walking from human data. In *Robot Motion and Control 2011*, volume 422, pages 89–116. Springer, 2012.
- [4] A. D. Ames. Human-inspired control of bipedal walking robots. *IEEE Transactions on Automatic Control*, 59(5):1115–1130, May 2014.
- [5] A. D. Ames, K. Galloway, J. W. Grizzle, and K. Sreenath. Rapidly exponentially stabilizing control lyapunov functions and hybrid zero dynamics. *IEEE Transactions on Automatic Control*, 59(4):876–891, 2014.
- [6] A. D. Ames and M. J. Powell. Towards the unification of locomotion and manipulation through control lyapunov functions and quadratic programs. In *Control of Cyber-Physical Systems, Lecture Notes in Control and Information Sciences*, pages 219–240. Springer, 2013.
- [7] M. Bellaccini, L. Lanari, A. Paolillo, and M. Vendittelli. Manual guidance of humanoid robots without force sensors: Preliminary experiments with NAO. In *Proceedings of International Conference on Robotics and Automation*, pages 1184–1189. IEEE, 2014.
- [8] P. Bouyer, N. Markey, N. Perrin, and P. Schlehuber-Caissier. Timed-automata abstraction of switched dynamical systems using control funnels. In *Proceedings of International Conference on Formal Modeling and Analysis of Timed Systems*, pages 60–75. Springer, 2015.
- [9] R. R. Burridge, A. A. Rizzi, and D. E. Koditschek. Sequential composition of dynamically dexterous robot behaviors. *The International Journal of Robotics Research*, 18(6):534–555, 1999.
- [10] B. G. Buss, A. Ramezani, K. A. Hamed, B. A. Griffin, K. S. Galloway, and J. W. Grizzle. Preliminary walking experiments with underactuated 3d bipedal robot marlo. In *Proceedings of International Conference on Intelligent Robots and Systems*, pages 2529–2536. IEEE, 2014.

- [11] K. Byl and R. Tedrake. Metastable walking machines. *The International Journal of Robotics Research*, 28(8):1040–1064, 2009.
- [12] S. Candido, Y.-T. Kim, and S. Hutchinson. An improved hierarchical motion planner for humanoid robots. In *Proceedings of the 8th IEEE-RAS International Conference on Humanoid Robots*, pages 654–661, 2008.
- [13] C. Chevallereau, G. Abba, Y. Aoustin, F. Plestan, E. Westervelt, C. C. de Wit, and J. W. Grizzle. Rabbit: A testbed for advanced control theory. *IEEE Control Systems Magazine*, 23(5):57–79, 2003.
- [14] C. Chevallereau, J. W. Grizzle, and C.-L. Shih. Asymptotically stable walking of a five-link underactuated 3-d bipedal robot. *IEEE Transactions on Robotics*, 25(1):37–50, 2009.
- [15] Ch. Chevallereau, J. W. Grizzle, and Ch. Shih. Asymptotically stable walking of a five-link underactuated 3-d bipedal robot. *IEEE Transactions on Robotics*, 25(1):37–50, 2009.
- [16] J. H. Choi and J. W. Grizzle. Planar bipedal walking with foot rotation. In *Proceedings of American Control Conference*, pages 4909–4916, 2005.
- [17] S.-J. Chung and M. Dorothy. Neurobiologically inspired control of engineered flapping flight. *Journal of guidance, control, and dynamics*, 33(2):440–453, 2010.
- [18] S. H. Collins, M. Wisse, and A. Ruina. A three-dimensional passive-dynamic walking robot with two legs and knees. *The International Journal of Robotics Research*, 20(7):607–615, 2001.
- [19] D. C. Conner, H. Choset, and A. A. Rizzi. Integrating planning and control for single-bodied wheeled mobile robots. *Autonomous Robots*, 30(3):243–264, 2011.
- [20] S. Dalibard, A. Nakhaei, F. Lamiroux, and J.-P. Laumond. Whole-body task planning for a humanoid robot: a way to integrate collision avoidance. In *Proceedings of 9th IEEE-RAS International Conference on Humanoid Robots*, pages 355–360, 2009.
- [21] N. Dantam, A. Hereid, A. D. Ames, and M. Stilman. Correct software synthesis for stable speed-controlled robotic walking. *Robotics: Science and Systems*, 2013.
- [22] V. Duchaine and C. M. Gosselin. General model of human-robot cooperation using a novel velocity based variable impedance control. In *EuroHaptics Conference and Symposium on Haptic Interfaces for Virtual Environment and Teleoperator Systems*, pages 446–451. IEEE, 2007.
- [23] K. Erbatur and O. Kurt. Natural zmp trajectories for biped robot reference generation. *IEEE Transactions on Industrial Electronics*, 56(3):835–845, 2009.

- [24] E. Frazzoli, M. A. Dahleh, and E. Feron. Maneuver-based motion planning for nonlinear systems with symmetries. *IEEE Transactions on Robotics*, 21(6):1077–1091, 2005.
- [25] J. Furusho and A. Sano. Sensor-based control of a nine-link biped. *The International Journal of Robotics Research*, 9(2):83–98, 1990.
- [26] K. Galloway, K. Sreenath, A. D. Ames, and J. W. Grizzle. Torque saturation in bipedal robotic walking through control lyapunov function-based quadratic programs. *IEEE Access*, 3:323–332, 2015.
- [27] G. Ganesh, A. Albu-Schaffer, M. Haruno, M. Kawato, and E. Burdet. Biomimetic motor behavior for simultaneous adaptation of force, impedance and trajectory in interaction tasks. In *Proceedings of IEEE International Conference on Robotics and Automation (ICRA)*, pages 2705–2711, 2010.
- [28] R. D. Gregg and M. Spong. Reduction-based control of three-dimensional bipedal walking robots. *The International Journal of Robotics Research*, 29(6):680–702, 2009.
- [29] R. D. Gregg and M. W. Spong. Reduction-based control of three-dimensional bipedal walking robots. *The International Journal of Robotics Research*, 29(6):680–702, May 2009.
- [30] R. D. Gregg, A. K. Tilton, S. Candido, T. Bretl, and M. W. Spong. Control and planning of 3-d dynamic walking with asymptotically stable gait primitives. *IEEE Transactions on Robotics*, 28(6):1415–1423, 2012.
- [31] E. Gribovskaya, A. Kheddar, and A. Billard. Motion learning and adaptive impedance for robot control during physical interaction with humans. In *Proceedings of IEEE International Conference on Robotics and Automation (ICRA)*, pages 4326–4332, 2011.
- [32] D. W. Grieve. Gait patterns and the speed of walking. *Journal of Biomedical Engineering*, 3:119–122, 1968.
- [33] J. W. Grizzle, G. Abba, and F. Plestan. Asymptotically stable walking for biped robots: Analysis via systems with impulse effects. *IEEE Transactions on Automatic Control*, 46(1):51–64, 2001.
- [34] J. W. Grizzle, J. Hurst, B. Morris, H.-W. Park, and K. Sreenath. Mabel, a new robotic bipedal walker and runner. In *Proceedings of American Control Conference*, pages 2030–2036. IEEE, 2009.
- [35] W. M. Haddad and V. Chellaboina. *Nonlinear Dynamical Systems and Control: A Lyapunov-Based Approach*. Princeton University Press, 41 William Street, Princeton, New Jersey, USA, 2008.

- [36] K. A. Hamed, B. G. Buss, and J. W. Grizzle. Exponentially stabilizing continuous-time controllers for periodic orbits of hybrid systems: Application to bipedal locomotion with ground height variations. *The International Journal of Robotics Research*, 35(8):977–999, 2016.
- [37] K. A. Hamed and J. W. Grizzle. Event-based stabilization of periodic orbits for underactuated 3-D bipedal robots with left-right symmetry. *IEEE Transactions on Robotics*, 30(2):365–381, 2014.
- [38] K. Harada, E. Yoshida, and K. Yokoi, editors. *Motion Planning for Humanoid Robots*. Springer-Verlag, 2010.
- [39] K. Hauser, T. Bretl, J.-C. Latombe, K. Harada, and B. Wilcox. Motion planning for legged robots on varied terrain. *The International Journal of Robotics Research*, 27(11-12):1325–1349, 2008.
- [40] H. Hirukawa, S. Hattori, K. Harada, Sh. Kajita, K. Kaneko, F. Kanehiro, K. Fujiwara, and M. Morisawa. A universal stability criterion of the foot contact of legged robots-adios zmp. In *Proceedings of IEEE International Conference on Robotics and Automation*, pages 1976–1983, 2006.
- [41] N. Hogan. Impedance control: An approach to manipulation: Part illapplications. *Journal of Dynamic Systems, Measurement, and Control*, 107(2):17, 1985.
- [42] R. Ikeura and H. Inooka. Variable impedance control of a robot for cooperation with a human. In *Proceedings of IEEE International Conference on Robotics and Automation*, volume 3, pages 3097–3102, 1995.
- [43] Y. Inoue, T. Tohge, and H. Iba. Cooperative transportation by humanoid robots: Learning to correct positioning. In *Proceedngs of Hybrid Intelligent Systems (HIS)*, pages 1124–1134, 2003.
- [44] Y. Inoue, T. Tohge, and H. Iba. Object transportation by two humanoid robots using cooperative learning. In *Proceedings of the Congress on Evolutionary Computation (CEC)*, volume 1, pages 1201–1208, 2004.
- [45] A. Isidori. *Nonlinear Control Systems*, volume 1. Springer, 1995.
- [46] I. Kato. The hydraulically powered biped walking machine with a high carrying capacity. In *Proceeding of the 4th International Symposium on External Control of Human Extremities*, pages 410–421, 1972.
- [47] R. Kelly, R. Carelli, M. Amestegui, and R. Ortega. On adaptive impedance control of robot manipulators. In *Proceedings of IEEE International Conference on Robotics and Automation*, pages 572–577, 1989.

- [48] H. K. Khalil. *Nonlinear Systems*. Prentice hall, Upper Saddle River, New Jersey, 3 edition, 2002.
- [49] H. Kim, J. An, J. Moon, and D. Kim. Simulation based for intelligent control system of multi - humanoid robots for dynamic load carrying. In *Proceedings of International Conference on Control Automation and Systems (ICCAS)*, pages 101–104, 2010.
- [50] H. Kimura, Y. Fukuoka, and A. H. Cohen. Adaptive dynamic walking of a quadruped robot on natural ground based on biological concepts. *The International Journal of Robotics Research*, 26(5):475–490, 2007.
- [51] S. Kolathaya and A. D. Ames. Achieving bipedal locomotion on rough terrain through human-inspired control. In *IEEE International Symposium on Safety, Security, and Rescue Robotics (SSRR)*, pages 1–6, 2012.
- [52] S. Kolathaya and A. D. Ames. Parameter sensitivity and boundedness of robotic hybrid periodic orbits. *IFAC-PapersOnLine*, 48(27):377–382, 2015.
- [53] J. Kuffner, S. Kagami, K. Nishiwaki, M. Inaba, and H. Inoue. Dynamically-stable motion planning for humanoid robots. *Autonomous Robots*, 12(1):105–118, 2002.
- [54] J. Kuffner, K. Nishiwaki, S. Kagami, M. Inaba, and H. Inoue. Motion planning for humanoid robots. In *Robotics Research. The Eleventh International Symposium*, pages 365–374. Springer, 2005.
- [55] S. Kuindersma, R. Deits, M. Fallon, A. Valenzuela, H. Dai, F. Permenter, T. Koolen, P. Marion, and R. Tedrake. Optimization-based locomotion planning, estimation, and control design for the atlas humanoid robot. *Autonomous Robots*, 40:429–455, 2016.
- [56] A. D. Kuo. Energetics of actively powered locomotion using the simplest walking model. *Journal of biomechanical engineering*, 124(1):113–120, 2002.
- [57] A. J. Laub. *Matrix Analysis for Scientists and Engineers*. Siam, 2005.
- [58] S. M. LaValle and J. J. Kuffner. Randomized kinodynamic planning. *The International Journal of Robotics Research*, 20(5):378–400, 2001.
- [59] Y. Li and S. S. Ge. Human–robot collaboration based on motion intention estimation. *IEEE/ASME Transactions on Mechatronics*, 19(3):1007–1014, 2014.
- [60] D. Liberzon. *Switching in Systems and Control*. Birkhäuser, Boston, 2003.
- [61] A. Majumdar and R. Tedrake. Robust online motion planning with regions of finite time invariance. In *Algorithmic Foundations of Robotics X*, pages 543–558. Springer, 2013.

- [62] I. R. Manchester and J. Umenberger. Real-time planning with primitives for dynamic walking over uneven terrain. In *Proceedings of IEEE International Conference on Robotics and Automation (ICRA)*, pages 4639–4646, 2014.
- [63] A. E. Martin, D. C. Post, and J. P. Schmiedeler. The effects of foot geometric properties on the gait of planar bipeds walking under hzd-based control. *The International Journal of Robotics Research*, 33(12):1530–1543, 2014.
- [64] N. H. McClamroch. A singular perturbation approach to modeling and control of manipulators constrained by a stiff environment. In *Proceedings of IEEE Conference on Decision and Control*, pages 2407–2411, Tampa, Florida, December 1989.
- [65] T. McGeer. Passive dynamic walking. *The international journal of robotics research*, 9(2):62–82, 1990.
- [66] S. G. McGill and D. D. Lee. Cooperative humanoid stretcher manipulation and locomotion. In *Proceedings of IEEE-RAS International Conference on Humanoid Robots*, pages 429–433, 2011.
- [67] H. Miura and I. Shimoyama. Dynamic walk of a biped. *The International Journal of Robotics Research*, 3(2):60–74, 1984.
- [68] B. Morris and J. W. Grizzle. A restricted poincaré map for determining exponentially stable periodic orbits in systems with impulse effects: Application to bipedal robots. In *Proceedings of IEEE Conference on Decision and Control*, pages 4199–4206, Seville, Spain, December 2005.
- [69] B. Morris and J. W. Grizzle. Hybrid invariant manifolds in systems with impulse effects with application to periodic locomotion in bipedal robots. *IEEE Transactions on Automatic Control*, 54(8):1751–1764, 2009.
- [70] M. S. Motahar, S. Veer, J. Huang, and I. Poulakakis. Integrating dynamic walking and arm impedance control for cooperative transportation. In *Proceedings of IEEE/RSJ International Conference on Intelligent Robots and Systems*, pages 1004–1010, Hamburg, Germany, September 2015.
- [71] M. S. Motahar, S. Veer, and I. Poulakakis. Composing limit cycles for motion planning of 3d bipedal walkers. In *Proceedings of IEEE Conference on Decision and Control*, pages 6368–6374, Las Vegas, December 2016.
- [72] M. S. Motahar, S. Veer, and I. Poulakakis. Steering a 3d limit-cycle walker for collaboration with a leader. In *Proceedings of IEEE/RSJ International Conference on Intelligent Robots and Systems*, Vancouver, September 2017.

- [73] U. Nagarajan, G. Kantor, and R. Hollis. Integrated motion planning and control for graceful balancing mobile robots. *The International Journal of Robotics Research*, 32(9-10):1005–1029, 2013.
- [74] Q. Nguyen, A. Hereid, J. W. Grizzle, A. D. Ames, and K. Sreenath. 3d dynamic walking on stepping stones with control barrier functions. In *Proceedings of 55th Conference on Decision and Control (CDC)*, pages 827–834. IEEE, 2016.
- [75] Q. Nguyen and K. Sreenath.  $L_1$  adaptive control for bipedal robots with control lyapunov function based quadratic programs. In *Proceedings of American Control Conference (ACC), 2015*, pages 862–867. IEEE, 2015.
- [76] Q. Nguyen and K. Sreenath. Optimal robust control for bipedal robots through control lyapunov function based quadratic programs. In *Proceedings of Robotics: Science and Systems*, 2015.
- [77] Q. Nguyen and K. Sreenath. Safety-critical control for dynamical bipedal walking with precise footstep placement. *IFAC-PapersOnLine*, 48(27):147–154, 2015.
- [78] K. Nishiwaki, W. Yoon, and S. Kagami. Motion control system that realizes physical interaction between robot’s hands and environment during walk. In *Proceedings of IEEE-RAS International Conference on Humanoid Robots*, pages 542–547, 2006.
- [79] P.-Y. Oudeyer, O. Ly, and P. Rouanet. Exploring robust, intuitive and emergent physical human-robot interaction with the humanoid acrobat. In *Proceedings of IEEE-RAS International Conference on Humanoid Robots*, pages 120–127, 2011.
- [80] C. A. C. Parker and E. A. Croft. Experimental investigation of human-robot cooperative carrying. In *Proceedings of IEEE/RSJ International Conference on Intelligent Robots and Systems (IROS)*, pages 3361–3366, 2011.
- [81] P. A. Parrilo. *Structured semidefinite programs and semialgebraic geometry methods in robustness and optimization*. PhD thesis, California Institute of Technology, 2000.
- [82] F. Popescu, J. M. Hidler, and W. Z. Rymer. Elbow impedance during goal-directed movements. *Experimental brain research*, 152(1):17–28, 2003.
- [83] M. B. Popovic, A. Goswami, and H. Herr. Ground reference points in legged locomotion: Definitions, biological trajectories and control. *The International Journal of Robotics Research*, 21(12):1013–1032, 2005.
- [84] M. Powell, A. Hereid, and A. D. Ames. Speed regulation in 3d robotic walking through motion transitions between human-inspired partial hybrid zero dynamics. In *Proceedings of IEEE International Conference on Robotics and Automation*, 2013.

- [85] M. J. Powell, H. Zhao, and A. D. Ames. Motion primitives for human-inspired bipedal robotic locomotion: walking and stair climbing. In *Proceedings of IEEE International Conference on Robotics and Automation (ICRA)*, pages 543–549, 2012.
- [86] J. E. Pratt. *Exploiting inherent robustness and natural dynamics in the control of bipedal walking robots*. PhD thesis, 2000.
- [87] M. M. Rahman, R. Ikeura, and K. Mizutani. Investigation of the impedance characteristic of human arm for development of robots to cooperate with humans. *JSME International Journal Series C*, 45(2):510–518, 2002.
- [88] C. O. Saglam and K. Byl. Robust policies via meshing for metastable rough terrain walking. In *Robotics: Science and Systems*, 2014.
- [89] Y. Sakagami, R. Watanabe, C. Aoyama, S. Matsunaga, N. Higaki, and K. Fujimura. The intelligent asimo: System overview and integration. In *Proceedings of IEEE/RSJ International Conference on Intelligent Robots and Systems*, volume 3, pages 2478–2483. IEEE, 2002.
- [90] L. Sciavicco. *Modelling and Control of Robot Manipulators*. Springer, 2000.
- [91] K. Seo, S.-J. Chung, and J.-J. E. Slotine. Cpg-based control of a turtle-like underwater vehicle. *Autonomous Robots*, 28(3):247–269, 2010.
- [92] H. Seraji and R. Colbaugh. Force tracking in impedance control. *The International Journal of Robotics Research*, 16(1):97–117, 1997.
- [93] C.-L. Shih, J. W. Grizzle, and C. Chevallereau. From stable walking to steering of a 3d bipedal robot with passive point feet. *Robotica*, 30(07):1119–1130, 2012.
- [94] R. W. Sinnet and A. D. Ames. 3D bipedal walking with knees and feet: A hybrid geometric approach. In *Proceedings of IEEE Conference on Decision and Control held jointly with the Chinese Control Conference*, pages 3208–3213, Shanghai, P.R. China, December 2009.
- [95] R. W Sinnet, S. Jiang, and A. D. Ames. A human-inspired framework for bipedal robotic walking design. *The International Journal of Biomechatronics and Biomedical Robotics*, 2013.
- [96] M. W. Spong. Passivity based control of the compass gait biped. In *Proceedings of IFAC World Congress*, pages 19–24, Beijing, China, 1999. Citeseer.
- [97] M. W. Spong and F. Bullo. Controlled symmetries and passive walking. *IEEE Transactions on Automatic Control*, 50(7):1025–1031, 2005.
- [98] M. W. Spong, S. Hutchinson, and M. Vidyasagar. *Robot Modeling and Control*, volume 3. Wiley New York, 2006.

- [99] K. Sreenath, H. W. Park, I. Poulakakis, and J. Grizzle. A compliant hybrid zero dynamics controller for stable, efficient and fast bipedal walking on MABEL. *The International Journal of Robotics Research*, 30(9):1170–1193, 2011.
- [100] O. Stasse, P. Evrard, N. Perrin, N. Mansard, and A. Kheddar. Fast foot prints re-planning and motion generation during walking in physical human-humanoid interaction. In *Proceedings of 9th IEEE-RAS International Conference on Humanoid Robots*, pages 284–289, 2009.
- [101] B. Stephens. *Push recovery control for force-controlled humanoid robots*. PhD thesis, Carnegie Mellon University Pittsburgh, Pennsylvania USA, 2011.
- [102] T. Sugihara, Y. Nakamura, and H. Inoue. Real-time humanoid motion generation through zmp manipulation based on inverted pendulum control. In *Proceedings of IEEE International Conference on Robotics and Automation*, volume 2, pages 1404–1409, 2002.
- [103] R. Tedrake, I. R. Manchester, M. Tobenkin, and J. W. Roberts. Lqr-trees: Feedback motion planning via sums-of-squares verification. *The International Journal of Robotics Research*, 29(8):1038–1052, 2010.
- [104] T. Tsumugiwa, R. Yokogawa, and K. Hara. Variable impedance control based on estimation of human arm stiffness for human-robot cooperative calligraphic task. In *Proceedings of IEEE International Conference on Robotics and Automation*, volume 1, pages 644–650, 2002.
- [105] S. Veer, M. S. Motahar, and I. Poulakakis. On the adaptation of dynamic walking to persistent external forcing using hybrid zero dynamics control. In *Proceedings of IEEE/RSJ International Conference on Intelligent Robots and Systems*, pages 997–1003, Hamburg, Germany, September 2015.
- [106] S. Veer, M. S. Motahar, and I. Poulakakis. Adaptation of limitcycle walkers for collaborative tasks: A supervisory switching control approach. In *Proceeding of IEEE/RSJ International Conference on Intelligent Robots and Systems*, Vancouver, September 2017.
- [107] S. Veer, M. S. Motahar, and I. Poulakakis. Almost driftless navigation of 3D limit-cycle walking bipeds. In *Proceeding of IEEE/RSJ International Conference on Intelligent Robots and Systems*, Vancouver, 2017.
- [108] M. Vukobratović and B. Borovac. Zero-moment point - thirty five years of its life. *The International Journal of Humanoid Robotics*, 1(01):157–173, 2004.
- [109] M. Vukobratovic, B. Borovac, D. Surla, and D. Stokic. *Biped Locomotion, Scientific Fundamentals of Robotics 7*. Springer-Verlag, 1989.

- [110] T. Wang, C. Chevallereau, and D. Tlalolini. Stable walking control of a 3D biped robot with foot rotation. *Robotica*, 32(04):551–570, 2014.
- [111] E. R. Westervelt, J. W. Grizzle, C. Chevallereau, J. H. Choi, and B. Morris. *Feedback Control of Dynamic Bipedal Robot Locomotion*. CRC Press, Boca Raton, FL, 2007.
- [112] E. R. Westervelt, J. W. Grizzle, and D. E. Koditschek. Hybrid zero dynamics of planar biped walkers. *IEEE Transactions on Automatic Control*, 48(1):42–56, 2003.
- [113] H. Xu, Y. Zhang, J. Yang, G. Zhou, and L. Caccetta. Practical exponential set stabilization for switched nonlinear systems with multiple subsystem equilibria. *Journal of Global Optimization*, pages 1–10, 2015.
- [114] X. Xu and G. Zhai. Practical stability and stabilization of hybrid and switched systems. *IEEE Transactions on Automatic Control*, 50(11):1897–1903, 2005.
- [115] J. Yamaguchi, E. Soga, S. Inoue, and A. Takanishi. Development of a bipedal humanoid robot-control method of whole body cooperative dynamic biped walking. In *Proceedings of IEEE International Conference on Robotics and Automation*, volume 1, pages 368–374, 1999.
- [116] J.-I. Yamaguchi, A. Takanishi, and I. Kato. Development of a biped walking robot compensating for three-axis moment by trunk motion. In *Proceedings of IEEE/RSJ International Conference on Intelligent Robots and Systems*, volume 1, pages 561–566, 1993.
- [117] T. Yang, E. R. Westervelt, A. Serrani, and J. P. Schmiedeler. A framework for the control of stable aperiodic walking in underactuated planar bipeds. *Autonomous Robots*, 27(3):277–290, 2009.
- [118] E. Yoshida, C. Esteves, I. Belousov, J. P. Laumond, T. Sakaguchi, and K. Yokoi. Planning 3-d collision-free dynamic robotic motion through iterative reshaping. *IEEE Transactions on Robotics*, 24(5):1186–1198, 2008.
- [119] H. Yoshida, K. Inoue, T. Arai, and Y. Mae. Mobile manipulation of humanoid robots—a method of adjusting leg motion for improvement of arm’s manipulability. In *Proceedings of IEEE/ASME International Conference on Advanced Intelligent Mechatronics*, volume 1, pages 266–271, 2001.
- [120] M. Zucker, S. Joo, M. X. Grey, C. Rasmussen, E. Huang, M. Stilman, and A. Bobick. A general-purpose system for teleoperation of the DRC-HUBO humanoid robot. *Journal of Field Robotics*, 32(3):336–351, 2015.